GEAR TECHNOLOGY

The Journal of Gear Manufacturing

SEPTEMBER/OCTOBER 1986

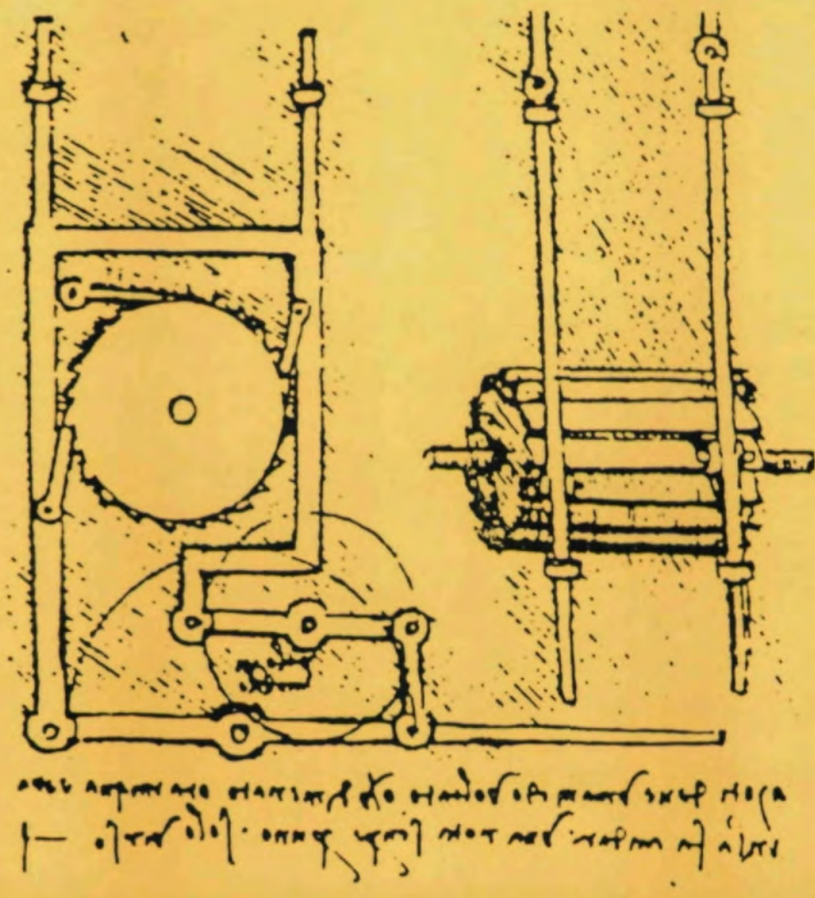

Improved Gear Life Through Controlled Shot Peening

Analysis of Highly-Loaded Gears Using the Modified-Scoring Index Method

Tooth Strength Study of Spur Planet Gears

Pressure Angle Changes for Circular Cut Spiral Bevel Gears

Gears for Non-Parallel Shafts


AMERICAN PFAUTER
LORENZ
ETTLINGEN
MAAG
ZURICH
KAPP

RANDALL PUBLISHING
1401 Lunt Avenue
P.O. Box 1426
Elk Grove, IL 60007
(312) 437-6604

TYPOGRAPHY:
Kenric Graphics, Inc.
Elk Grove Village, IL

PRINTING:
TCR Graphics
Streamwood, IL

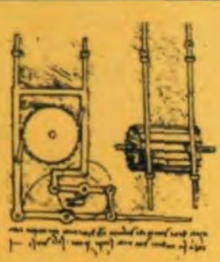

The Advanced Technology of Leonardo Da Vinci 1452-1519

COVER

Leonardo, the engineer, was fascinated by the mechanical arts. One of his life-long interests was in the improvement of the way in which machines harnessed and used the forces of motion.

Our cover sketch shows one of Leonardo's many studies of the reciprocating-to-rotary motion problem. In the right hand design, the motion transference takes place when the pawls on the vertical rods engage the rachets on the cylinder. On the downstroke, the pawls slide past the ratchets; on the upstroke, pawls and rachets meet, turning the cylinder.

GEAR TECHNOLOGY

The Journal of Gear Manufacturing

CONTENTS — PAGE NO.

FEATURES

DEPARTMENTS

September/October 1986 — Vol. 3, No. 5

GEAR TECHNOLOGY, The Journal of Gear Manufacturing (ISSN 0743-6858) is published bimonthly by Randall Publishing Co., Inc., 1425 Lunt Avenue, P. O. Box 1426, Elk Grove Village, IL 60007. GEAR TECHNOLOGY, The Journal of Gear Manufacturing is distributed free of charge to qualified individuals and firms in the gear manufacturing industry. Subscription rates for non-qualified individuals and firms are: $30.00 in the United States, $50.00 for foreign countries. Second-Class postage paid at Arlington Heights, IL and at additional mailing office.

Postmaster: Send address changes to GEAR TECHNOLOGY, *The Journal of Gear Manufacturing*, 1425 Lunt Avenue, P. O. Box 1426, Elk Grove Village, IL 60007.

MANUSCRIPTS: We are requesting technical papers of every sort from manufacturers of gear making machinery and related equipment, universities, and engineers. Articles should be of an educational and training nature with general appeal to anyone having anything to do with the purchase of materials or machinery, or the design, manufacture, testing or processing of gears. Subjects sought are solutions to specific problems, explanations of new: technology, techniques, designs, processes, and alternative manufacturing methods. These can range from the "How to . . ." of gear cutting (BACK TO BASICS) to the most advanced technology. All manuscripts submitted will be carefully considered. However, the Publisher assumes no responsibility for the safety or return of manuscripts. Manuscripts must be accompanied by a self-addressed, self-stamped envelope, and be sent to GEAR TECHNOLOGY, The Journal of Gear Manufacturing, P.O. Box 1426, Elk Grove, IL 60007, (312) 437-6604.

Purdy gets it all together.

PRECISELY

Critical parts of world famous helicopters are made and assembled at Purdy. A CNC machining system, highly flexible and computer controlled, allows Purdy to offer perfection, beyond precision, in meeting the most complex specifications . . . on time, with cost efficiency.

Purdy Gears complete the parts.

Now Purdy gear box housings are complete with Purdy gears, which Purdy cuts in fast cutting cycles. Zeiss measuring machines compute the track and depth of stock removal and check for accuracy. Purdy also machines RSR cutting blades.

PURDY

Beyond Precision

The Purdy Corporation, 586 Hilliard St., Manchester, CT 06040 Telephone: (203) 649-0000

CIRCLE A-33 ON READER REPLY CARD

EDITORIAL

"It's show time!" Ready or not, on Sept. 3, the biennial International Machine Tool Show opens at McCormick Place, Chicago. Planning a show that encompasses displays from over 1000 companies from 29 nations and an associated technical conference presenting more than 200 papers on 50 topics has not been without its problems. The question of McCormick Place North's readiness has been an off-again-on-again-off-again issue all summer. That, along with all the inherent problems in organizing a show of this magnitude has called for creativeness, flexibility and a certain amount of courage on the part of the IMTS's organizers and exhibitors. Now, however, coming down the home stretch, planners and exhibitors are optimistic about the show's success.

These same kinds of attitudes seem to be required of manufacturing people as they contemplate the future of the industry. Business conditions at this time are startlingly diverse. An executive of an oil pump jack manufacturing company has stated that his company won't be coming to the show so it can "use the money to pay the light bills." On the other hand a defense industry manufacturer comments, "Business has never been better." However, most exhibitors and manufacturers are approaching the show with cautious optimism.

Other factors that will affect future business conditions over the coming year and even farther into the future are changes in interest rates, exchange rates, and the new tax bill. With these many unknown factors affecting the industry, resourcefulness, sensitivity to change and a tough-minded attitude will be required of manufacturers to insure that they have enough financial wherewithal and skilled personnel to remain competitive.

The companies that are still in business today are survivors. Many of our weak and inefficient companies are already gone, and in many cases new companies have risen from their ashes. Survivors and newcomers alike have learned the need for both new and efficient machinery and equally flexible and efficient ways of doing business.

"The show must go on" in the machine tool industry as well as at McCormick Place. We do not have the luxury of waiting for all the pieces to fall into place before we make the business decisions that will keep us competitive. No matter what happens in Congress, in the Federal Reserve System, or in the international economy, we must continue to push ahead doing the best we can with what we have, because, ready or not, "It's show time!"

Michael Goldstein
Editor/Publisher

GUEST EDITORIAL

LONG ON HIGH TECHNOLOGY — SHORT ON HIGH TECHNOLOGISTS

At the present time, technology seems to be moving faster than our ability to educate people in its utilization. This is particularly true of the manufacturing engineering profession.

Donald Zook
President, SME

For example, enormous progress has been made in the area of CAD/CAM. Hardware to support computer graphics has been developed and designed with amazing speed. In the last five years, the microminiaturization of electronic components has increased the power of these units beyond our wildest dreams.

Software development has kept pace with the progress in hardware. Computer programs and advanced computer graphics have been developed to help us design, test, and process parts. The potential of this technology is enormous.

Unfortunately, the technical education of our engineers has not developed at the same pace. Since design, testing and processing were formerly done by numerous individuals from different disciplines, it is difficult to find a single individual who can perform all of these functions utilizing CAD/CAM. Consequently, while the technology is available, the qualified individual to make the best use of the technology is not.

We are able to provide assistance in some areas through the application of artificial intelligence or canned knowledge, so that a given individual does not have to be an expert in every field, but this support is not enough. Such assistance has not developed at the same pace as the technology itself; furthermore, such dependence on artificial intelligence is no substitute for the solid training of talent.

In both academic circles and in the industry, we must become more aware of the need to put the same emphasis on the development of our people as we have put on the development and installation of tools. Unless we can provide products that perform to the satisfaction of our customers in terms of function, durability, and cost, they will go elsewhere. Without utilizing all of the talent, as well as the technology at hand, we will not remain competitive in today's market.

In short, we must become equally long on high technologists.

Donald Zook

Don Zook

President
Society of Manufacturing Engineers

***MR. DONALD ZOOK,** is President of the Society of Manufacturing Engineers (SME). He is presently employed as the Assistant Director of Manufacturing for the Caterpillar, Inc. in Peoria, Illinois. A member of SME since 1967, Mr. Zook has chaired several international committees, including a special Battelle Study entitled "The Manufacturing Engineer — Past, Present, and Future." Zook earned BS and MS degrees from the University of Illinois and is a past instructor at Bradley University. He is a registered Professional Engineer (PE) and a Certified Manufacturing Engineer (CMfgE).*

Before you buy a CNC Gear Inspection System, ask these four questions

1. Can we get complete inspection of both gears and cutting tools?

With the M & M 2000 QC System, the answer is yes. The system will test lead and involute profile characteristics of internal or external gears and splines. It is the only universal gear tester available which provides true index testing without expensive attachments. In addition, we have fully-developed software for checking hobs, shaver cutters, shaper cutters, and other cylindrical parts such as worms and cams.

Hob Pressure Angle Check

Shaver Cutter Lead Check

2. Can you customize software to meet our quality-inspection specifications?

At M & M Precision, we write and develop our own inspection software. Our technical team can and has implemented inspection specifications into specific software for individual requirements. Our current library includes line/curve fitting as well as modified K-chart analysis routines.

Line/Curve Fitting

Modified K-Chart Analysis

3. OK, you can inspect gears and cutting tools. What else is available to aid us in quality control of the manufacturing process?

At M & M Precision, we have fully integrated such advanced software packages as Statistical Process Control and Tooth Topography into our standard testing software. Our SPC program can identify non-random variations and provide early warning of variations which are approaching tolerance limits. Our Tooth Topography software features automatic testing of lead and involute at multiple locations and provides two- and three-dimensional graphics.

SPC Run Chart

Topological Map

4. Do you have the technical support team and installation experience to back up the hardware and software provided?

At M & M Precision, we have a technical team with over 45 man-years of experience in developing CNC gear inspection hardware and software. All software for our QC 2000 System has been developed in-house. In addition, we have working installations at these leading companies:

- General Motors
- TRW
- Ford Motor
- Warner Gear
- Cincinnati Milacron
- Chrysler
- Pratt & Whitney
- Rocketdyne

For details on our advanced QC 2000 System and available software, contact M & M Precision Systems, 300 Progress Road, West Carrollton, Ohio 45449, 513/859-8273.

Visit us at Booth #6097, IMTS '86.

M&M PRECISION SYSTEMS

AN ACME-CLEVELAND COMPANY

ADVERTISER'S INDEX FOR IMTS

*Indicates New Advertiser or Change in Booth Number

(In-house exhibition)
American Pfauter
925 E. Estes Ave.
Elk Grove, IL 60007
(312) 640-7500

Booth 6243
McCormick North Level 2 (COSA)
Forest City Gear
11715 Main Street
Roscoe, IL 61073
(815) 623-2168

Booth 8818
McCormick Place West
Fromag GmbH
R. J. Kemp, Representative
38 W510 Lake Charlotte Ct.
St. Charles, IL 60174

Booth #4454
McCormick, East Level 3
GMW Machinery Inc.
Gear Machinery Division
1665 Tonne Avenue
Elk Grove Village, IL 60007
(312) 364-4530

Booth #3333
McCormick, North
The Gleason Works
1000 University Avenue
Rochester, NY 14692
(716) 473-1000

Booth B2740*
McCormick, West
Illies America, Inc.
5420 Newport Drive
Rolling Meadows, IL 60008
(312) 577-1144

Booth #6598*
McCormick, North
Klingelnberg Corporation
15200 Foltz Industrial Parkway
Strongsville, OH 44136
(216) 572-2100

Booth #5252
McCormick, North
Liebherr Machine Tool
290 South Wagner Rd.
Ann Arbor, MI 48103
(313) 769-3521

Booth #6097*
McCormick, North
M & M Precision Systems
300 Progress Road
West Carrollton, OH 45499
(513) 859-8273

Booth #6281
McCormick, North
Mitsubishi Heavy Industries America, Inc.
873 Supreme Drive
Bensenville, IL 60106
(312) 860-4220

Booth #6279*
McCormick, North
Perez Machine Tool Co.
11 Ginger Court
East Amherst, NY 14051
(716) 688-6982

Booth #6068*
McCormick, North
Precision Technology
211 E. 18th Street
New York, NY 10003

Booth #6343
McCormick, North
StarCut Sales, Inc.
23461 Industrial Park Drive
Farmington Hills, MI 48024
(313) 474-8200

IMTS
The world of manufacturing technology

1986 INTERNATIONAL MACHINE TOOL SHOW
September 3-11, 1986 • Chicago, Illinois, USA

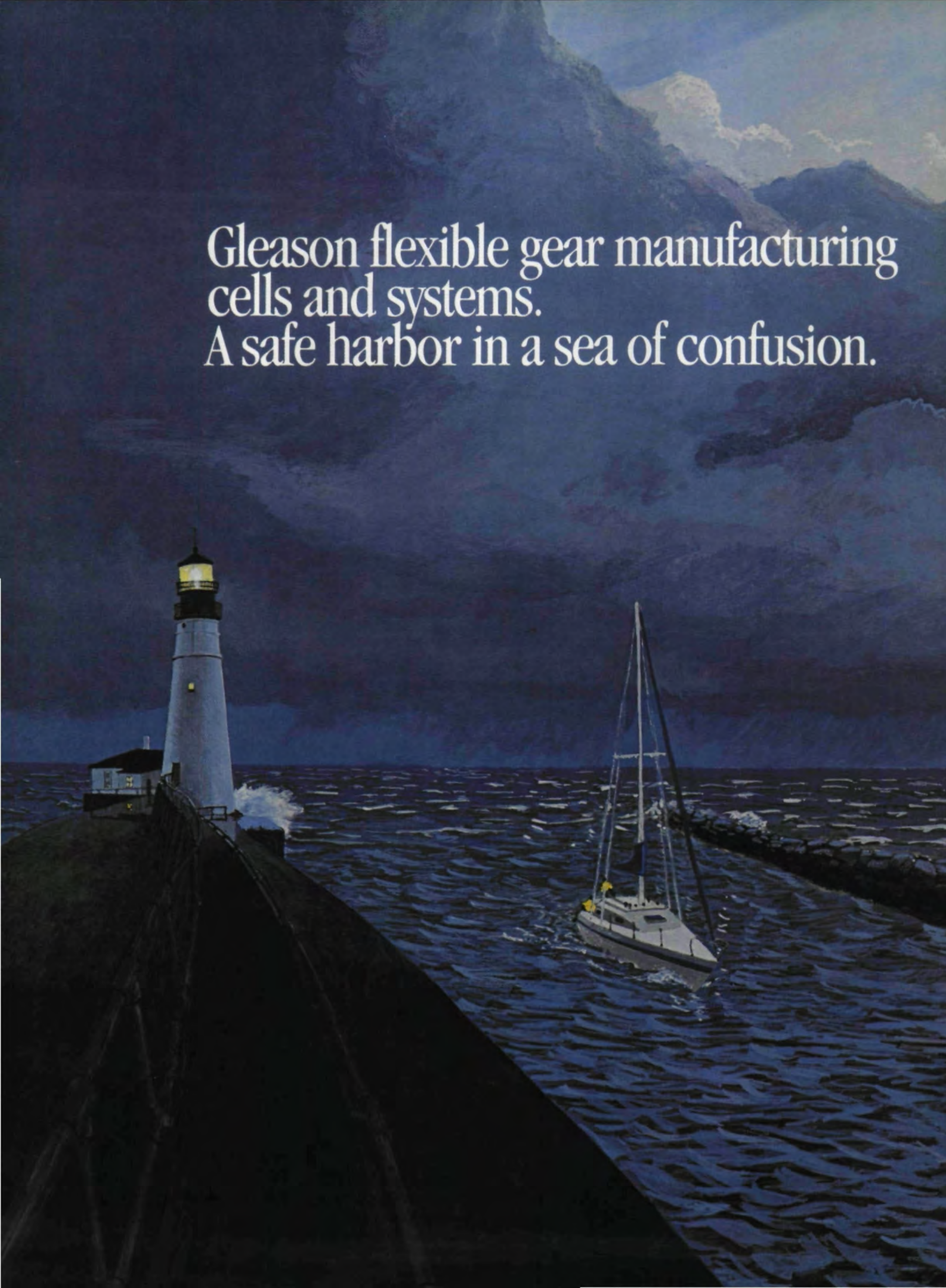
Gleason flexible gear manufacturing cells and systems.
A safe harbor in a sea of confusion.

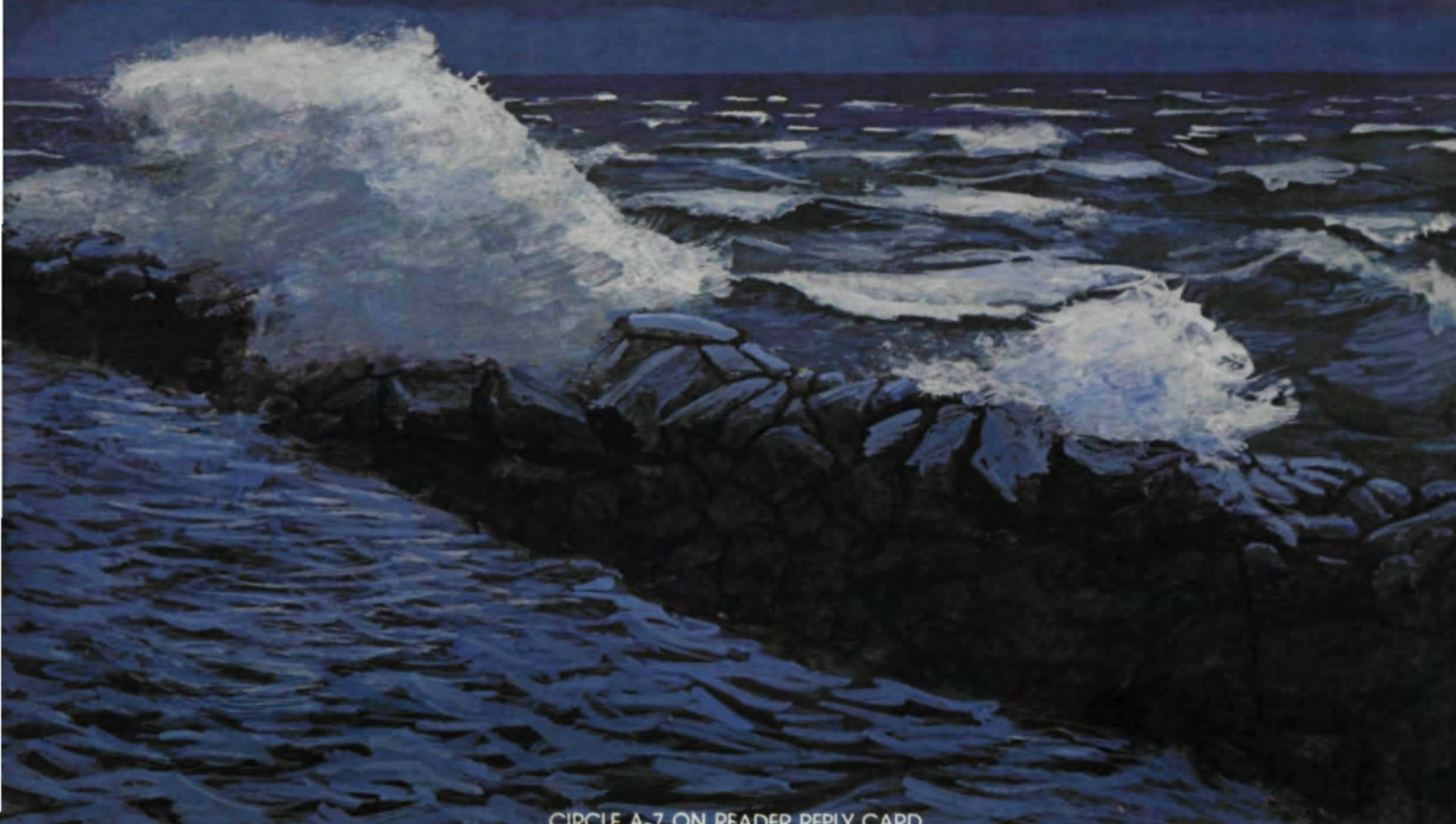

Improved Gear Life Through Controlled Shot Peening

by
N.K. Burrell
Metal Improvement Co.
Paramus, New Jersey

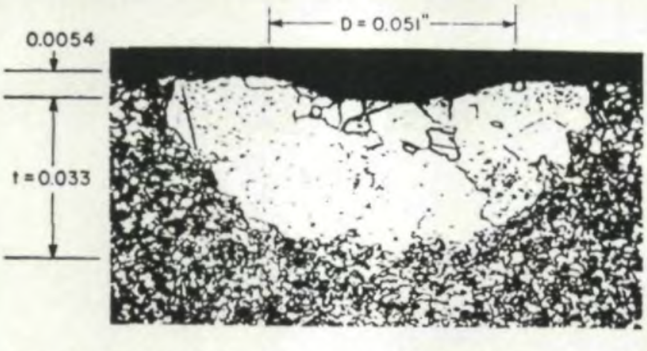

Fig. 1 – Effect of shot impacting a part at 90° impingement angle.(1)

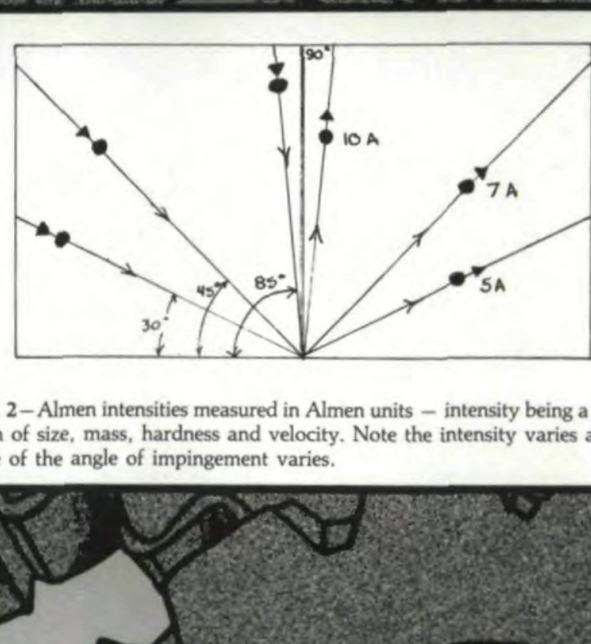

Fig. 2 – Almen intensities measured in Almen units – intensity being a function of size, mass, hardness and velocity. Note the intensity varies as the size of the angle of impingement varies.

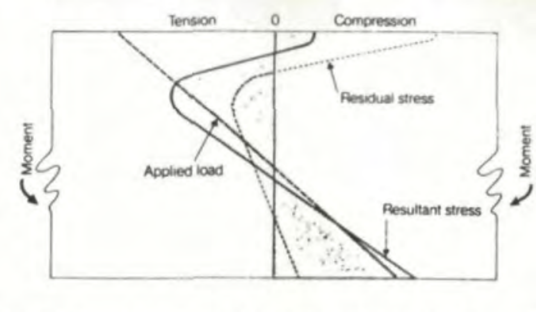

Fig. 3 – Qualitative illustration of distribution of stress in a beam which has been shot peened on upper surface.(4)

Abstract

Evaluating dynamic loads in gear design has always been a major design consideration. In addition to stresses due to applied loads, however, the impact of residual stresses must also be considered. Shot peening as described in this paper produces beneficial residual compressive stresses under strictly controlled conditions. Compressive stress prevents or limits failure in gearing due to fatigue failures at the fillet and pitting failure at the pitch line, as well as providing other benefits for gear designers and users.

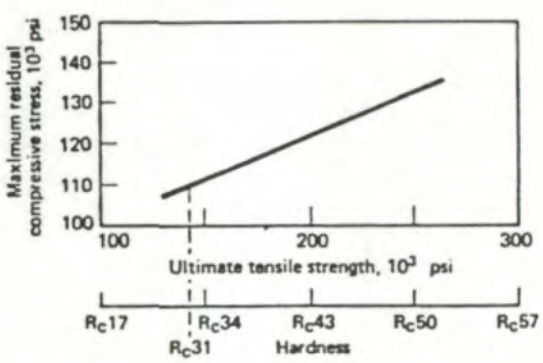

Fig. 4 – Ultimate tensile strength and surface hardness determine the residual stresses after peening.

AUTHOR:

MR. N. K. BURRELL *is the Midwest Director of Marketing for the Metal Improvement Company of Paramus, New Jersey. He has twenty years' experience in shot peening technology, and has served as a consultant specializing in problems of metal fatigue on gears and other mechanical components. He is the author of numerous papers for ASM, SAE, AGMA, SME, as well as other technical articles for trade journals. Mr. Burrell holds a BSME from the University of Illinois.*

The search for greater gear life involves improvement in cost, weight and increased power output. There are many events that affect gear life, and this paper addresses those relating to fatigue, gear tooth pitting, fatigue strength losses due to the heat treating processes and shot peening technique. The capability of shot peening to increase fatigue strength and surface fatigue life, eliminate machine marks which cause stress risers, and to aid in lubrication when properly *controlled*, suggests increased use and acceptance of the process.

Fatigue failures usually occur as follows: the first phase is the initiation of a crack at the surface that contains either residual tensile stresses (caused by manufacturing procedures) or applied tensile stresses (external stresses caused by gear tooth loading). This phase is followed by crack propagation through the part, as at the root of a gear tooth where tensile loads are greatest. In time, catastrophic failure occurs when the cross section of the part is no longer capable of carrying the applied load.

Shot peening benefits derive basically from the fact that a crack will not initiate in, or propagate through, a compressively stressed layer.

When spherical media of controlled size and shape strike the surface at an angle of impingement approaching normal, they induce a compressive layer in the material. The depth of the area affected is about equal to the diameter of the dimple, and the total affected surface area is about twice the size of the dimple.

In Fig. 1 we see the effect of shot which impacts the part at an impingement angle of 90°. As angles of impingement vary from 90° to 45° and smaller, the depth of compressive stress induced in the same material by shot of equal size, mass and hardness impelled at the same velocity will induce stresses of increasingly shallower depth, as shown in Fig. 2. Angle of impingement is but one of the variables that deserve the closest possible control and is covered in more detail later in this article.

If the part is peened by a great number of shot under controlled conditions, so that the edges of the dimples caused by these shots all touch or overlap, a consistent uniform layer of compressive stress is formed.

Fig. 3 shows qualitatively the distribution of stress in a beam which has been shot peened on the upper surface. The broken residual stress line shows the beam in equilibrium with no external forces. The area under the stress distribution curve in the regions of compressive stress must be equal to the corresponding area under the curve in the region of tensile stress. The sum of the moments of these areas must be equal to zero.

The solid line shows the resultant stress after a bending moment is applied. This resultant stress will be equal to the algebraic sum of the residual stress after shot peening and the stress due to the applied load at that depth.

Note especially that after loading, shown by the intermittant broken line, the peened surface still retains a compressive stress. This stress will inhibit formation of surface cracks and takes advantage of the fact that a crack will not propagate in a compressively stressed layer. The magnitude of the residual compressive stress shown at or just slightly below the surface of the peened member will be approximately 50% to 60% of the ultimate tensile strength of the base material. (See Fig. 4).

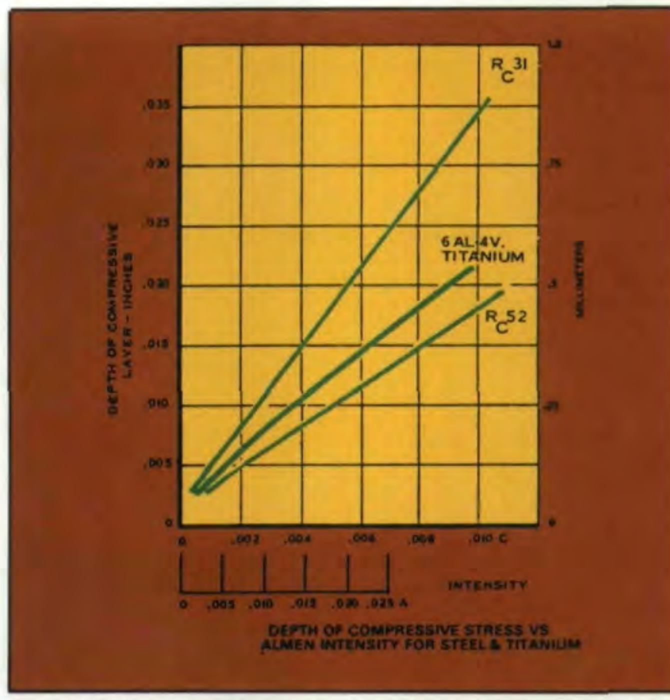

Fig. 5 – Depth of compressive stress vs Almen intensity for steel and titanium.[4]

Since the amount of energy imparted to the shot peened surface is a function of the mass, velocity and hardness of the shot, the hardness of the material being peened will also determine the depth of compressive stress. The variables are in addition to the aforementioned angle of impingement.

The standard for measuring energy applied to the work piece is the *Almen* strip. A good description of the detail of this method of specifying intensity can be found in Mil Spec 13165B Amendment II.[3] Note in Fig. 5 that as the hardness of the work piece increases, the depth of the compressive layer decreases – presuming the factors of shot size, mass, velocity, hardness and angle of impingement remain constant. Control of the depth of compressive stress is very important because the designer or user of shot peening must take other factors into consideration when selecting the intensity. These factors are wear, general erosion, if any, possibility of foreign object damage, surface finish requirements, an acceptable level of compensating tensile stress, etc. On very thin parts, depth of compressive stress can be a very important matter since, as a general rule, the depth of compression should not exceed 10% of the thickness of material per side in order to keep tensile core stresses to an acceptable maximum.

Finally, as we see in Fig. 4, it is extremely important to be sure that the design load is such that tensile stresses resulting from that load are kept below the level of the residual compressive stresses. These are a function of the ultimate tensile strength of the material being peened and generally are in the range of 50% to 60% of the ultimate tensile strength (UTS) cuts of the base material. A tensile load level maximum is generally accepted to be 40% to 50% of the UTS of the material being peened.

The main effects of controlled shot peening on gears are as follows:

1. Improved fatigue strength of the gear tooth in the root fillet.

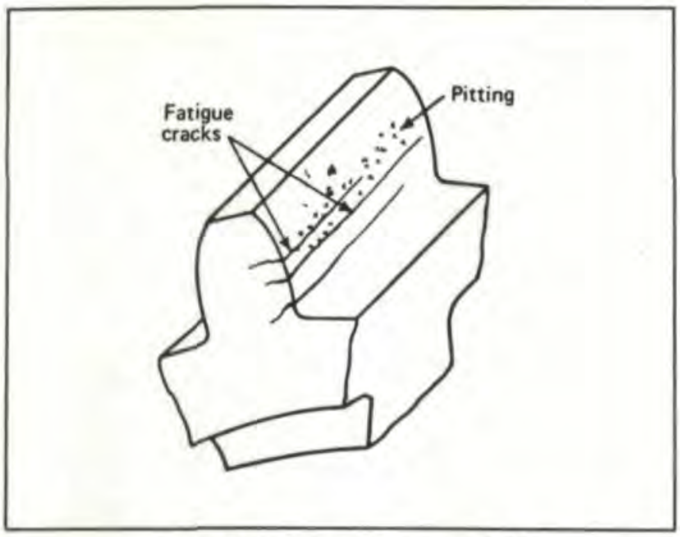

Fig. 6 – Typical pits and fatigue cracks[7]

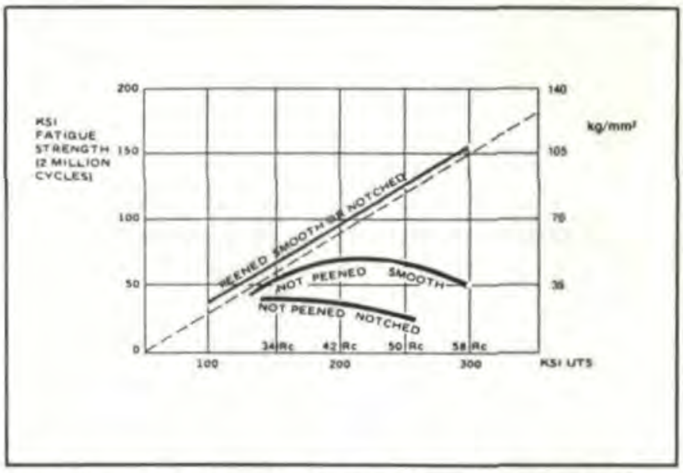

Fig. 7 – Comparison of peened and unpeened fatigue limits for smooth and notched specimens as a function of ultimate tensile strength of steel.

2. Increased surface fatigue life to reduce pitting and increase durability (See Fig. 6).

Another benefit accruing from shot peening gears is improved lubrication of the gear by virtue of the many small reservoirs (dimples) that can store lubricant at the point where it is most needed; thus, negating the squeegee effect of the rolling/sliding contact of two very smooth surfaces. Of course, other considerations must be met to determine the amount of dimpling that can be tolerated or obtained. Another benefit is the elimination of continuous machine lines on the gear tooth flank by peening in the "green" state.

Typically, a gear's surface hardness is increased to allow it to carry higher loads by heat treating. Hardening by carburizing, nitriding or other hardening processes can cause dimensional changes which may require remachining. Note, too, that on through hardened gears, as tooth hardness increases above 43 RC (about 200,000 psi), fatigue strength actually decreases (See Fig. 7).

As hardness increases, the reduction in fatigue strength in both notched and unnotched unpeened steel specimens occurs at about 45 RC. This drop in fatigue life is believed to be due to increased notch sensitivity and brittleness. With peening the strength level can be raised by using higher hardness, a practice regularly used by the aircraft industry. It must be remembered that when peening hardened gears or any other hardened material, it is extremely important that the peening media be at least as hard as the part being peened. This is necessary to generate maximum compressive stress in the gear. A significant decrease in fatigue strength will be noted if the hardness of the peening media does not at least equal the hardness of the part or specimen being peened.

In addition, it is important to recognize and to take into account the residual tensile stresses induced on the gear tooth profile and root during grinding. These tensile stresses can be overcome by shot peening to induce beneficial compressive stresses.

If the roughness of the tooth flanks produced by the shot peening is objectionable, the flanks may be shaved rather than masked before peening; however, control of surface temperatures during lapping and honing operations is important.

The greatest increases in gear life, when comparing peened versus non-peened, are found in through hardened gearing. Shot peening of through hardened pinions can yield as much as 30% improvement in fatigue limit. A 33% increase on induction hardened 4140 material is reported. The same authors also stated that nitrided steel surface tests showed moderate results[8].

Today, gears are frequently shot peened after carburizing. Fig. 8 shows how shot peening can stretch fatigue life of carburized gears or make it possible to use smaller transmissions for larger loads. Increases of 15-40% are commonly found.

Of course, proper selection of shot size and hardness is an important consideration. Special hardness (55-65 RC) shot is recommended for case-hardened carburized gears in order to give a higher magnitude of compressive stress. (See Figs. 9, 10, 11).

Townsend and Zaretsky stated that shot peening produces residual subsurface stresses in steel in addition to the residual stresses produced by case carburizing, hardening and grinding. They theorized that the additional residual stresses induced by shot peening should account for the increased life of carburized and hardened A151 spur gears. Subsequent tests showed an increase of 40% for the shot peened gears over the standard gears at a depth of maximum shear stress in addition to a 350% increase at a depth of 0.5 mil. Further, there was an increase in surface pitting fatigue of 1.6 times that of non-shot peened gears[9].

As a result of the growth in confidence in the shot peening process, Lloyd's Register of Shipping[10] allows an increase of tooth loading for both wear and strength of up to 20% for controlled shot peened gears.

The term "controlled" is extremely important and leads us to a discussion of shot peening controls and the changes that are now taking place that allow the peener to accurately meet the requirements set forth by the design engineers. With controlled conditions of shot peening, the designers can establish specifications that they have confidence will be met by their

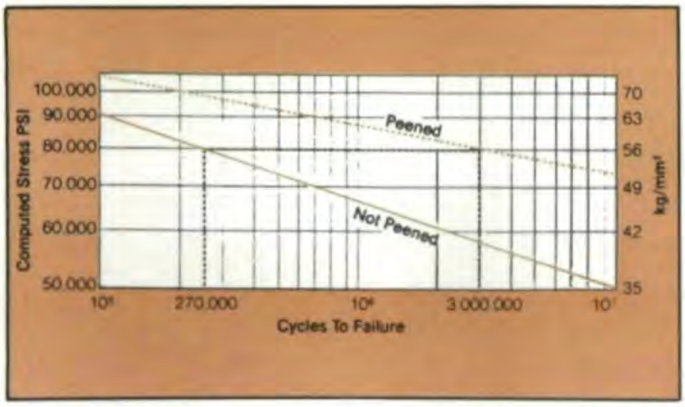

Fig. 8 – Effect of shot peening on carburized gears.[4]

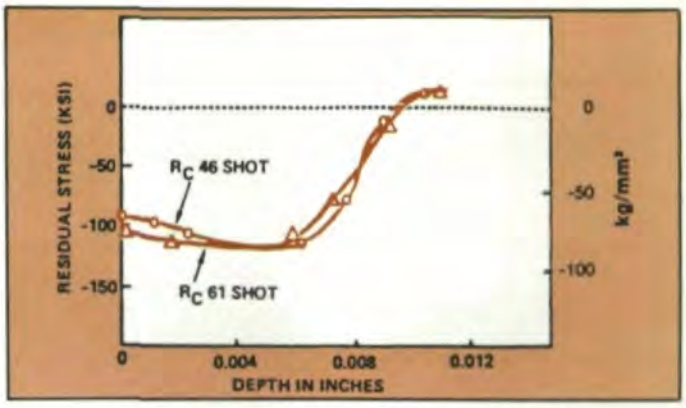

Fig. 9 – Peening 1045 steel at RC 48 with 330 shot.

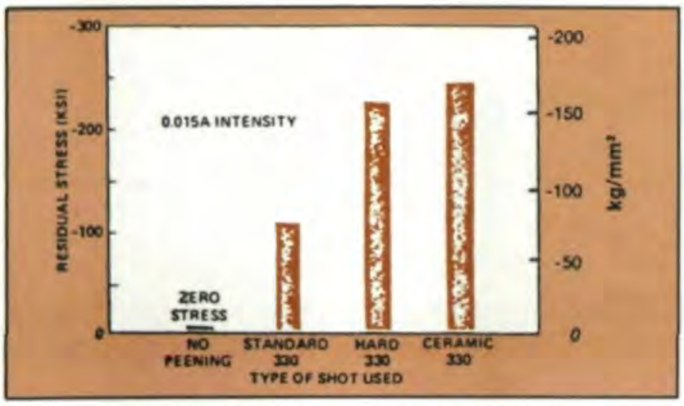

Fig. 10 – Peening 1045 steel at RC 62 with 330 shot.

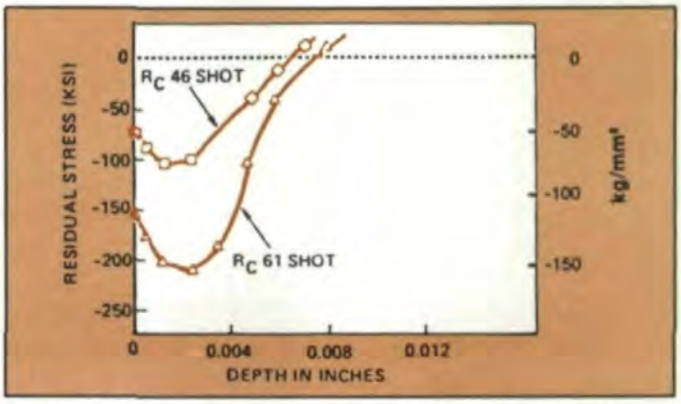

Fig. 11 – Residual stresses induced on 300M using various shot.

shot peening service. There is still no non-destructive method of inspection, other than for coverage (Peenscan). This problem has been largely alleviated through the use of microprocessor controlled shot peening equipment.

As covered previously, the Almen strip measures intensity for a given set of conditions of shot size, shot velocity, shot hardness and angle of impingement.[3] MIL-S-13165B also gives specifications for both steel and glass shot, which cover screening tolerances of new shot by size, set limits on hardness where applicable, specify uniformity of shot in the machine and set standards for shape with allowable deviations.

Shot quality *is important* to successful peening and must be continuously monitored. Vigilance is especially necessary on those machine installations where a single size shot is run continuously. The temptation to add make up shot whenever reduced flow is noted without checking, screening and sizing the old shot seems to be irresistable to production people. Inevitably, quality of peening becomes degraded as the shot breaks down into odd sizes and increasing numbers of broken particles. Concurrently, those expected improvements in fatigue will slowly and quietly degrade as well.

The third item to consider is coverage. Since the discovery of shot peening in the late 20's, the 10X magnifying glass has been the recommended tool for checking coverage. Specifications generally require full or complete (100%) coverage (See Fig. 12). Others call for 125%, feeling that the additional insurance of 25% will guarantee the 100% coverage actually required for good peening. The uncertainties of measuring or checking coverage have become so great that one of the largest aircraft manufacturers in the United States has specified 200% coverage on certain critical parts in the hope of getting at least 100% coverage on all of the part during manufacture, a sad commentary on the 10X glass as an inspection tool. The borescope (See Fig. 12A) while allowing examination of cavities and holes, suffers from the same limitations of limited field and mobility in contoured areas.

The obvious limitations of the 10X glass are its small field, making total inspection of large parts a physical impossibility along the short focal length, and not permitting inspection for coverage of critical clevises, roots, radii and holes, where there is not sufficient room to get the glass close enough to focus on the peened surface. On very hard parts, RC 55 and above, it is often difficult to determine whether the part has been covered, and many times shot peeners have been required by customers' inspectors to peen very hard parts from 500-600% coverage simply to assure these inspectors that the coverage is complete.

Now there is a process for measuring coverage that does away with the problems of the glass. This process, Peenscan, uses a non-elastic ultra violet (UV) sensitive compound that is painted or sprayed on the part prior to peening and dur-

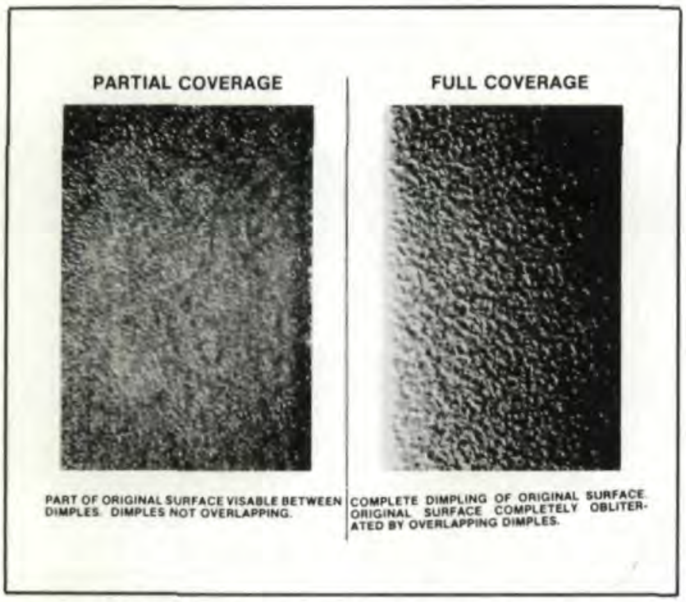

Fig. 12—Partial and complete shot peening coverage.

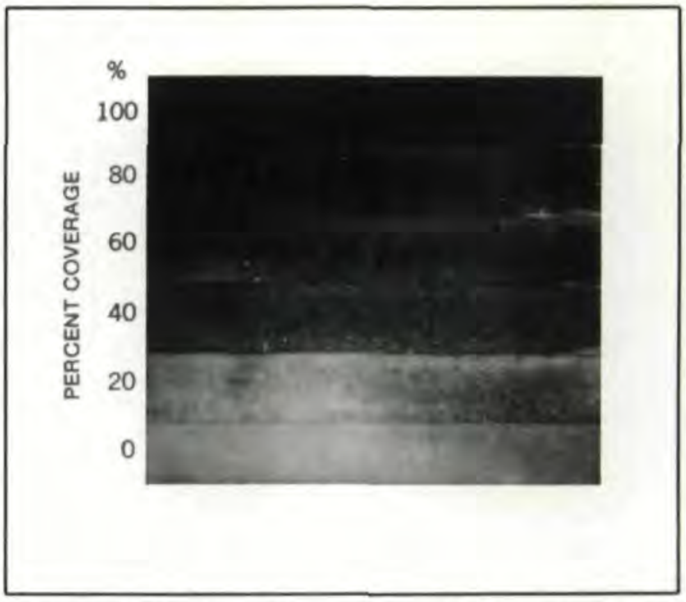

Fig. 13—Varying degrees of coverage shown by Peenscan process.[4]

ing the set up operation. When the coated part is peened, this material, Dyescan, comes under direct impingement and will be removed only in those areas which have been struck at reasonable angles. Removal of the UV material is gradual and is completed when the part is totally covered by shot peening. When inspected with a UV light, areas improperly peened will show evidence of some material remaining as a white shadow of varying intensity, depending upon the degree of coverage actually obtained. See Fig. 13. Note variation of color under UV light from full fluorescence at 0% coverage to complete black, which denotes full coverage.

This process is outlined in the MIL-S13165B[3] and has been accepted by the entire defense agency.

The Peenscan process is used to set up automatic equipment and as a control in production on a statistical sampling basis.

Having assured ourselves of the questions of intensity and coverage, we now come to the most recent developments in controlling the shot peening process. Though the industry has had automatic equipment for a number of years, the shot peening operators have never satisfied most gear manufacturers on the inability to control the process completely and accurately. Therefore, the improvements in fatigue life produced by peening have never been assigned values for the gear designer to use in designing gears. Thus, the benefits of shot peening have largely been used as "insurance policies" or as "band-aids" to cover mistakes made in manufacture and design or to allow increased loads to be put on gearing already designed and in production.

The advent of microprocessor controlled shot peening machinery is causing a change in this philosophy. The concept of total control of the shot peening process has been successfully developed, and many of these machines are in service today. Once a successful shot peening process has been developed and the process variables determined, this process can be precisely duplicated time after time. This requires that all of the process variables be constantly monitored with high and low limits set on each. The variables normally monitored are shot flow, air pressure or wheel speed, turntable or roller speed, and nozzle oscillation. If desirable, the nozzles can be programmed to vary their rate of travel across the part or turn on or off at prescribed intervals during the cycle. If any of the variables wander outside of the preset limits, the peening cycle is aborted at that point with a print-out made of the malfunction. At the end of each peening cycle, a printout is made of each of the process variables. This information can also be stored on floppy discs for ease of physical storage.

With the advent of this latest state-of-the-art equipment, it is now time for the gear and transmission industry to establish values for controlled shot peening. This step would put shot peening in a new perspective as a tool for designers to be used in manufacturing quality gearing.

(continued on page 64)

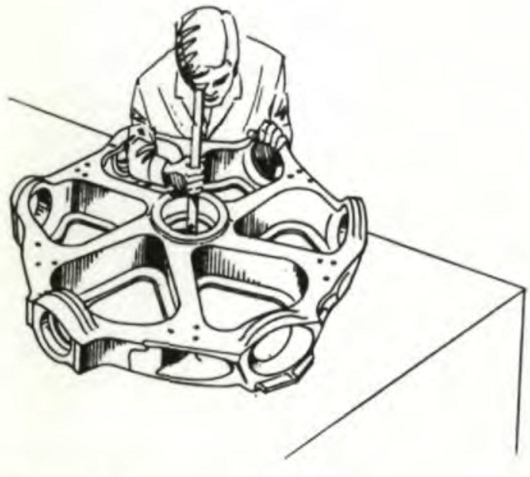

Fig. 12a (Left)—Examination of helicopter hub assembly with a boroscope.

Practical Analysis of Highly-Loaded Gears by Using the Modified-Scoring Index Calculation Method

by
M. Hirt and T. Weiss and J. Stockmaier
Zahnraderfabrik Renk

Introduction

The power of high speed gears for use in the petrochemical industry and power stations is always increasing. Today gears with ratings of up to 70,000 kW are already in service. For such gears, the failure mode of scoring can become the limiting constraint. The validity of an analytical method to predict scoring resistance is, therefore, becoming increasingly important.

A simplified calculation procedure suitable for high power, high speed gearing and based on the Winter and Michaelis integral temperature method is presented.

Scoring itself can be described as a momentary flashing of the oil film because of high loads and high speeds. Flashing of the oil film results in metal-to-metal contact and instantaneous welding in small local spots. These small welds are torn apart as fast as they are formed. The sliding action of the teeth causes the torn-out weld to be dragged across the mating surface, creating a gouge or score mark; hence, the name failure mode scoring. The typical appearance of a scored test gear is shown in Fig. 1.

The pitting resistance of gear teeth increases by the square of the hardness. In a given gear set, a change in hardness from 300 Brinell Hardness Number to Rockwell C 57 increases the pitting resistance by over 200%. Pitting failures, therefore, are unlikely in RC 57 gearing.

In contrast to this, the resistance to breakage of a gear tooth increases with the first power of the hardness. Therefore, a gear set of 300 BHN that has balanced pitting characteristics and bending strength becomes unbalanced at RC 57.

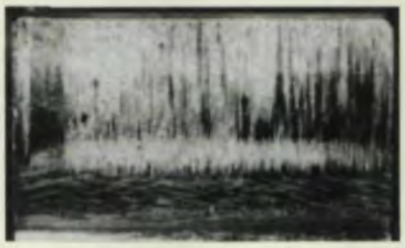

Fig. 1 – Carburized test gear with scoring failure.

The size of the teeth must be increased to gain the additional strength required in bending. For this reason, hardened and ground gears characteristically have larger teeth (lower tooth numbers) than their through-hardened predecessors.

The scoring resistance of the gear teeth is not significantly affected by hardness. Sliding velocity, surface finish, oil film anti-weld agents (copper and silver plating, or extreme pressure (EP) additives in the oil) have a much greater influence on this mode of failure.

Gear diameter and tooth size affect the tangential and sliding velocities during the tooth engagement cycle. Tangential velocity, in turn, affects the thickness of the elastohydrodynamic oil film, while sliding velocity affects the heat generated therein. Good gear tooth action results when the peripheral velocity is high enough to produce an oil film thick enough to keep the asperities of the tooth surfaces from touching, and when, at the same time, the sliding velocities are low enough to avoid the generation of excessive heat and flashing of the oil. Therefore, the rise with regard to scoring is of greater importance in using case carburized gears than in using through-hardened gears.

Scoring Calculation Methods

Two early calculation methods were established by J.O. Almen and J.C. Straub in the mid 1930's. They used the PV and PVT factors. P, V and T represent contact stress, sliding

AUTHORS:

DR. MANFRED HIRT *studied mechanical engineering at the Technical University of Munich and received his doctorate in 1974. Dr. Hirt is presently manager of the Design Department at RENK, the gear manufacturer in Augsburg, Germany. He is the author of several publications on gear calculations, stress measurements, high speed gearing ISO-calculation, quality of gears and case carburizing.*

DR. TONI WEISS *studied general mechanical engineering at the Technical University of Munich. He earned his PhD in 1983 and has worked as a research assistant at the Institute for Machine Elements. He has done work in the areas of heat treatment, strength and durability of gears and gear calculation. Presently he is product manager for Industrial Gears at RENK, Augsburg, W. Germany.*

MR. HANS STOCKMAIER *received his degree in mechanical engineering from Oskar-von-Miller Polytechnikum, Akademie für Angewandte Technik, Munich. He is manager of the Calculation Department for Gear Systems, Zahnraderfabric RENK, Augsburg, W. Germany.*

velocity and distance.

During the late 1930's, H. Blok of Delft Technical Institute developed a flash temperature theory which was based on the conversion of friction energy to heat and, in turn, to a local peak temperature.

Later, Bruce W. Kelley, Caterpillar Tractor Company, described certain modifications to the Blok approach required to correlate test and field experience, notably the surface roughness. This information was presented in AGMA 219.04, 1953.

An allowable specific load intensity expressed in terms of the tangential load per unit of face per unit of diameter was developed by G. Niemann, Technical University, Munich, in 1960. While this criterion had certain usefulness in low speed gears, it was too pessimistic for gears with pitch line velocities over 20 meters per second (m/s).

In 1962, Darle W. Dudley[5] presented an equation for a scoring criterion number above which scoring might be encountered and suggested more elaborate analyses be made. AGMA Standard 217.01,[2] 1965, contains an adaptation of the Kelley/Blok work, especially tailored to aerospace spur and helical gears, and also contains the Dudley scoring index as a simplified quick check for aerospace type gears.

EHD film thickness criteria were used for several years, but because they were designed mainly for mineral oils with a high portion of additives, they do not work correctly. Also, the real oil-pressure, temperature and roughness in the oil film is not known.

More recently, at the Technical University of Munich, analytical and experimental work under the direction of H. Winter has resulted in further refinements of the Kelley/Blok work. This information was presented in AGMA Technical Paper P 219.17,[8] 1983, and is called the integral temperature method. This method is based on a mean integrated tooth flank temperature in contrast to a local peak temperature as used by Blok. Additional refinements include consideration of tooth geometry effects (profile and addendum modification, gear ratio, length of the line of action and tooth size), surface coatings, EP additives, material effect, surface roughness, etc. Since the integral temperature method is generalized approach applicable to many types of gears (spur, bevel, single and double helical) and to a broad range of sizes and speeds, a large number of influencing factors have been included in the calculations. This improves the accuracy of the method, but also makes it relatively complicated to work with.

Integral Temperature Method

The integral temperature method developed by Winter and Michaelis has been adopted as DIN/ISO 3990, Part 4.[4] With this method, a mean integrated tooth flank temperature is determined and compared to an allowable value established from gear tests using the specific lubricant involved. Mean values are used for the coefficient of friction and for the load distribution.

The mean flash temperature calculated is multiplied by empirical factors and added to the bulk temperature, T_M.

$$T_I = T_M + 1.5\ T_{Flm} \qquad (1)$$

This mean tooth flank temperature, T_I (also called the integral temperature), corresponds to a measurable tooth flank temperature which could be verified by thermocouples.

The bulk temperature, T_M, can, in turn, be determined from the oil inlet temperature and is added to a percentage of the mean flash temperature.

$$T_M = 1.2\ T_{oil} + 0.\ 84\ T_{Flm} \qquad (2)$$

The factors 1,5, 1,2, and/or 0, 84 result from the adaptation of the measured flank and/or bulk temperature to the calculation method and are to be considered constant parameters. Thus, the mean tooth flank temperature becomes:

$$T_I = 1.2\ T_{oil} + 2.34\ T_{Flm} \qquad (3)$$

The mean flash temperature, T_{Flm}, is dependent on the geometry, the material, the speed, and the load parameters.

$$\left[T_{Flm} + \mu_B\ \frac{X_M X_{BE}}{X_{Ca} X_Q} X_\epsilon \frac{W^{3/4}\ V^{1/2}}{a^{1/4}}\right] \qquad (4)$$

where

- μ_B = mean coefficient of friction
- X_M = material factor
- X_{BE} = factor for geometry, Hertzian pressure and sliding velocity at the pinion tip
- X_{Ca} = factor for tip relief
- X_ϵ = contact ratio factor
- X_Q = rotation factor.

Mean values for these influencing factors, diagrams, and/or calculation formulae are given in DIN/ISO 3990.

The factor of safety against scoring, S_{SI}, then results in

$$S_{SI} = \frac{T_{SI}}{T_I} \qquad (5)$$

These temperature calculations are based on the flash temperature T_{FL} according to Blok. The contact temperature then is determined by

$$T_C = T_M + T_{FL} \qquad (6)$$

and the flash temperature is given by

$$T_{Fl} = 2.52\ (\mu)\left[\frac{F_{bt}}{b}\right]^{3/4}\left[\frac{n}{60}\right]^{1/2}\left[(R_{(1)})^{1/2} - (\frac{R_2}{u})^{1/2}\right]/R^{1/4} \qquad (7)$$

- μ = gear ratio
- n = pinion speed, rpm
- F_{bt} = tangential tooth load, N
- b = face width, mm
- μ = local friction coefficient
- R_1, R_2 = radii of curvature, mm
- R = $\frac{R_1\ R_2}{R_1 + R_2}$ relative radius of curvature, mm.

Utilizing this equation, contact temperature curves, T_C, can be plotted as a function of the line of contact (Fig. 2). For the integral temperature calculation method, a large

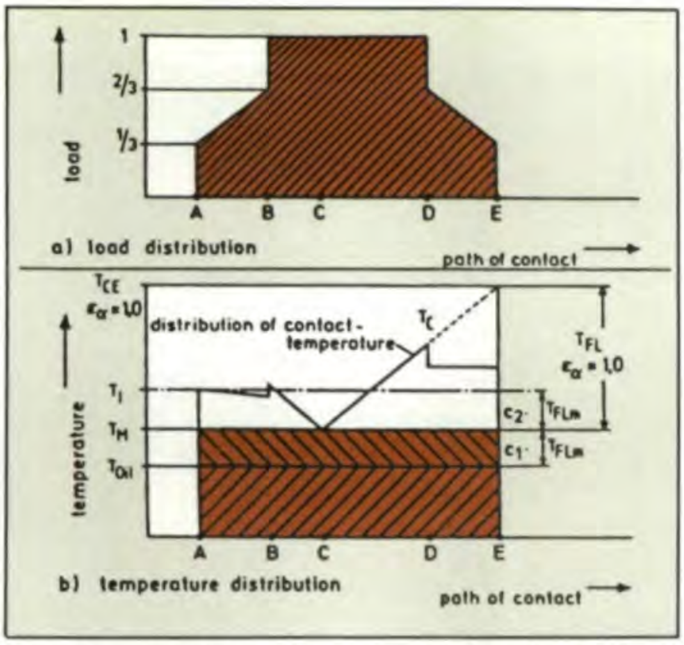

Fig. 2 – Assumptions for integral temperature calculation: load distribution and temperature distribution at contact line.

number of gear tests were used to determine the allowable temperature T_{SI} according to formula 5.

Modified-Scoring-Index Calculation

Based on the integral temperature calculation, a method was developed which can be used for typical applications such as high-speed units in turbomachinery[1] or as shown below for turbine-marine gearing. For the range of applications certain constants were introduced.

Equation 4, as developed by Winter and Michaelis and as adopted by DIN/ISO, is relatively complex and is usually handled in a computer program. One of the attractive aspect of the well-known Dudley scoring index, or AGMA 217.01, is its simplicity and the ease with which it can be determined with a hand-held calculator.

The range of the variables in Equation 4 when applied to high speed turbogearing, is shown first. The more or less standard practices followed in the design, manufacture and operation of high quality turbogearing with respect to tooth geometry, contact ratio, profile modifications, surface finish and lubricant permit assigning constant values to the following variables:

μ_B coefficient of friction	$\mu_B = 0.03$
X_M material factor	$X_M = 50$
X_{Ca} tip relief factor	$X_{Ca} = 1.15$
X_Q rotation factor	$X_Q = 1.00$

The resulting simplification to Equation 4 is an easy-to-use calculation procedure expressly applicable to high speed gearing. The product of the terms X_{BE} and X_ε and is equated to a geometry factor X_{GEO}, accounting for the number of teeth, contact ratio, radii of curvature, and ratio, and constant values for the terms μ_B, X_M, X_{Ca}, and X_Q are substituted in Equations 3 and 4. The result is:

$$T_{IM} = 1.2\ T_{oil} + X_{GEO}\ SI_M \qquad (8)$$

SI_M = Modified Scoring Index

$$SI_M = \frac{3\ w^{3/4}\ v^{1/2}}{a^{1/4}} \qquad (9)$$

The load, w, is the tangential force per unit face width.

$w = F_{bt}/b$, N/mm
v = circumferential speed, m/s
a = center distance, mm

For example, the load, w, should include all overload effects from non-uniform load distributions and/or from actual operating conditions.

As can be easily verified, the modified scoring index, SI_M, Equation 9, is similar in form to the AGMA 217 scoring index. For example:

$$\text{AGMA Scoring Index} = \frac{W^{3/4} n_p^{1/2}}{P_d^{1/4}} \qquad (10)$$

W = tangential force per unit face width
n_p = pinion speed, rpm
P_d = diametral pitch.

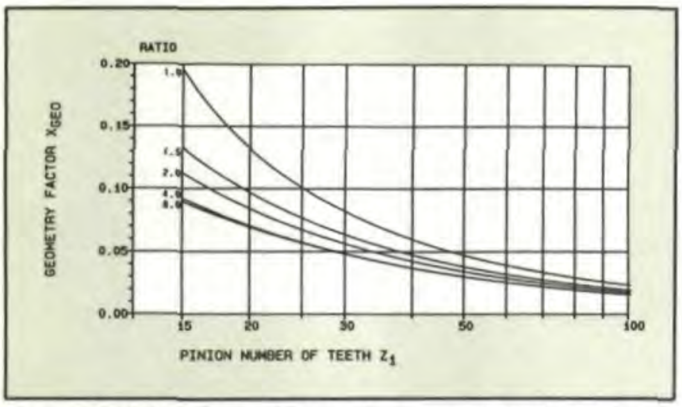

Fig. 3 – Modified Scoring Index Method: Geometry factor for helix angle of 27.5° and addendum and modification factor $X_1 = 0$.

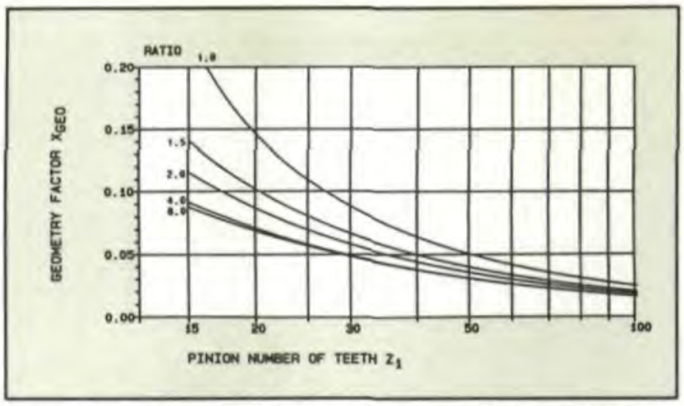

Fig. 4 – Modified Scoring Index Method: Geometry factor for helix angle of 27.5° and addendum modification factor $X_1 = 0.2$.

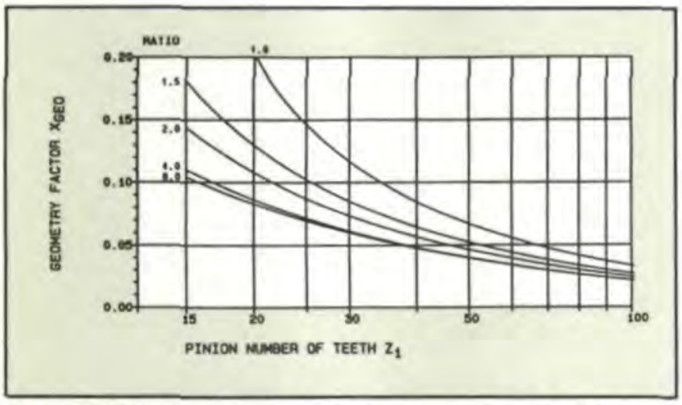

Fig. 5 – Modified Scoring Index Method: Geometry factor for helix angle of 27.5° and addendum modification factor $X_1 = 0.5$.

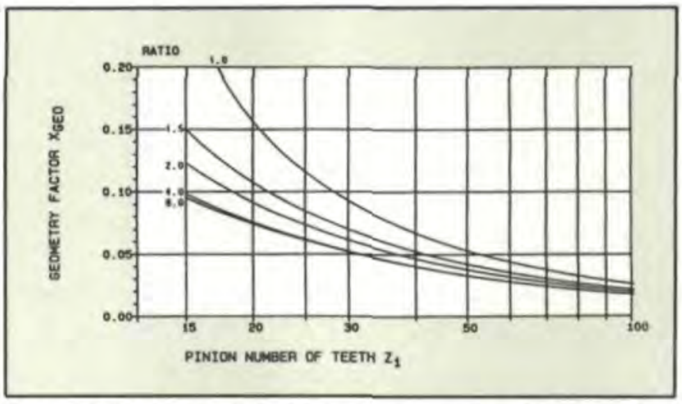

Fig. 6 – Modified Scoring Index Method: geometry factor for helix angle of 10° and addendum modification factor $X_1 = 0$.

The geometry factor, X_{GEO}, in Equation 8 considers the influence of tooth numbers, ratio, and addendum proportions in addition to tooth size. Geometry effects in Equation 10 are limited to tooth size only. Diagrams of X_{GEO} for teeth with zero-addendum modification or zero sum of addendum modification are shown in Figs. 3 through 8.

These diagrams are calculated for the typical high speed or marine turbine gearing:

a) single helical with helix angle of appr. 10°,
b) double helical with helix angle of appr. 27.5°,

and "normal" addendum modification factors 0, 0.2 and 0.5 at the pinion.

Furthermore, common European practice is to have the sum of modification factors of pinion and gear near zero. Similarly to the integral temperature calculation, the safety margin for the modified method can be found by:

$$S_{SIM} = \frac{T_{IS}}{T_{IM}} \tag{11}$$

Using Equation 8 and allowable values of T_{IS} from Equation 4, or Table 1, the safety margin for scoring resistance can be determined.

An adequate margin of safety exists when the S_{SIM} value of Eequation 11 is 1,6 or greater. As a quick design check, the permissible modified scoring index, SI_{MP}, can be used from Table 1. The values shown include normal safety factors and are based on average gear geometry.

Applications of Modified Scoring Index Method

The following will show how the different constant figures for this modified method were determined with regard to high speed and turbine marine gearing.

Coefficients of Friction

A curve of the coefficient of friction as a function of the pitch line velocity is shown in Fig. 9. Surface roughness, Ra, must be 0.5 μm or better (after running-in). The curves shown are believed to be flat beyond 70 m/s. A value of $\mu_B = 0.03$ has been taken for high speed gears. For pitch line velocities below 30 m/s, a slightly larger value should be used. The points in Fig. 9 are marking typical applications for high speed and marine gearing.

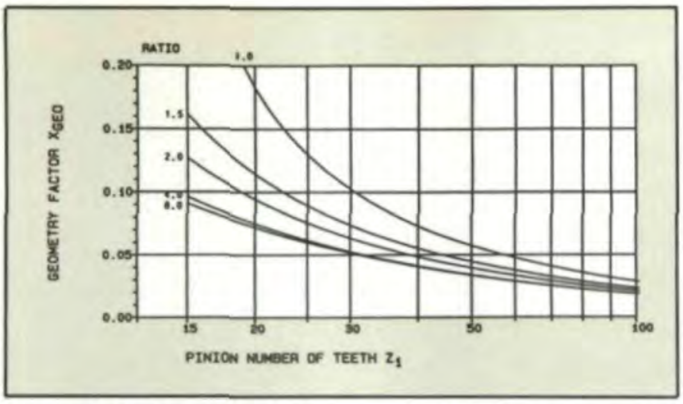

Fig. 7 – Modified Scoring Index Method: geometry factor for helix angle of 10° and addendum modification factor $X_1 = 0.2$.

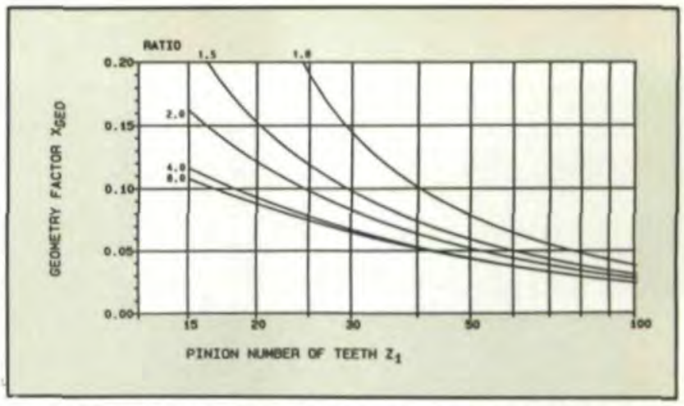

Fig. 8 – Modified Scoring Index Method: geometry factor for helix angle of 10° and addendum modification factor $X_1 = 0.5$.

Table 1 Allowable Temperature T_{IS}, Loads and Indices for Several Commonly Used Oils

Oil Type	ISO Viscosity grade SAE Viscosity grade	FZG-Test Load-stage	Ryder Gear Test, ppi app.	T_{IS}	Permissible Modified Scoring Index SI_{MP}
Turbine-Oil	ISO VG 46	6	1,500	160°C	900
Special Turbine Oil	ISO VG 46	7*	2,200	180°C	1,150
Turbine-Oil	ISO VG 100	7*	2,200	180°C	1,150
Motor-Oil	SAE 30	>8	>3,000	>200°C	>1,400
		9	4,000	235°C	1,850

*If pinion and/or wheel copper plated one to two load-stages higher

Tip relief factor.

With optimal profile modification and normal contact ratios, tip relief factor X_{Ca} can be assigned a value of 1.15.

Addendum Proportions.

When addendum proportions are kept within the range of standard to 50% long and short, the rotation factor, X_Q, can be taken as unity.

A standard addendum set is defined as having mating pinion and gear with addendums equal to 100% X Module, mm. The maximum departure from the standard addendum is 150% x Module (driver) mating with 50% x Module (driven). The summation addendum lengths shorter and longer than standard should equal 100%.

Material Factor, X_M, is considered a constant of 50 for normal steel gears.

Lubrication.

Pressure fed lubrication by spray jet is mandatory.

Typical Examples.

The following three groups of practical examples will be analysed by the exact Integral Temperature Method and the Modified Scoring Index Method. Tables 2 to 4 show the main technical data of these three gear groups, which are

a) High speed gears for powers of 7,300 kW to 70,000 kW, Table 2,

Table 2 Technical data, load and oil quality of typical examples of high speed gears

Gearing No.	Power P kW	Ratio i	Pitch line velocity v m/s	Unit load K ·(F_{bt}/b) N/mm	Oil type	ISO Viscosity grade (SAE)	FZG-Test DIN 51 354 Load stage	Plant
1	70,000	1.2	137	1,860	Special Turbine-Oil	ISO VG 46	(7) 9	Gas Turbine/Generator Pinion copper plated
2	19,500	5.8	116	800	Turbine-Oil	ISO VG 46	6	Motor/Compressor
3	7,300	1.9	139	435	Turbine-Oil	ISO VG 46	6	Motor/Compressor

Table 3 Technical data, load and oil quality of typical examples of marine turbine gears

Gearing No.	Power P kW	Ratio i	Pitch line velocity v m/s	Unit load K ·(F_{bt}/b) N/mm	Oil type	ISO Viscosity grade (SAE)	FZG-Test DIN 51 354 Load stage	Plant
4	3,500	2.6	71	630	Turbine-Oil	ISO VG 46	6	Steam Turbine/Propeller 1. Stage
5	3,500	5.1	44	640	Turbine-Oil	ISO VG 46	6	Steam Turbine/Propeller 2. Stage
6	19,000	4.6	30	2,770	Turbine-Oil	ISO VG 100	7	Gas Turbine/Propeller
7	3,800	1.1	56	740	Turbine-Oil	ISO VG 100	7	Gas Turbine/Propeller
8	10,250	8.2	35	1,720	Turbine-Oil	ISO VG 100	7	Gas Turbine/Propeller

Table 4 Technical data, load and oil quality of typical examples of marine diesel drives

Gearing No.	Power P kW	Ratio i	Pitch line velocity v m/s	Unit load K ·(F_{bt}/b) N/mm	Oil type	ISO Viscosity grade (SAE)	FZG-Test DIN 51 354 Load stage	Plant
9	3,750	1.0	24	1,300	Turbine-Oil	ISO VG 100	7	Diesel-Engine/Propeller
10	7,400	5.3	39	1,500	Motor-Oil	SAE 30	8	Diesel-Engine/Propeller

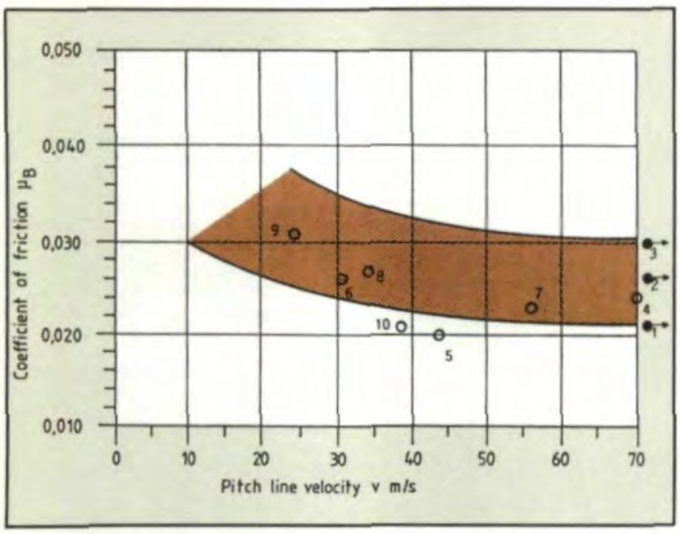

Fig. 9 – Typical calculated coefficients of friction and scattering field for marine and high speed applications.

b) Marine turbine gears for powers of 3,500 to 19,000 kW, Table 3,

c) Marine diesel gears for powers of 3,700 to 7,400 kW, Table 4.

Besides the main geometrical data, loading data such as unit load are also given. For these gears the factor of safety against scoring according to the modified scoring index method versus the safety factor according to integral temperature method is shown in Fig. 10. A good relation can be recognized which proves that the simplied method is working satisfactorily.

Additionally, Fig. 11 gives a relation between the scoring load stage (FZG) and the permissible modified scoring index together with the practical modified scoring index used in the gears. One can see that a certain safety margin exists between the data points and the limit line. All these gears have been

(continued on page 26)

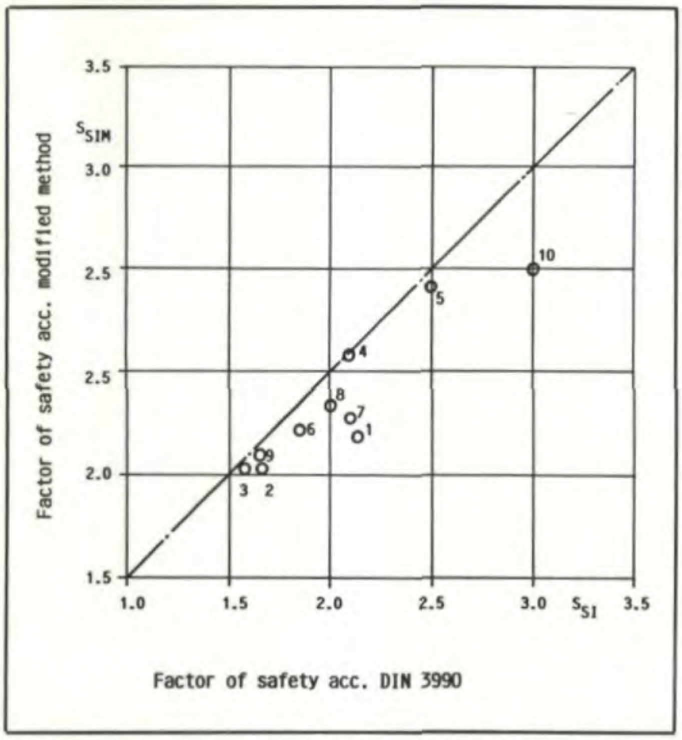

Fig. 10 – Calculated scoring safety factors according Integral Temperature Method versus scoring safety factors according Modified Scoring Index Method.

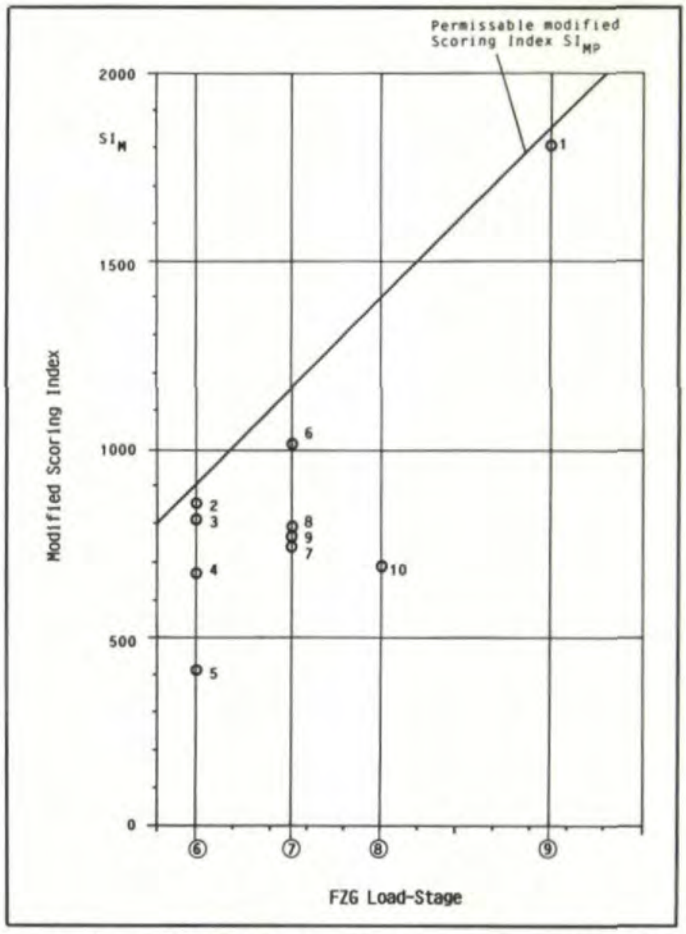

Fig. 11 – Practical Modified Scoring Index values SI_M for typical applications versus allowable SI_M values and FZG load stages.

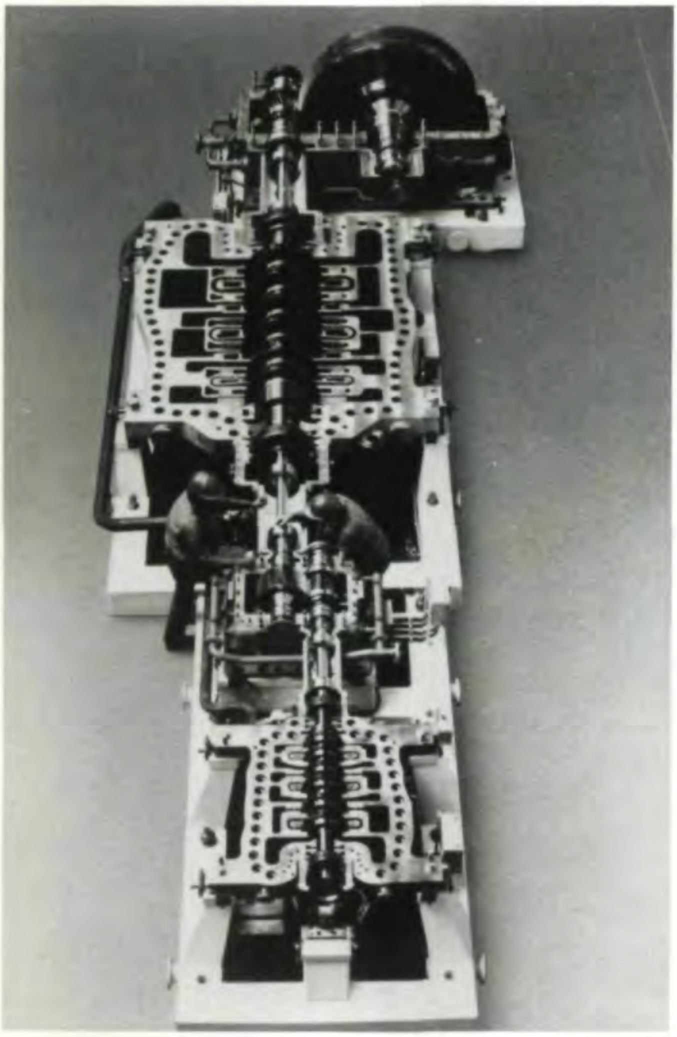

Fig. 12 – Total view of a high- and low-pressure gas compressor unit equipped with high speed gears, Ref. Nos. 2 and 3.

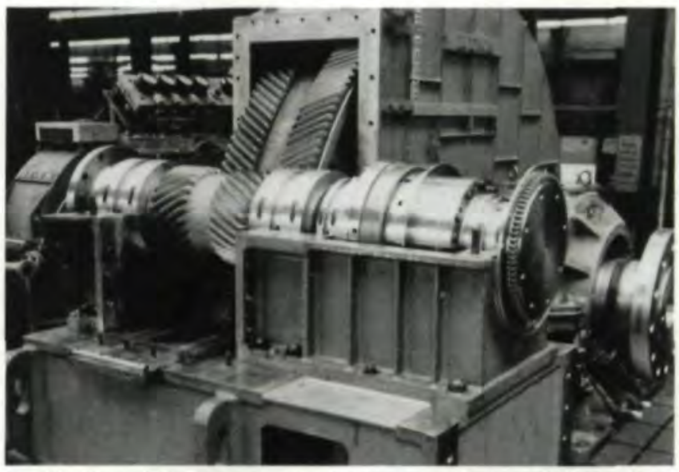

Fig. 13 – Typical Navy gear, main pinion at output stage, Ref. No. 8.

operating for years without scoring problems. Fig. 12 shows a photograph of the gears mentioned in Table 2, reference numbers 2 and 3. Fig. 13 provides an impression of a modern marine gear for a navy ship. As mentioned, these gears proved high scoring capacity under load. Therefore, the application of the modified scoring index seems to be acceptable to calculate the real scoring resistance of high speed and turbine marine gears.

(continued on page 64)

Tooth Strength Study of Spur Planet Gears

Raymond J. Drago
Bapa R. Uppaluri
Boeing Vertol Company
Philadelphia, PA

Abstract

The finite-element method (FEM) has been applied to three spur planet gears to determine the tooth strength. Models for each gear were created using different constraint conditions and model parameters. Comparison of the results of the models with experimental data reveals the need to integrate the effect of the individual roller loads on the model. The effect of roller-bearing support on the gear tooth root and fillet stresses has been demonstrated to be a significant factor in gear load capacity.

The use and application of a system of updated finite-element pre- and postprocessors used in the analysis are briefly explained. One planet gear's static strain survey test data are presented and compared with both the FEM analytical predictions and conventional AGMA results. The usefulness of the FEM preprocessor and postprocessor in minimizing the test effort is pointed out.

Introduction

In the design of any new gear drive, the performance of previous similar designs is very carefully considered. In the course of evaluating one such new design, the authors were faced with the task of comparing it with two similar existing systems, both of which were operating quite successfully. A problem arose; however, when it was realized that the bending stress levels of the two baselines differed substantially. In order to investigate these differences and realistically compare them to the proposed new design, a three-dimensional finite-element method (FEM) approach was applied to all three gears. The general FEM methodology was similar to that which the authors have applied extensively to spiral-bevel gears.[1-4] The basic accuracy of this system and its ability to accurately predict the stress levels of complex spiral-bevel gears has also been established.

Since all three systems are simple epicyclic drives, the planet gear of each was chosen for detailed evaluation. Although similar, as Fig. 1 shows, there are some substantial differences in the detailed construction and supporting structure for each.

Planet gears B and C are supported by double-row cylindrical roller bearings while planet gear A is supported by a double-row spherical bearing. The backup ratio (rim

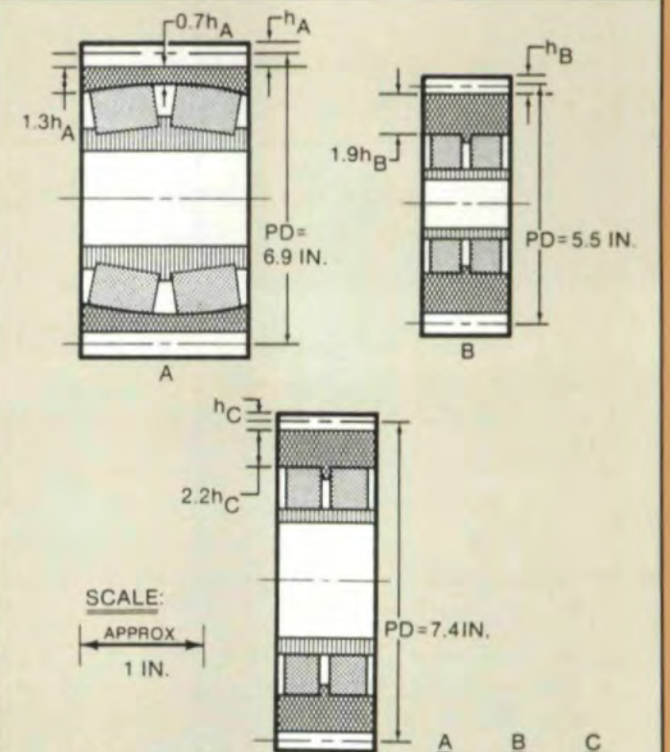

	A	B	C
DIAMETRAL PITCH (IN.)	4.8	7.8	5.8
AGMA BENDING STRESS (KSI)	37.0	66.2	41.4
HORSEPOWER/FACE WIDTH	187.5	206.0	353.3
TANGENTIAL LOAD/FACE WIDTH	3,418	3,712	3,544
MOMENT OF INERTIA OF RIM	0.06	0.04	0.12
HORSEPOWER/POUND (APPROX) (GEAR ONLY)	45	18	65

Fig. 1—Comparison of Three Planet Gears

AUTHORS:

MR. RAYMOND J. DRAGO *is a Senior Engineer with the Advanced Power Train Technology of Boeing's Vertol Company. Drago's current interests lie in the areas of applied mathematics, kinematics, analytical gear system design and synthesis, finite element analysis, and computer programming. He has also been pursuing ongoing studies in the analysis, design, manufacture, assembly, and testing of many gear systems. He holds a Bachelor of Mechanical Engineering Degree from the City University of New York and a Masters Degree in Structural Engineering from Pennsylvania State University.*

DR. BAPA UPPALURI *is a Senior Engineer in the Power Train Technology Department of Boeing Vertol Company. His areas of study focus on stress analysis, finite element methods using NASTRAN, ANSYS, WECAN, fatigue analysis, and computer programming. He earned a M.S.M.E. and a Ph.D. from Georgia Tech.*

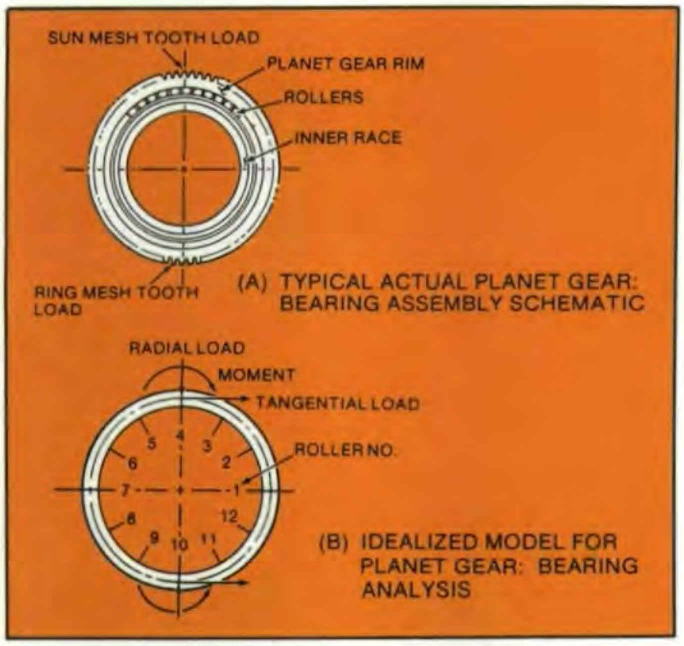

Fig. 2—Planet Ring Program Analysis Model

thickness/whole depth), while similar for B and C, is quite different for A. The pitch diameters of planet gears A and C are similar while that for B is somewhat smaller.

Experience with other thin-rimmed gears has indicated that such gears must be modeled very carefully, in three dimensions, with all individual roller loads applied as constraint conditions.[6,7]

Method of Analysis

The method used was simple in concept, though rather complex in execution. The general procedure used for each gear was as follows:

1. **Reference Baseline** — Run each gear through AGMA-type gear analysis computer program in order to produce a common reference point.
2. **Define Roller Reaction Loads** — Analyze each planet gear/bearing system with computer program RINGEAR to define individual roller reaction loads and obtain inner- and outer-rim stress approximations.
3. **Preprocessing** — Model each gear using the FEM preprocessor.[3]
4. **NASTRAN FEM Analysis** — Load each model with appropriate sun mesh, ring mesh, and individual roller loads and execute NASTRAN analysis.
5. **Postprocessing** — Evaluate NASTRAN results using Boeing Vertol postprocessor and plot results.[3]

Once all of the data are available, they must be evaluated so that specific conclusions may be drawn.

In order to establish confidence in the comparative accuracy of this approach, the results of the planet gear A analysis were compared to the experimental data which were obtained from a strain survey. As will be obvious when the basic FEM tooth stresses are presented later, the correlation between test and FEM results is quite good.

Reference Baseline

Using general methodology[8] (but with all modifying factors set equal to unity), the AGMA tooth fillet bending stresses were calculated in order to provide a common frame of reference. These stresses, shown in Fig. 1, indicate that planet gear B is, by far, more highly stressed than either A or C. As the FEM analysis will show; however, this is not actually the case.

Define Roller Reaction Loads

In order to obtain an accurate estimate of the actual tooth root and fillet stresses, the FEM model must realistically simulate the actual structure being analyzed. Perhaps the single most common (and most devastating) error made in applying FEM to gearing is the failure to properly model the gear and its constraint conditions. In the case of the planet gears, the temptation to use a simply supported two-dimensional model is great. To do so, however, will yield apparently reasonable, but actually very misleading results.

Because of the dual function of the blank (gear teeth on the OD and bearing journal on the ID), the gear must be modeled not only with both sun and ring loads applied but

TABLE I. INPUT DATA FOR RIM STRESS AND DEFLECTION PROGRAM

First Card	Integer equal to number of cases being run
Second Card	Title for case
Third Card	Number of planets, pressure angle, helix angle, sun gear torque
Fourth Card	Ring gear pitch diameter, sun gear pitch diameter, planet gear pitch diameter, planet gear centroid diameter
Fifth Card	Ring gear centroid diameter, backup I and backup area, C distance to ID, C distance to OD
Sixth Card	Same information as above but for sun gear
Seventh Card	Same information as Card 5 but for ring gear at bolt holes
Eighth Card	I/C to planet gear root diameter, I/C to planet gear inside diameter, number of rollers per row, planet backup cross section area, planet backup moment of inertia
Ninth Card	Planet bearing effective roller length, diametral clearance, roller ID (hollow roller), inner race out of round
Tenth Card	Planet bearing roller diameter, bearing pitch diameter, bearing contact angle, planet speed relative to post

TECHNICAL CALENDAR

September 17-19, 1986
Ohio State University Gear Noise Seminar
Columbus, OH

The three-day course will cover general noise measurements and analysis, causes of gear noise, gear noise reduction techniques, dynamic modeling, gear noise signal analysis, and modal analysis of gear boxes.

For further information contact:
Mr. Richard Frasher at (614) 422-8143.

September 22-24, 1986
ASME Professional Development
Short Course Program
McCormick Center Hotel
Chicago, Illinois

Fundamentals of Gear Design

Introductory course in gear design for designers, users and beginning gear technologists. Emphasis will be on proper design, selection and application.

For further information contact: Susan Chen at ASME (212) 581-5267.

October 5-8, 1986
AGMA Fall Technical Conference & Gearing Exhibit
Hyatt Regency Chicago in Chicago, IL

AGMA's Fall Technical Meeting will provide a forum for discussion of the design and manufacture of gears, flexible couplings and mechanical power transmission products. This year there will be an exhibit of gear generating machinery, gear design hardware and software, as well as other products of use to the industry.

For further information contact:
Rich Norment or Wendy Allen at
(703) 684-0211.

November 11-13, 1986
SME Gear Processing and Manufacturing Clinic
Chicago, IL

Call for Papers: The Society of Manufacturing Engineers has issued a call for papers for this meeting. Please submit all papers on or before July 15th. The clinic will also include vendor tabletop
exhibits.

For more information, contact Joseph A. Franchini at SME (313) 271-1500, ext. 394.

November 19-21, 1986
Seminar: Gear System Design for Minimum Noise
University of Wisconsin

This course provides an overview of noise control in gear sysem design and offers practical design information with a minimum of acoustical theory. The course is for engineers who design or specify gears or gear drives.

For additional information contact:
John Leaman at (414) 224-4189.

VIEWPOINT

"VIEWPOINT" provides an opportunity for readers to discuss problems and questions facing our industry.

Please address your questions and answers to: VIEWPOINT, GEAR TECHNOLOGY, P.O. Box 1426, Elk Grove Village, IL 60007.

I recently had the opportunity to read GEAR TECHNOLOGY, The Journal of Gear Manufacturing. I was impressed with the subject matter.

This journal would be extremely useful to me in my function as Sperry New Holland's gear design specialist. We design and manufacture spur and helical gears for our agricultural and construction equipment. We also specify straight, spiral, and hypoid bevel gears to be supplied by vendors.

T. L. Stiefvater
Sperry New Holland
New Holland, PA 17557

Gentlemen:

In the past several issues of Gear Technology I have been looking for a source to do some gear tooth inspection work on a contract basis. To date, I have not been able to locate a source from your magazine, which I consider a good source of information. My needs are in the bevel gear area to measure tooth profiles. Would you be able to give me several names of firms who do this type of work? I would prefer that these sources be in a 120 mile radius of St. Marys, PA.

Trusting you will be of some service to us, we remain

Thomas J. Engel
PROMETECH
Manager, Quality Assurance

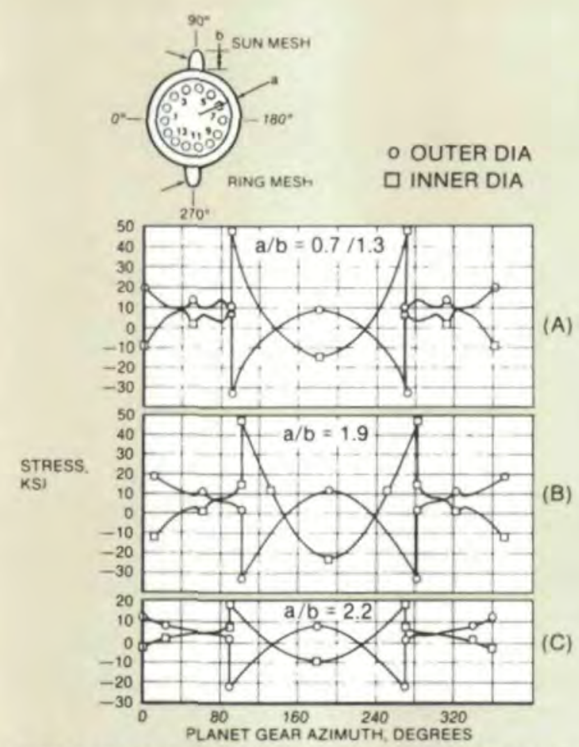

Fig. 3 – Planet Gear Rim Stress Approximation

also with the individual roller reaction loads applied. In order to define the individual roller loads, a separate analysis simulates (as shown in Fig. 2) the planet as a simple ring with the sun and ring as applied loads and each roller providing a reaction point.

The idealized loading is statically equivalent to the actual loading and comprises radial and tangential loads and a moment which act at the centroid of the cross section of the backup rim. Data input to the computer program, Table I, is simple and direct.

The computer program used in this analysis (which is based, in part, on the analysis presented) was originally developed to provide a ring bending analysis for planet gears.[9] Thus, in addition to calculating the roller reaction loads, an estimate of the ring stresses at the root centerline is provided. As the stress concentration effect of the fillet is not considered here, this estimate is unconservative.

While these stress calculations do not consider the stress concentration effects due to the tooth root, they do provide some insight into the relative response of the three gears. The results, plotted in Fig. 3 and summarized in Table II, clearly show that A and B are stressed to about the same level while C is substantilly lower.

If considering only the ring stresses, one would have to conclude that A and B would perform about the same while C is conservatively loaded, despite the disparity of their AGMA stresses. Such a conclusion is, however, in the overall sense, premature at this point; but it does point to the need for a much more detailed analysis of these seemingly simple gears.

TABLE II. SUMMARY OF PLANET RIM FATIGUE STRESSES FROM RING PROGRAM

Planet	At Outside Diameter[1]		At Inside Diameter	
	Steady (psi)	±Alternating (psi)	Steady (psi)	±Alternating (psi)
A	−6,611	26,480	16,503	31,439
B	−6,813	25,701	12,183	34,831
C	−4,845	17,414	4,335	14,119

1. Does not include stress concentration due to tooth root fillets

TABLE III. SPUR AND HELICAL GEAR TOOTH CONTACT LINE PROGRAM INPUT DATA

Card 1 INN (Alphanumeric title, 76 columns)
("INN" is control: 1 = read, 2 = stop)

Card 2	Symbol	Case Number 1	2	3	4
Number of teeth, pinion	XPN				
Number of teeth, gear	XNG				
Diametrical pitch (+trans, −norm)	PD				
Pressure angle (+trans, −norm)	Phi				
Tooth thickness, pinion	TTP				
gear	TTG				
Outside radius, pinion	ROP				
gear	ROG				
Card 3					
Helix angle (+R/H pinion, −L/H pinion)	PSI				
Center distance factor	CDO				
Top land edge break, pinion	EB				
gear	EB				
Face width, pinion	FP				
gear	FG				
Pinion or gear drive (1.2)	IDRIVE				
Pinion direction of rotation (CW=1, CCW=2	IROT				

Preprocessing

The preprocessing step comprises two parts: tooth contact line definition and actual grid-by-grid FEM model definition.

Contact Line Analysis

The accurate application of gear tooth loads in the finite-element method required the coordinates of the contact lines from the beginning of mesh to the end. Computer programs have been developed to generate the contact lines for spur, helical, and bevel gear meshes based on the theory of conjugate action. The program generates contact lines on three adjacent teeth at regular angular position intervals from start to end of mesh. It also generates the unit inward normal vectors at the contact coordinates, which are subsequently used as the load vectors in the NASTRAN analysis.[3]

Table III illustrates the very simple input data required by the spur gear tooth contact line program.[2, 3]

Model Geometry Definition

The gear preprocessor computer program, developed by the authors, was used to create all three models used in this analysis.[2, 3] It generates a gear finite-element model built of solid CIHEX1 elements. As many teeth as needed can be molded, together with or without integral front and/or back shafting. It can automatically generate the executive, case control, and bulk data decks (with force cards) for COSMIC-NASTRAN linear static analysis. With a little manual editing of the data deck, in order to add boundary conditions (SPC/MPC/SPC1) or to combine loads if necessary, a complete NASTRAN analysis can be performed. Table IV presents the input data required for this preprocessor.

NASTRAN FEM Analysis

The data deck generated by the preprocessor requires some manual editing before being submitted for a NASTRAN analysis. The preprocessor employs a unit load distribution along the tooth contact lines to generate the NASTRAN force cards. The torque applied to the gear tooth due to this unit loading is calculated and provided as output. This unit loading torque must be multiplied by a load factor to obtain the actual torque transmitted by the gear. This is accomplished by means of the load cards in the NASTRAN data deck where linear combinations of forces are created. In addition, proper boundary conditions must be imposed on the model for the static analysis. The restraints must reflect the manner in which the gear is supported by its bearings; this is done by means of SPC or SPC1 or MPC cards in the NASTRAN program. Finally, the number of load cases to be run, the output data required from each load case, the plot options, etc, must be edited before submitting the NASTRAN job.

Each NASTRAN load case consists of many tooth load cases, each of which simulates the instantaneous contact loads at the sun/planet and planet/ring gear meshes. This allows the FEM model to simulate the response of the planet gear during a strain survey so that the data from both can be easily compared.

Postprocessing

The postprocessor reads the voluminous NASTRAN stress output file and generates stress tables and plots at the tooth fillet or root for each load case. The postprocessor interpolates the stress at adjacent grids to yield fillet and root stress distributions for all load cases individually and as a composite for a full mesh cycle. The resultant stresses are then summarized in the form of plots of maximum alternating and peak tension stress as functions of face width for both fillet and root locations for one complete gear revolution.[2, 3]

Results

The results of this analysis are best presented by comparing the stresses at three locations in the tooth fillet area, as defined in Fig. 4. The fillet location is the critical section implicit in the AGMA stress approach. The root location is often critical for thin-rimmed hollow gears, because, at the central root location, the tooth bending and ring bending stresses combine to yield high stress levels.

While the results of a purely analytical study are of interest, it is imperative that experimental verification of new methods be provided so that their validity can be evaluated. Fortunately, a substantial base of experimental data exists for one of the planet gears (A). These data, for both root and fillet locations, will be superimposed on the FEM results for comparative purposes.

Before the stress results are examined, however, some planet gear stiffness data are obtained from the ring analysis

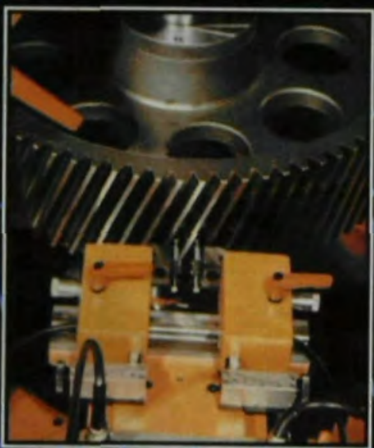

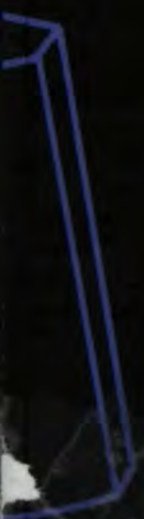

TABLE IV. SPUR AND HELICAL GEAR GEOMETRIC PREPROCESSOR INPUT DATA

Card No.	Item	Format/Location
1	A. Title	Alphanumeric-1-80
2	A. Letters "ELEM"	Real, 1-4
	B. No. of teeth in gear	Real, 5-14
	C. No. of full teeth modeled	Real, 15-24
	D. No. of layers of elements along face	Real, 25-34
	E. No. of rows of elements in half tooth	Real, 35-44
	F. No. of rows of elements in half blank	Real, 45-54
3	A. Letters "FULL"	Real, 1-4
	B. Location no. of full tooth	Real, 5-14
	C. Location no. of full tooth	Real, 15-24
	D. Location no. of full tooth	Real, 25-34
	E. Location no. of full tooth	Real, 35-44
	F. Location no. of full tooth	Real, 45-54
	G. Location no. of full tooth	Real, 55-64
	(Repeat Card 3 if more than six full teeth are generated)	
4	A. Letters "PROF"	Real, 1-4
	B. Tooth blank factor ($\approx$0.95)	Real, 5-14
	C. Kink factor ($\approx$0.95)	Real, 15-24
	D. No. of grids on profile	Real, 25-34
	E. No. of grids on centerline of tooth	Real, 35-44
5	A. Letters "PROF"	Real, 1-4
	B. Line no. of profile grid no. 1	Real, 5-14
	C. Line no. of profile grid no. 2	Real, 15-24
	D. Line no. of profile grid no. 3	Real, 25-34
	E. Line no. of profile grid no. 4	Real, 35-44
	F. Line no. of profile grid no. 5	Real, 45-54
	G. Line no. of profile grid no. 6	Real, 55-64
	(Repeat Card 5 if needed; lines 1 and 58 should be included)	
6	A. Letters "LODL" for loading left face of tooth	Real, 1-4
	B. Tooth no. is FEM model to be loading	Real, 5-14
	C. Tooth no. is contact program generating contact line	Real, 15-24
	D. Mesh position no. is contact program generating contact line	Real, 25-34
7	A. Letters "SPUR"	Real, 1-4
	B. Gear inner radius	Real, 5-14
	C. Gear outer radius	Real, 15-24
	D. Gear base radius	Real, 25-34
	E. Gear pitch radius	Real, 35-44
	F. Gear fillet radius	Real, 45-54
	G. Gear Fillet tangency radius	Real, 55-64
8	A. Letters "SPUR"	Real, 1-4
	B. No. of teeth	Real, 5-14
	C. Face width, in.	Real, 15-24
	D. Helix angle, degrees +LH, −RH	Real, 25-34
	E. Pressure angle, degrees	Real, 35-44
	F. Arc tooth thickness, in.	Real, 45-54

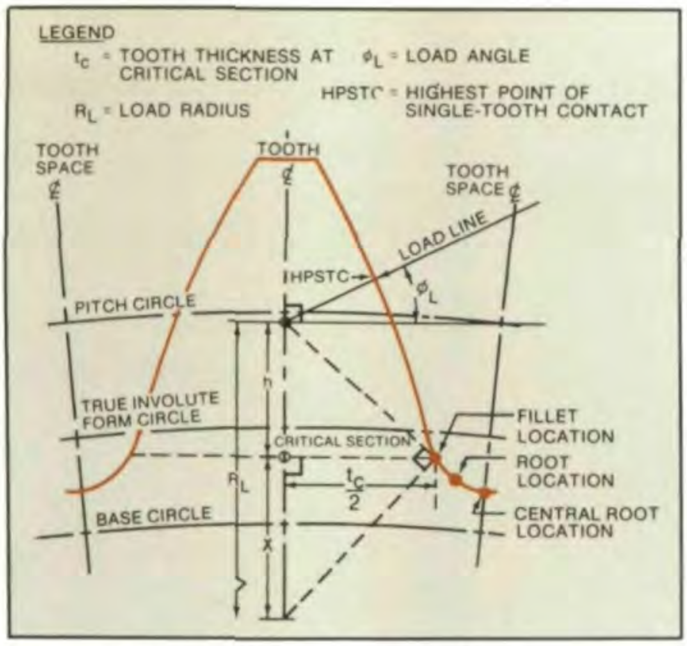

Fig. 4 – Tooth Form Stress Layout Schematic

and used to define the roller loads.

Ring Deflections

The stress results from the ring analysis have already been presented. As noted, they are of comparative interest only because they do not reflect the stress concentrations caused by the tooth roots. The ring program also provides the radial ring deflection at each roller location. This information is used to define the reaction loads. Additionally, however, it can provide some insight into the rigidity of the gears. As Table V shows, these deflections are far from insignificant in aircraft transmissions.

The need to include this effect in the overall analysis of the planet gear stresses should be understood.

Fillet Stresses

Fig. 5 shows the fillet stress results for all three planet gears with the experimental results for planet gear A also superimposed on that plot. Since muliple strain gages were applied to muliple teeth, both the range of measured data and the mean are shown. The calculated and measured values for planet gear A are in very close agreement.

If the analysis is similarly accurate for planet gears B and C, the fillet stresses for all three gears are much closer than the simple AGMA results would indicate. In fact, although the AGMA stresses for planet gear B are much higher than for A, the FEM analysis indicates that the alternating stresses for both gears are about equal. Interestingly, the fillet alternating stress level for planet gear C is actually lower than that for either A or B.

Root Stresses

Very similar results were obtained at the root location (Fig. 6). The correlation between test an analysis was again quite good, especially for the alternating stresses. As was the case with the fillet stresses, the maximum alternating root stresses on planet gears A and B are quite close. However, the peak stress level on planet gear B is significantly higher than that on planet gear A, while that on planet gear C is higher than either A or B. The alternating stress on planet gear C is actually lower than that for either of the other planets.

Central Root Stresses

The tooth fillet and root stresses described above are useful in evaluating the capacity of the gear teeth as influenced by many factors, including the behavior of the ring that supports the teeth. Due to the complex loading applied to this ring, the basic ring stresses are also of interest. (The authors

TABLE V. RADIAL RIM DEFLECTIONS AT ROLLERS

Roller No.*	Radial Deflection (in.)		
	Planet A	Planet B	Planet C
1	0.0025	0.0024	0.0022
2, 14	0.0028	0.0026	0.0023
3, 13	0.0030	0.0028	0.0025
4, 12	0.0031	0.0027	0.0025
5, 11	0.0023	0.0016	0.0015
6, 10	−0.0019	−0.0019	−0.0017
7, 9	−0.0065	−0.0055	−0.0050
8	−0.0083	−0.0070	−0.0064

*See Figure 2 for roller numbering scheme.

have investigated at least one planet gear failure which was traced to excessive central root stresses). The RINGEAR program approximates these stresses through the idealization shown in Fig. 3. However, the effect of the tooth fillets (which are stress risers on the ring OD) is not included. By looking at the FEM results for a central root location, a more accurate picture of these ring stresses (Fig. 7) can be obtained. Comparing these charts with those shown in Fig. 3 shows the effect of the tooth loading and the tooth fillets. The effect of the thinner planet gear A ring on the stress distribution as compared to the stiffer planet gear C ring is also apparent.

The maximum tension and compression peaks for most gears are associated with the tooth mesh itself. From Fig. 7, however, it can easily be seen that the compressive stress due to the ring bending, independent of the mesh contact, exceeds that due to the tooth mesh itself. The alternating stress at this location is thus defined by combining the peak tension due to the tooth mesh with the peak compressive stress due to the ring bending. This is a critical consideration and can be the governing factor in defining the load capacity of thin-rimmed, roller-supported planets.

Summary

Although the basic AGMA tooth fillet stresses for the three planets evaluated here differ substantially, their fatigue (alternating) stress levels are surprisingly similar, as the summary in Table VI shows.

The conventional AGMA tooth bending stresses are closer to the FEM peak tension stresses (Table VI) at the fillet location than at the root location. This may be attributed to the fact that the effect of rollers is more predominant at the tooth root than at the tooth fillet. The roller effect is not considered in AGMA calculation.

Discussion

The correlation between the static-strain survey test data and the FEM results for planet gear A is in general about 15 percent. Considering the possible test variations to be about 10 percent by themselves, this level of correlation appears to be quite acceptable.

The effect of rollers on the tooth stresses appears to be a function of the backup rim's rigidity and tooth loads. Planet gear C has the largest backup rim moment of inertia and produces a tensile steady stress (Table VI) at all locations considered. Planet gear A has half the backup rim rigidity and twice the tooth load. The FEM analysis predicted compressive steady stresses at tooth root and fillet locations as verified by test data.

Although in all three cases considered here, the critical stress location is not at the central root location, the possibility of this location's becoming critical is certainly obvious. A small additional stress concentration, for example, would tip the scales. Generally, in the absence of integral roller bearings, maximum tooth stresses occur during the mesh. Futhermore, the magnitude of the peak stresses with rollers could be higher than those without rollers. As pointed out earlier, this effect is a function of the rigidity of backup rim and tooth load.

An interesting observation, or more correctly, conjecture,

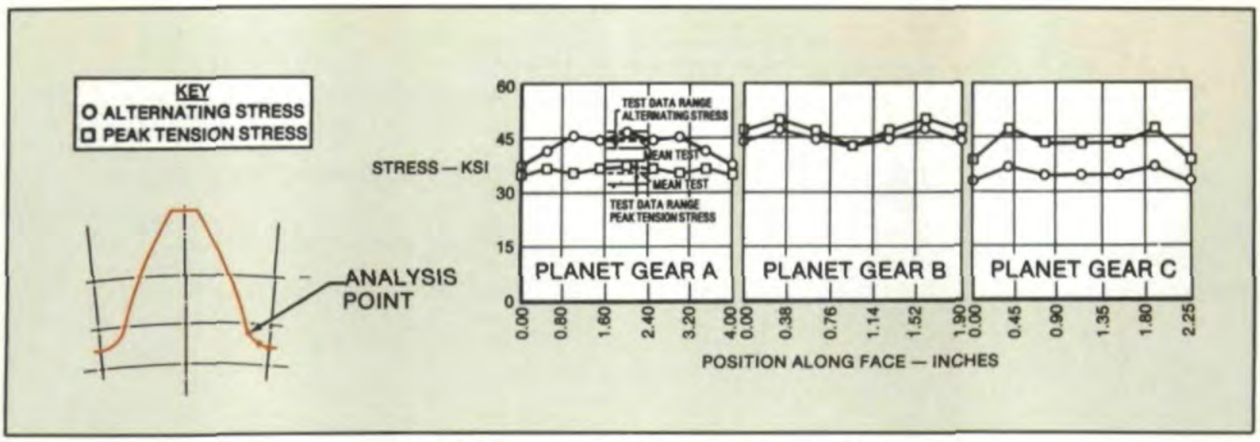

Fig. 5 – FEM Gear Tooth Fillet Stresses Versus Face Width

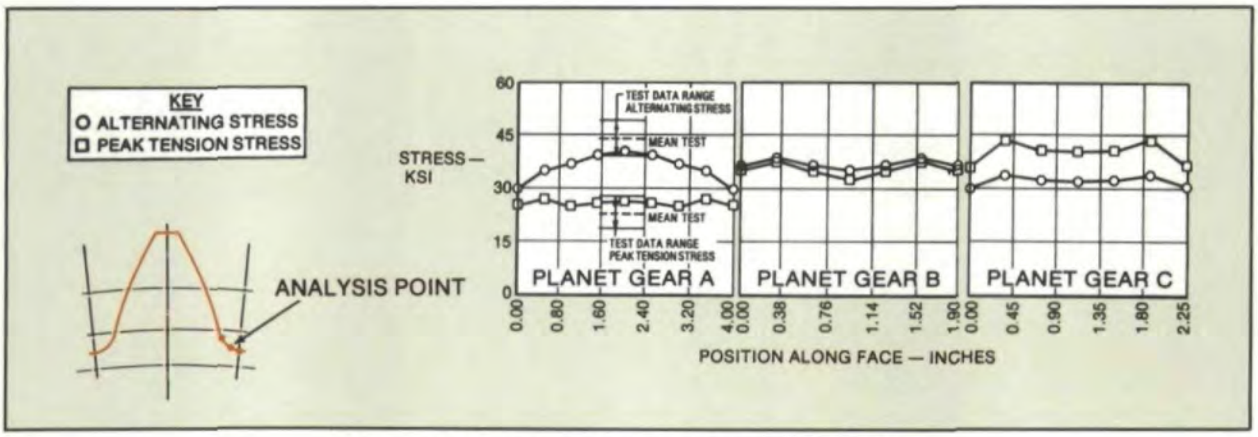

Fig. 6 – FEM Gear Tooth Root Stresses Versus Face Width

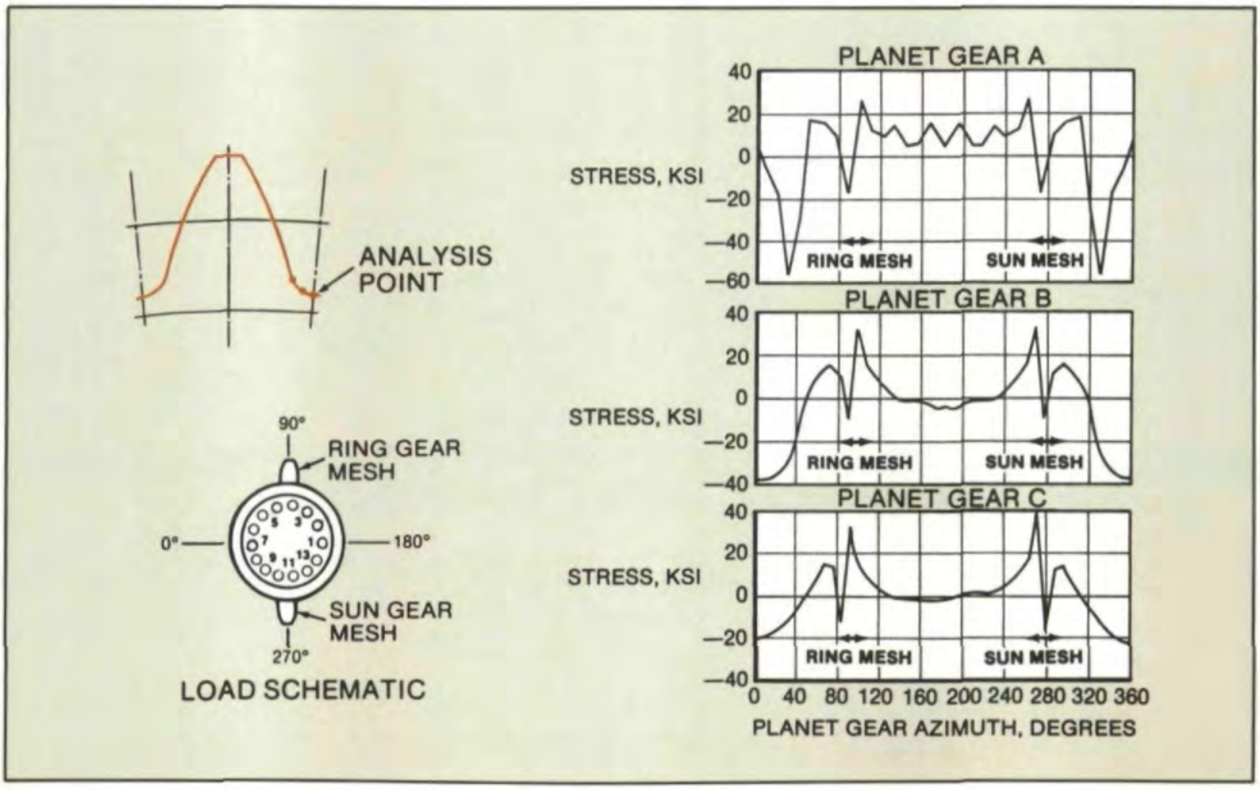

Fig. 7 – FEM Central Root Stresses

TABLE VI. SUMMARY OF PREDICTED STRESSES

Stress Item	Planet A (ksi)	Planet B (ksi)	Planet C (ksi)
AGMA *Tooth bending at sun mesh*[1]	*37.0*	*66.2*	*41.4*
FEM peak tension at tooth fillet[2]	38.1	50.8	40.4
FEM fatigue stress at tooth fillet[2,3]	− 9.7±47.8	+2.8±48.0	+10.6±37.2
FEM fatigue stress at tooth root[2,3]	−14.2±40.9	−1.1±38.7	+ 9.8±33.0
FEM fatigue stress at central root[2,3]	−14.2±41.8	−4.5±35.3	+16.5±31.3

NOTES: 1. Does not consider effect of roller loads
2. Includes effect of bearing roller loads
3. Considers both sum mesh and ring mesh

comes to mind based on these data. In some designs, the planet gear is supported by an integral, fluid-film bearing. Since such a bearing provides a fully distributed load reaction rather than discrete individual (roller) reaction loads, it is possible that such planet gears may be designed with thinner rims than their roller-bearing-supported counterparts. This possibility has not been investigated so far and could be undertaken in the future.

The AGMA and FEM calculated peak tension stresses for planet gears A and C agree rather well; those for planet gear B do not. A possible explanation for this is the AGMA stress correction factor. The smaller fillet radii on finer pitch gears tend to produce comparatively large values for the stress correction factor. These values may be somewhat pessimistic for finer pitch gears. The empirical relation used to calculate this factor is based on work by Dolan and Broughamer which used relatively large models; thus the extrapolation to small fillets may be in error.

Conclusions

After carefully studying all the data, the following specific conclusions were reached:

1. Despite the apparent large differences in the AGMA stress levels for the three planet gears, their alternating stresses are quite similar.
2. The FEM analysis described, using the gear preprocessor and postprocessor, is a reliable tool for analyzing spur planetary gears with integral roller bearings.
3. In critical applications which typically involve extensive testing (strain surveys), the FEM analysis could be substituted for selected test conditions after establishing correlation with some known test conditions, thereby reducing test time, cost, and effort.
4. The effect of the ring bending-induced compressive stress on the alternating stress in the tooth root is not negligible and may be the governing factor in some circumstances.

Recommendations

Thus far, the gear finite-element model generated by the preprocessor is used successfully in predicting the tooth stresses for spur and spiral-bevel gears by a linear static analysis. The potential which exists for extending this methodology is substantial. Consider the following examples:

1. The same FEM model could probably be used in a dynamic analysis to predict the gear natural frequencies and normal mode shapes.
2. A nonlinear, static, FEM analysis, wherein the tooth contact loads are a function of the tooth deflections, could shed more light on tooth load distribution along the contact lines and tooth load sharing among adjacent gear teeth.
3. A comprehensive program of parametric study of spur, helical, and bevel-gear tooth stresses with respect to diametral pitch, backup rigidity, contact pattern, and load distribution might be undertaken with the ultimate goal of arriving at optimally minimum-weight aircraft

transmission gears.

4. The effect of the thermal deformation of transmission housings, particularly lightweight magnesium, aluminum, or composite housings such as those usually used in aerospace applications, is to cause gear misalignment. This shifts the contact pattern on the gear tooth and causes higher tooth stresses than in the case of perfectly aligned gears, and might lead to premature fatigue failure. The use of the FEM analysis for a better understanding of this problem and its solution should be considered.
5. The expression used for the stress-correction factor in the AGMA method should be reviewed for applicability to small fillets.

References

1. DRAGO, RAYMOND J., On The Automatic Generation of FEM Models for Complex Gears – A Work-In-Progress Report, American Gear Manufacturers Association Aerospace Gearing Meeting, San Diego, CA, February 1982.
2. DRAGO, RAYMOND J., and UPPALURI, BAPA R., Large Rotorcraft Transmission Technology Development Program, Vol. 1, NASA Report CR-168116, National Aeronautics and Space Administration, Cleveland, OH, February 1983.
3. DRAGO, RAYMOND J., and UPPALURI, BAPA R., Computer Program Users Manual, Vol. II, Large Rotorcraft Transmission Technology Development Program, NASA Report CR-168117, National Aeronautics and Space Administration, Cleveland, OH, February 1983.
4. DRAGO, RAYMOND J., SAMANICH, N.E. and MACK, J.C., Development of Large Rotorcraft Transmissions, American Helicopter Society, Thirty-Ninth Annual Forum, St. Louis, MO, May 1983.
5. DRAGO, RAYMOND J., Results of an Experimental Program Utilized to Verify a New Gear Tooth Strength Analysis, American Gear Manufacturers Association, Fall Technical Meeting, Montreal, Canada, October 1983.
6. DRAGO, RAYMOND J., and PIZZIGATI, G.A., Some Progress in the Accurate Evaluation of Tooth Root and Fillet Stresses in Light Weight, Thin Rimmed Gears, AGMA Paper No. 229.21, American Gear Manufacturers Association Fall Technical Meeting, Washington, DC, October 1980.
7. DRAGO, RAYMOND J., BROWN, F.W., and FAUST, H.S., Recent Advances in the Evaluation of Stresses in High Speed, Light Weight, Highly Loaded Gearing, International Conference on Reliability, Stress Analysis, and Failure Prevention, San Francisco, CA, August 1980.
8. AGMA Standard for Rating the Pitting Resistance and Bending Strength of Spur and Helical Involute Gear Teeth, AGMA 218, American Gear Manufacturers Association, Arlington, VA.
9. JONES, A.B., and HARRIS, T.A., Analysis of a Rolling Element Idler Gear Bearing Having a Deformable Outer-Race Structure, Journal of Basic Engineering, June 1983.

This article was previously presented at the AGMA Fall Technical Meeting in October 1984. Paper No. 84FTM1.

Pressure Angle Changes in the Transverse Plane for Circular Cut Spiral Bevel Gears

by
Ronald Huston
University of Cincinnati
Cincinnati, Ohio

and

John J. Coy
NASA Lewis Research Center
Cleveland, Ohio

Abstract

This article examines pressure angle changes along a tooth for circular cut spiral bevel crown gears. The changes are measured in the transverse planes for various cutter profiles. Three cases are considered: 1) a straight line profile; 2) a circular profile; and 3) an involute profile. In each case, the heel-to-toe variation is approximately 3, depending on the cutter radius. For conical gears, the variation is increased by the factor $1/\sin\alpha$ where α is the half-cone angle. Finally, it is shown that pressure angle variation occurs for all cutter profiles.

Introduction

Recently it has been suggested that the transverse plane may be very useful in studying the kinematics and dynamics of spiral bevel gears.[1,2] The transverse plane is perpendicular to the pitch and axial planes as shown in Fig. 1. Buckingham[3] has suggested that a spiral bevel gear may be viewed as a limiting form of a "stepped" straight-toothed gear as in Fig. 2. The transverse plane is customarily used in the study of straight toothed bevel gears.[4]

For spiral bevel gears the *normal* plane is often used for studying the kinematics and dynamics. One reason for this is that for smooth tooth surfaces the contact forces between mating teeth are transmitted in the normal plane; that is, the resultant force vector is in the normal plane. However, if friction is present, the resultant force vector is rotated out of the normal plane, and it becomes more nearly parallel to the transverse plane.

Therefore, in this brief article the pressure angle changes in the transverse planes are examined along the circular cut tooth. The balance of the article contains four parts. The first part provides some preliminary geometrical considerations. The next part contains the analysis. Applications are presented in the third part, and the final part makes some conclusions for mechanical design.

AUTHORS:

DR. RONALD L. HUSTON *is presently employed as a Professor of Mechanics in the Department of Mechanical and Industrial Engineering for the University of Cincinnati. He also serves as the Director of the University's Institute for Applied Interdisciplinary Research. Dr. Huston was awarded a Ph.D. in Engineering Mechanics, an M.S. in Engineering Mechanics, and a B.S. in Mechanical Engineering from the University of Pennsylvania.*

DR. JOHN J. COY *is employed by the U.S. Army Aviation Systems Command's Propulsion Directorate at the NASA Lewis Research Center in Cleveland. Presently, he serves as the Head, Rotercraft Section in the Aeronautics Directorate. He earned Ph.D., M.S. and B.S. Degrees in Mechanical Engineering through the University of Cincinnati. He is Chairman of the ASME Power Transmission and Gearing Committee and holds membership on the NATO/AGARD Propulsion Energetics Panel.*

Preliminary Geometrical Concepts

Consider the pitch plane and a circular-cut tooth centerline as shown in Fig. 3. X and Y are the Cartesian axes with origin at 0, the gear center. X_1 and Y_1 are axes parallel to X and Y with origin at C, the cutter center. C has X and Y coordinates (H, V). R_c is the mean "mean cutter radius"; that is, R_c is the distance from C to the tooth surface in the pitch plane. The cutter radius r_1 for other points on the tooth surface is a function of the elevation z of those points above or below the pitch plane. For example, for and "inside" tooth surface r_1 might be expressed as:

$$r_1 = R_c + F(z) \tag{1}$$

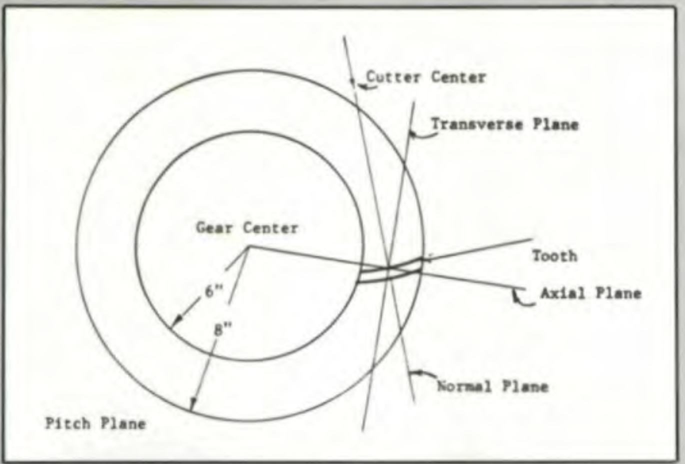

Fig. 1 – Spiral Bevel Crown Gear and Identifying Planes

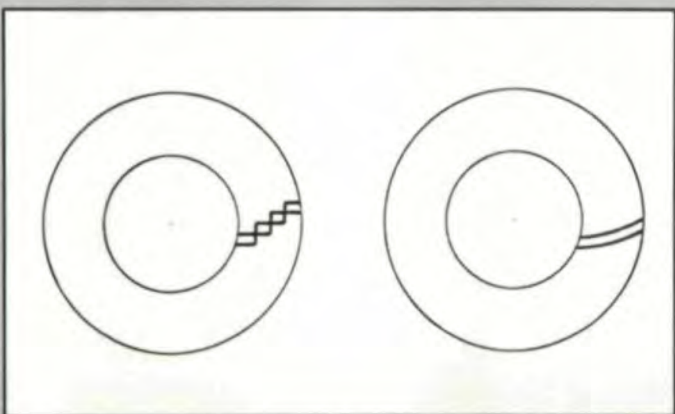

Fig. 2 – Spiral Bevel Gear as a Limiting Form of a "Stepped" Straight-Toothed Gear

where F(z) describes the cutter tooth geometry. Finally in Fig. 3, R_i and R_o are the inner ("toe") and outer ("heel") tooth radii and ψ_m is the spiral angle at the mean tooth radius R_m.

Consider a typical point P along the tooth centerline. Let r be the radial distance OP and let ϵ be the angle between OP and the X axis as shown in Fig. 4. Let X_2 and Y_2 be a third coordinate system and let its origin be C and let it be inclined at an angle ϵ to X_1 and Y_1. Then X_2 is parallel to OP. Finally, let ψ be the spiral angle at P as shown.

The angle ψ and the radial distance r are not independent, but are related by the expression[2,4]

$$\sin\psi = (r_2 + R_c^2 - H^2 - V^2)/2rR_c \qquad (2)$$

(This relation follows from the law of cosines with triangle OPC by noting that the cosine of the angle at P is $\sin\psi$.) If R_m is the mean tooth radius, Equation (2) may be expressed as:

$$\sin\psi = (r_2 - R_m^2 + 2R_mR_c \sin\psi_m)/2rR_c \qquad (3)$$

(This relation is obtained by noting in Fig. 3 that H and V may be expressed as $H - R_m - R_c\sin\psi_m$ and $V = R_c \cos\psi_m$.)

The tooth profile in the transverse plane at the typical point

Nomenclature

α	– Half-Cone Angle
ϵ	– Angle Between OP and the X-axis (Fig. 4)
ψ	– Spiral Angle
ψ_m	– Spiral Angle at the mean Tooth Radius
ϱ	– Radius of the Circular Profile and Involute Generating Circle
θ	– Pressure Angle in the Transverse Plane
θ_c	– Complement of the Pressure Angle
β	– Pressure Angle in the Normal Plane
ξ, η	– Coordinate System in the Normal Plane (Fig. 8)
a,b	– Coordinates of the Center of a Circular Tooth Profile (Fig. 7)
C	– Cutter Center
F(z)	– Function Defining the Cutter Tooth Geometry
H, V	– X and Y Coordinates of C
0	– Gear Center
r	– Radial Distance
r_1	– General Cutter Radius
R_c	– Mean Cutter Radius
R_i	– Inner ("Toe") Tooth Radius
R_o	– Outer ("Heel") Tooth Radius
R_m	– Mean Tooth Radius
X, Y	– Cartesian Axes with Origin at 0
X_1, Y_1	– Cartesian Axes with Origin at C
X_2, Y_2	– Cartesian Axes with Origin at C (Fig. 4)
z	– Elevation Above or Below the Pitch Plane

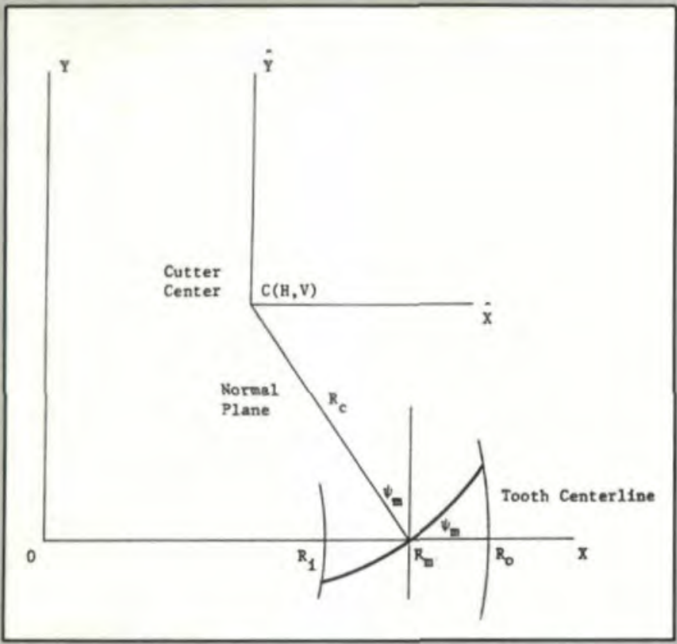

Fig. 3 – View of Pitch Plane and Tooth Centerline of Crown Gear

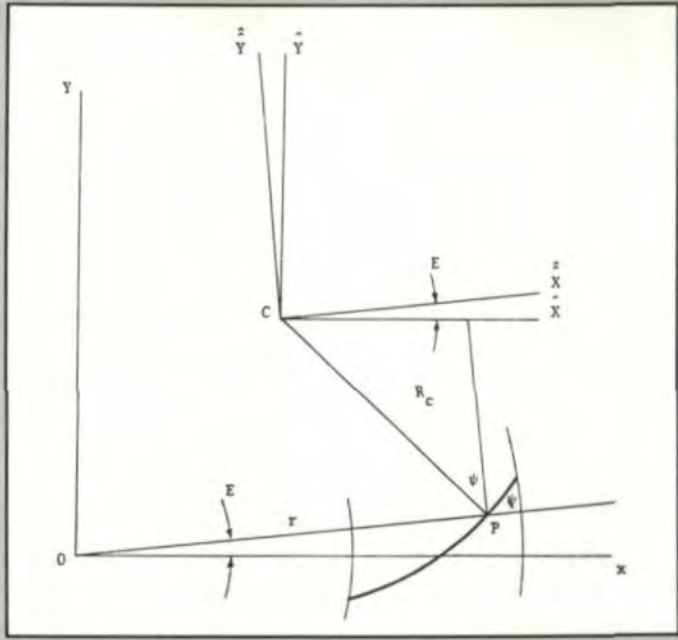

Fig. 4 – Coordinate Geometry for a Typical Point P on the Tooth Centerline

P depends upon r (or ψ). The following part of the article containing the central analysis, discusses these tooth profile changes between different transverse planes along the tooth centerline for various cutter profiles.

Analysis of Tooth Profile Changes Between Transverse Planes

Equation (1) provides a relationship between the cutter radius r_1 and the elevation z of a point on the tooth surface. By solving for z, the relationship may be expressed in the form:

$$z = f(r_1) \tag{4}$$

The cutter profile, described by the function F(z) of Equation (1), is thus also described by the function $f(r_1)$ in Equation (4); however, in Equation (4), the ensuing tooth surface is readily seen to be a surface of revolution. Equation (4) may also be viewed as providing a description of the tooth profile in the normal plane.

The cutter radius r_1 may be expressed in terms of the coordinates x_1, y_1 and x_2, y_2 in the form:

$$r_1 = (x_1^2 + y_1^2)^{1/2} = (x_1^2 + y_2^2)^{1/2} \tag{5}$$

Hence, by comparing Equations (4) and (5), z may be considered to be a function of x_1 and y_1 or of x_2 and y_2. If x_1 or x_2 has a constant value, Equation (4) provides a description of the tooth profile in a *transverse* plane. For example, if $x_1 = R_c \sin\psi_m$, the tooth profile in the mid-transverse plane is

$$z = f\left([R_c^2 \sin^2\psi m + y_1^2]^{1/2}\right) = g(y_1, \psi_m) \tag{6}$$

That is, the elevation of a point on the tooth surface in the mid-transverse plane depends upon y_1. For a general transverse plane, Equation (6) may be expressed as:

$$z = f\left([R_c^2 \sin^2\psi + y_2^2]^{1/2}\right) = g(y_2, \psi) \tag{7}$$

Thus, the tooth profile in a general transverse plane depends upon the spiral angle ψ which, in turn, is a function of the radial distance r, through Equation (3).

Equation (7) can be used to study tooth profile changes between the transverse planes. For example, a comparison of $g(y_2, \psi)$ with $g(y_2, \psi_m)$ provides a measure of the modification of the transverse profile from the profile in the mid-transverse plane. Equation (7) is also useful for determining the pressure angle changes between the transverse planes. To see this, consider the profile in the transverse plane depicted in Fig. 5. Let θ be the pressure angle and let θ_c be its complement. Then, for the inside tooth surface $\tan\theta_c$ is:

$$\tan\theta_c = \partial z/\partial(y_2) = -(dz/dr_1)(\partial r_1/\partial y_2) \tag{8}$$

or

$$\tan\theta_c = -f'(r_1)\, y_2/r_1 \tag{9}$$

But since $\tan\theta_c = \cot\theta$, the pressure angle θ (in the transverse plane is

$$\theta = -\tan^{-1}[r_1/f'(r_1)y_2] \tag{10}$$

Equation (10) may be viewed as an algorithm which provides the pressure angle as a function of the radial distance r from the gear center. Moreover, it is a valid algorithm for any cutter profile.

Example Applications

Equation (10) was used to study the pressure angle changes

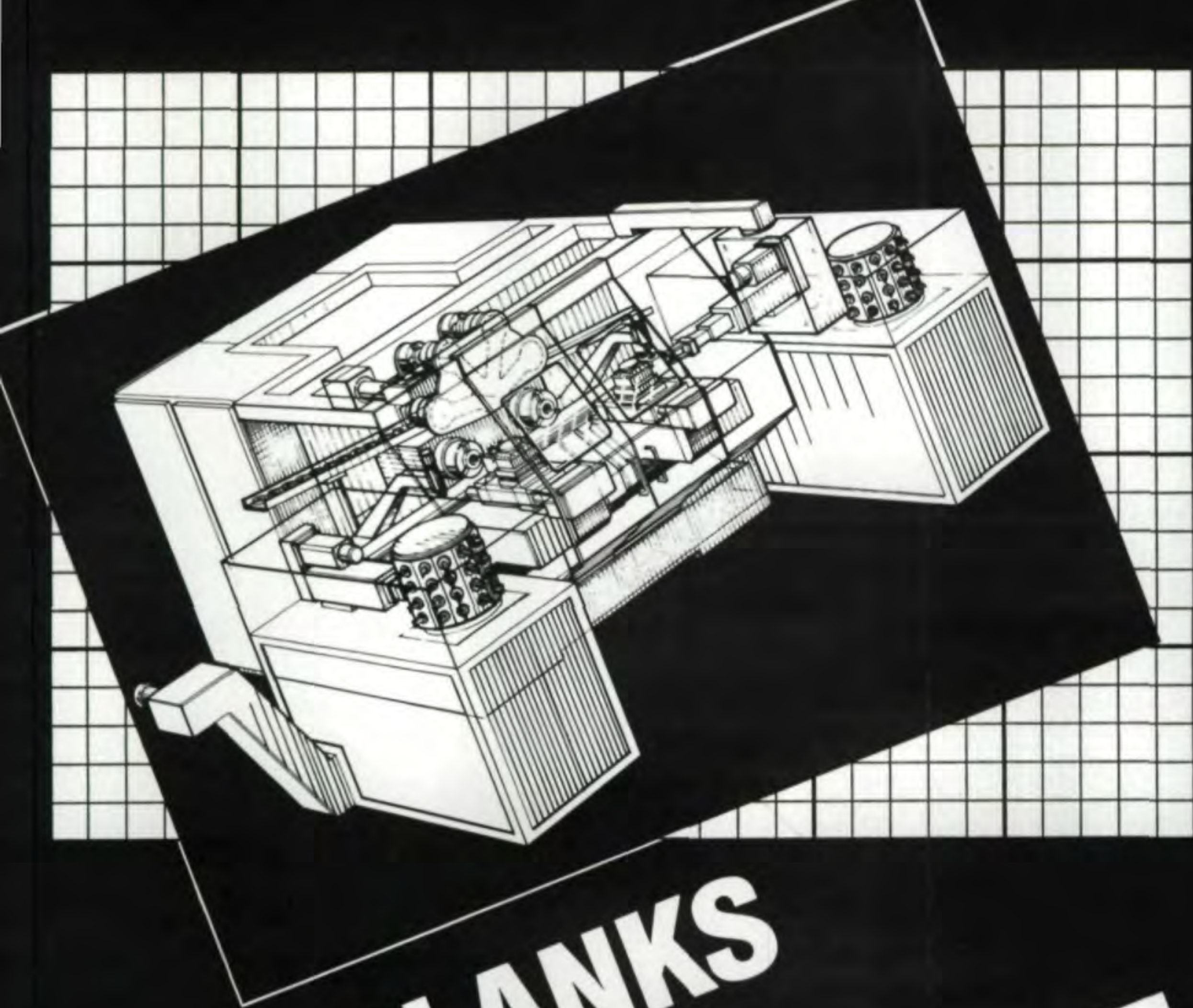

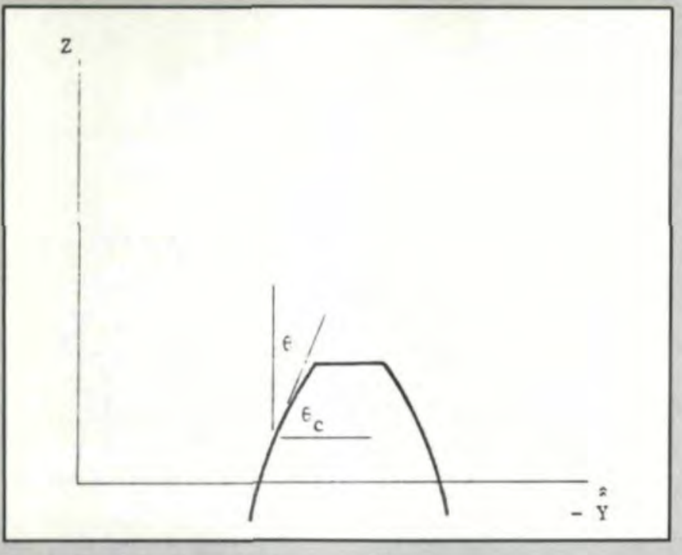

Fig. 5—Tooth Profile in the Transverse Plane

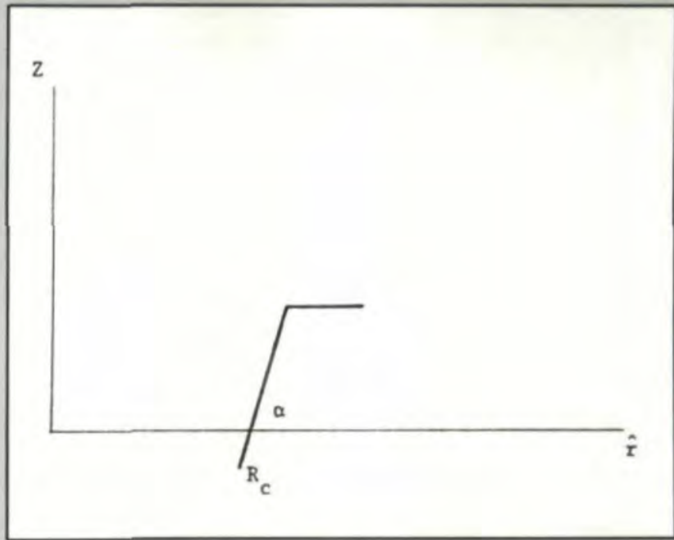

Fig. 6—Straight-Line Tooth Profile in the Normal Plane

through the transverse plane along the inside tooth surface for three cutter profile shapes: 1) a straight line profile, 2) a circular profile, and 3) an involute profile.

1. *Straight Line Cutter Profile.* Fig. 6 depicts a straight line tooth profile in the normal plane. In this case Equation (4) takes the form:

$$z = f(r_1) = (\tan\alpha)(r_1 - R_c) \qquad (11)$$

where R_c is the mean cutter radius and α is the cutter inclination. By substituting into Equation (10) we obtain the transverse plane pressure angle,

$$\theta = \tan^{-1}\{(\cot\alpha)\,[1 + (R_c/y_2)^2 \sin^2\psi]^{1/2}\} \qquad (12)$$

where we have replaced r_1 by $(R_c^2 \sin^2\psi + y_2^2)^{1/2}$ as in Equation (6). The spiral angle ψ may be expressed in terms of the radial distance r by either Equation (2) or (3). Hence, θ is a function of r.

Fig. 9 shows a computer drawn graph of θ in the pitch plane (that is, with $y_2 = -R_c\cos\psi$) for R_c + 6.0 in. (15.24cm), R_m = 7.0 in. (17.78cm), ψm =70°, and α =70.

2. *Circular Cutter Profile.* Fig. 7 depicts a circular tooth profile in the normal plane. In this case, the equation of the profile may be expressed as:

$$(z - b)^2 + (r_1 - a)^2 = \varrho_2 \qquad (13)$$

where a, b, and ϱ are the circle center coordinates and the circle radius as shown in Fig. 7. If α is the cutter inclination at the mean cutter radius, then a and b may be expressed as:

$$a = R_c + \varrho \sin\alpha \text{ and } b = -\varrho \cos\alpha \qquad (14)$$

Hence, Equation (4) may be expressed in the form:

$$z = f(r_1) = -\varrho \cos\alpha + [\varrho_2 - (r_1 - R_c - \varrho \sin\alpha)^2]^{1/2} (15)$$

Then by substituting into Equation (10), we obtain the transverse plane pressure angle:

$$\theta = \tan^{-1}\Big[\{(\varrho^2 - [(R_c^2 \sin^2\psi + y_2^2)^{1/2} - R_c - \varrho \sin\alpha]^2\}.$$
$$(R_c^2 \sin^2\psi + y_2^2)^{1/2}.$$
$$[(R_c^2 \sin^2\psi + y_2^2)^{1/2} - R_c - \varrho \sin\alpha]^{-1}\, y_2\Big] \qquad (16)$$

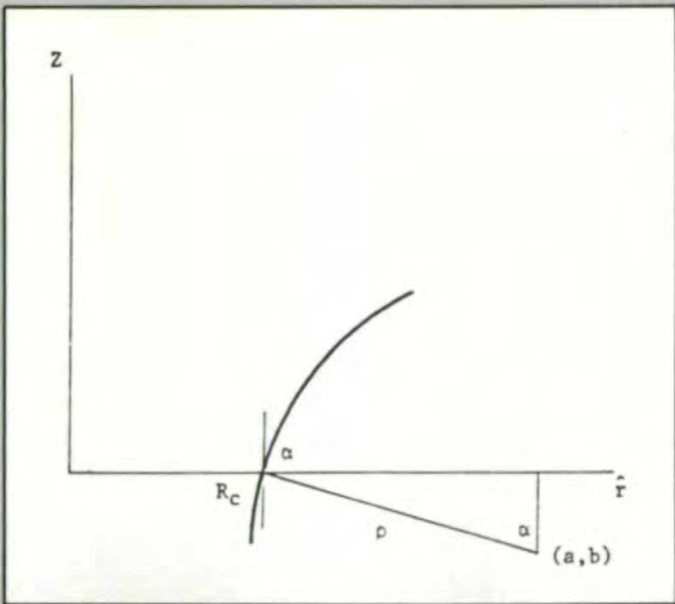

Fig. 7—Circular Tooth Profile in the Normal Plane

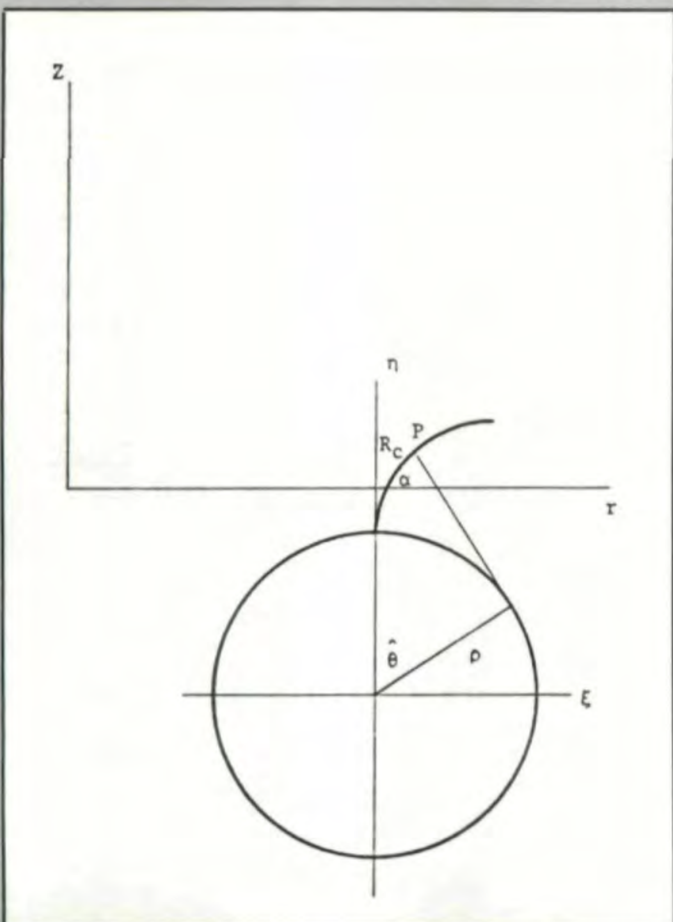

Fig. 8—Involute Tooth Profile in the Normal Plane Together with the Involute Generating Circle

where, as before, we have replaced r_1 by $(R_c^2\sin^2\psi + y_2^2)^{1/2}$.

Fig. 9 also shows a graph of Equation (16) for $R_c = 6.0$ in. (15.24 cm), $R_m = 7.0$ in. (17.78cm), $\varrho = 1.0$ in. (2.54cm), $\psi_m = 30°$, $\alpha = 70°$, and $y_2 = -R_c\cos\psi$.

3. *Involute Profile.* Fig. 8 depicts an involute tooth profile in the normal plane, together with the generating circle of the involute. In terms of the ξ, μ coordinate system, the coordinates of a typical point P on the involute curve may be expressed as:

$$\xi = \varrho\ (\sin\beta - \beta\cos\beta) \qquad (17)$$

and

$$\eta = \varrho\ (\cos\beta + \beta\sin\beta) \qquad (18)$$

where ϱ is the radius of the generating circle and β is the pressure angle in the normal plane. Equations (17) and (18) are parametric equations of the profile with β being the parameter. In the z, r_1 coordinate system these equations may be written as:

$$z = -\eta_0 + \varrho\ (\cos\beta + \beta\sin\beta) \qquad (19)$$

and

$$r_1 = R_c - \xi_0 + \varrho\ (\sin\beta - \beta\cos\beta) \qquad (20)$$

where ξ_0 and η_0 are the values of ξ and η when $\beta = (\pi/2) - \alpha$ (that is, ξ_0 and η_0 are the coordinates of the intersection of the profile and the r_1-axis.)

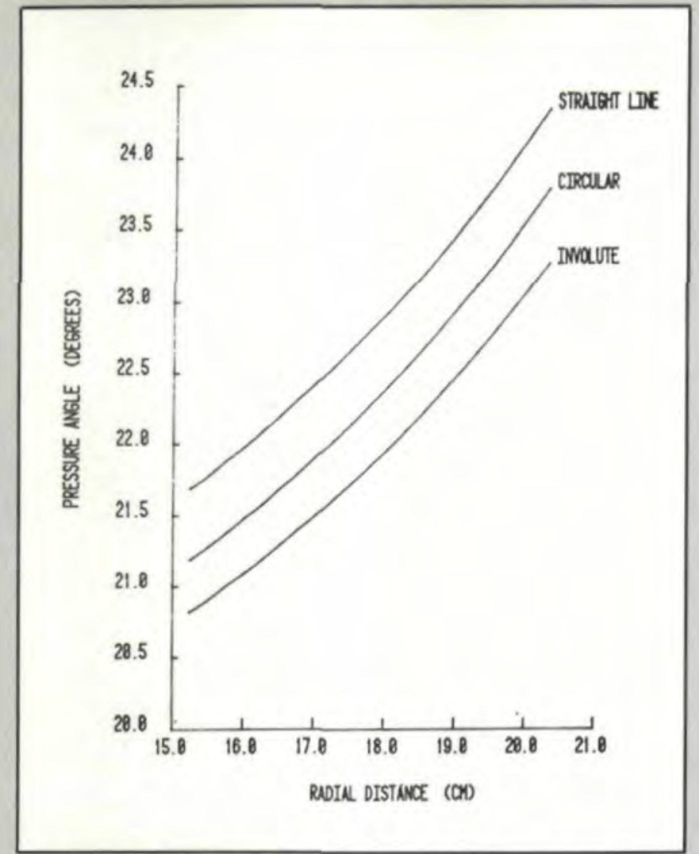

Fig. 9—Pressure Angle Variation for Three Cutter Profiles

In this case, the parametric Equations (19) and (20) replace Equation (4). In Equation (10), $f'(r_1)$ becomes

$$f'(r_1) = dz/dr_1 = (dz/d\beta)/(dr_1/d\beta) = \cot\beta \quad (21)$$

Hence, the pressure angle in the transverse plane is:

$$\theta = \tan^{-1}[\tan\beta\,(R_c^2\sin^2\psi + y_2)^{1/2}y_2] \quad (22)$$

where, as before, we have replaced r_1 by $(R_c^2\sin^2\psi + y_2)^{1/2}$, and where in this case, y_2 is related to β through Equation (20), leading to the expression:

$$y_2 = -\{[R_c - \xi_0 + \varrho(\sin\beta - \beta\cos\beta)]^2 - R_c\sin^2\psi\}^{1/2} \quad (23)$$

Finally, Fig. 9 also shows a graph of Equation (22) for $R_c = 6.0$ in. (15.24cm), $R_m = 7.0$ in. (17.78cm) $\varrho = 7.0$ in. (17.78cm), $\psi_m = 30$, $\beta = 20°$, and y_2 given by Equation (23).

Discussion and Conclusions

Fig. 9 shows the pressure angle variation in the transverse planes for the different cutter profile shapes. In each case the variation is similar, resulting in a pressure angle change of approximately 3° or 15% from heel to toe. For conical gears, this change in pressure angle would be enhanced by the factor $(1/\sin\alpha)$ where α is the half-cone angle.[6]

The effects of this pressure angle change on the gear kinematics, stress, and wear are unknown, but they could be significant.

Finally, the question arises as to whether it would be possible to adjust the cutter profile $f(r_1)$ so that the transverse plane pressure angle would be independent of r, the radial position on the gear. An examination of Equation (10) shows that f is not an explicit function of x_2 or y_2. This means it is *not* possible to adjust f to make $r_1/f'(r_1)y_2$ a constant. Therefore, the pressure angle changes exhibited in Fig. 9 will be similar for all circular cut gears regardless of the cutter profile.

References

1. HUSTON, R. L., and COY, J. J., "Surface Geometry of Circular Cut Spiral Bevel Gears," *Journal of Mechanical Design*, Vol. 104., 1982, pp. 743-748.
2. HUSTON, R. L., LIN, Y., and COY, J. J., "Tooth Profile Analysis of Circular Cut Spiral Bevel Gears," ASME Paper No. 82-Det-79, presented at the ASME Design and Production Engineering Technical Conferences, Arlington, VA 1982.
3. BUCKINGHAM, E., *Analytical Mechanics of Gears*, Dover, New York, 1963, p. 338.
4. BAXTER, M. L., "Basic Theory of Gear-Tooth Action and Generation," *Gear Handbook* (D. W. Dudley, Ed.), McGraw Hill, 1962, Chapter 1.
5. HUSTON, R. L. and COY J. J. "A New Approach to Surface Geometry of Spiral Bevel Gears—Part I: Ideal Gears," *Journal of Mechanical Design*, Vol. 103, No. 4, 1981, pp. 126-132.

ENGINEERING CONSTANTS

RULES AND FORMULA FOR GEAR SIZES

DIAMETRAL PITCH* SPUR GEARS

To Find	Having	Rule
Diametral Pitch	Circular Pitch	Divide 3.1416 by the Circular Pitch.
Diametral Pitch	Pitch Diameter and Number of Teeth	Divide Number of Teeth by Pitch Diameter.
Diametral Pitch	Outside Diameter and Number of Teeth	Divide Number of Teeth plus 2 by Outside Diameter.
Pitch Diameter	Number of Teeth and Diametral Pitch	Divide Number of Teeth by Diametral Pitch.
Pitch Diameter	Number of Teeth and Outside Diameter	Divide the product of Outside Diameter and Number of Teeth by Number of Teeth plus 2.
Pitch Diameter	Outside Diameter and Diametral Pitch	Subtract from the Outside Diameter the quotient of 2 divided by the Diametral Pitch.
Pitch Diameter	Addendum and Number of Teeth	Multiply Addendum by the Number of Teeth.
Outside Diameter	Number of Teeth and Diametral Pitch	Divide Number of Teeth plus 2 by the Diametral Pitch.
Outside Diameter	Pitch Diameter and Diametral Pitch	Add to the Pitch Diameter the quotient of 2 divided by the Diametral Pitch.
Outside Diameter	Pitch Diameter and Number of Teeth	Divide the Number of Teeth plus 2 by the quotient of Number of Teeth divided by Pitch Diameter.
Outside Diameter	Number of Teeth and Addendum	Multiply the Number of Teeth plus 2 by Addendum.
Number of Teeth	Pitch Diameter and Diametral Pitch	Multiply Pitch Diameter by the Diametral Pitch.
Number of Teeth	Outside Diameter and Diametral Pitch	Multiply Outside Diameter by the Diametral Pitch and subtract 2.
Thickness of Tooth	Diametral Pitch	Divide 1.5708 by the Diametral Pitch.
Addendum	Diametral Pitch	Divide 1 by the Diametral Pitch.
Root	Diametral Pitch	Divide 1.157 by the Diametral Pitch.
Working Depth	Diametral Pitch	Divide 2 by the Diametral Pitch.
Whole Depth	Diametral Pitch	Divide 2.157 by the Diametral Pitch.
Clearance	Diametral Pitch	Divide .157 by the Diametral Pitch.
Clearance	Thickness of Tooth	Divide thickness of Tooth at Pitch Line by 10.

*Diametral Pitch is the Number of Teeth to each inch of Pitch Diameter.

CIRCULAR PITCH† SPUR GEARS

To Find	Having	Rule
Circular Pitch	Diametral Pitch	Divide 3.1416 by the Diametral Pitch.
Circular Pitch	Pitch Diameter and Number of Teeth	Divide Pitch Diameter by the product of .3183 and Number of Teeth.
Circular Pitch	Outside Diameter and Number of Teeth	Divide Outside Diameter by the product of .3183 and the Number of Teeth plus 2.
Pitch Diameter	Number of Teeth and Circular Pitch	The continued product of the Number of Teeth, the Circular Pitch and .3183.
Pitch Diameter	Number of Teeth and Outside Diameter	Divide the product of Number of Teeth and Outside Diameter by Number of Teeth plus 2.
Pitch Diameter	Outside Diameter and Circular Pitch	Subtract from the Outside Diameter the product of the Circular Pitch and .6366.
Pitch Diameter	Addendum and Number of Teeth	Multiply the Number of Teeth by the Addendum.
Outside Diameter	Number of Teeth and the Circular Pitch	The continued product of the Number of Teeth plus 2, the Circular Pitch and .3183.
Outside Diameter	Pitch Diameter and the Circular Pitch	Add to the Pitch Diameter the product of the Circular Pitch and .6366.
Outside Diameter	Number of Teeth and Addendum	Multiply the Addendum by the Number of Teeth plus 2.
Number of Teeth	Pitch Diameter and Circular Pitch	Divide the product of Pitch Diameter and 3.1416 by the Circular Pitch.
Thickness of Tooth	Circular Pitch	One-half the Circular Pitch.
Addendum	Circular Pitch	Multiply the Circular Pitch by .3183.
Root	Circular Pitch	Multiply the Circular Pitch by .3683.
Working Depth	Circular Pitch	Multiply the Circular Pitch by .6366.
Whole Depth	Circular Pitch	Multiply the Circular Pitch by .6866.
Clearance	Circular Pitch	Multiply the Circular Pitch by .05.
Clearance	Tooth Thickness	1/10 the Thickness of Tooth at Pitch Line.

†Circular Pitch is the distance from the center of one tooth to the center of the next tooth, measured along the pitch circle.

ENGINEERING CONSTANTS

USEFUL INFORMATION

Circumference of a Circle = Diameter × 3.1416.

Diameter of a Circle = Circumference × .3183.

Area of a Circle = Diameter Squared × .7854.

Doubling the Diameter of a Circle Increases its Area Four Times.

Area of Rectangle = Length × Breadth.

Area of Triangle = Base × ½ Perpendicular Height.

Area of Elipse = Product of Both Diameters × .7854.

Area of Parallelogram = Base × Altitude.

Side of an Inscribed Cube = Radius of Sphere × 1.1547.

Side of an Inscribed Square = Diameter × 0.7071 or Circumference × 0.2251 or Circum. ÷ 4.4428.

Side of an Equal Square = Diameter × .8862.

Square:

A side × 1.4142 = Diameter of its Circumscribing Circle.

A side × 4.443 = Circumference of its Circumscribing Circle.

A side × 1.128 = Diameter of an Equal Circle.

A side × 3.547 = Circumference of an Equal Circle.

Dimensions of Equal Cube = Diameter of Ball × 0.806.

Cubic Inches in a Ball = Diameter Cubed × .5236.

Convex Surface of a Ball = Square the Diameter × 3.1416.

Cubic Contents of a Cone = Area of Base × ⅓ the Altitude.

Surface of Frustum of Cone or Pyramid = Sum of Circumference of Both Ends × ½ Slant Height + Area of both Ends.

Contents of Frustum of Cone or Pyramid = Multiply Area of Two Ends and Get Square Root. Add the Two Areas and × ⅓ Altitude.

Doubling the Diameter of a Pipe Increases its Capacity Four Times.

A Gallon of Water (U.S.Std.) Weighs 8⅓ Lbs. and Contains 231 Cubic Inches.

A Cubic Foot of Water Contains 7½ Gallons and Contains 1728 Cubic Inches and Weighs 62.4 Lbs. at a Temperature of about 62 Deg. F. The Weight Varies Slightly with the Temperature. To Find the Pressure in Pounds Per Square Inch of a Column of Water = Height of Column in Feet × .434. No Allowance is Made for Friction.

Area of a Sector of a Circle = One-half the Length of the Arc × Radius of the Circle.

Gasoline has a specific gravity of .72, and consequently weighs 5.96 pounds per gallon. This applies to 76° gasoline.

A foot-pound represents the work required to raise a weight of one pound to a height of one foot. There are 33,000 foot-pounds to a horse-power.

A British Thermal Unit represents the amount of heat required to raise the temperature of one pound of water one degree Fahrenheit at or near 39° F. Its symbol is B.T.U. There are 778 foot-pounds in a B.T.U.

There are 42.4 B.T.U. to a horsepower.

The thermal efficiency of a good internal combustion motor is from 30 to 35 per cent.

The mechanical efficiency of a good internal combustion motor should be between 85 and 90 per cent.

On direct drive, with an efficient transmission and differential, about 88 per cent of the power furnished by the motor should be delivered at the rear wheel.

Under the best conditions, about 75 per cent of the indicated horsepower of the engine should be available for useful work.

If the work performed at the rear wheels is reduced to heat units, it will be found that about 23 per cent of the energy represented by the heating value of the fuel is available as useful work.

The piston speed of a motor should not exceed 1,000 feet per minute.

The peripheral velocity of a cast iron flywheel should not exceed 5,000 feet per minute. Should it exceed this speed, there would be danger of the flywheel bursting from centrifugal force.

Atmosphere (14.7 lbs. per square inch) = 1.0335 kilogrammes per square centimetre.

1 Foot-pound = 0.1382 kilogrammetre.

1 lb. per square inch = 0.0703077 kilogramme per square centimetre = 0.7031 gramme per square millimetre = 5.170 centimetres of mercury at 0 degree centigrade.

1 Kilogramme per square millimetre = 1422.32 lbs. per square inch = 0.635 ton per square in.

1 Kilogramme per square centimetre = 14.2232 lbs. per square inch.

1 Gramme per square millimetre = 1.422 lbs. per square inch.

1 Kilogrammetre = 7.233 foot-pounds.

1 Gramme per square centimetre = 0.01422 lb. per square inch.

1 Calorie or French unit of heat = 3.968 British Thermal Units.

French mechanical equivalent of heat (425 kilogrammetres) = 3.074 foot-pounds per unit.

1 Calorie per square metre = 0.369 heat-units per square foot.

1 Calorie per kilogramme = 1.800 heat-units per lb.

English unit of heat, or heat-unit = 0.252 calorie.

English mechanical equivalent to one heat-unit (778 foot-pounds) = 10.67 kilogrammetres.

1 English heat-unit per square foot = 2.713 calories per square metre.

1 English heat-unit per lb. = 5.9 calorie per kilogramme.

BACK TO BASICS...

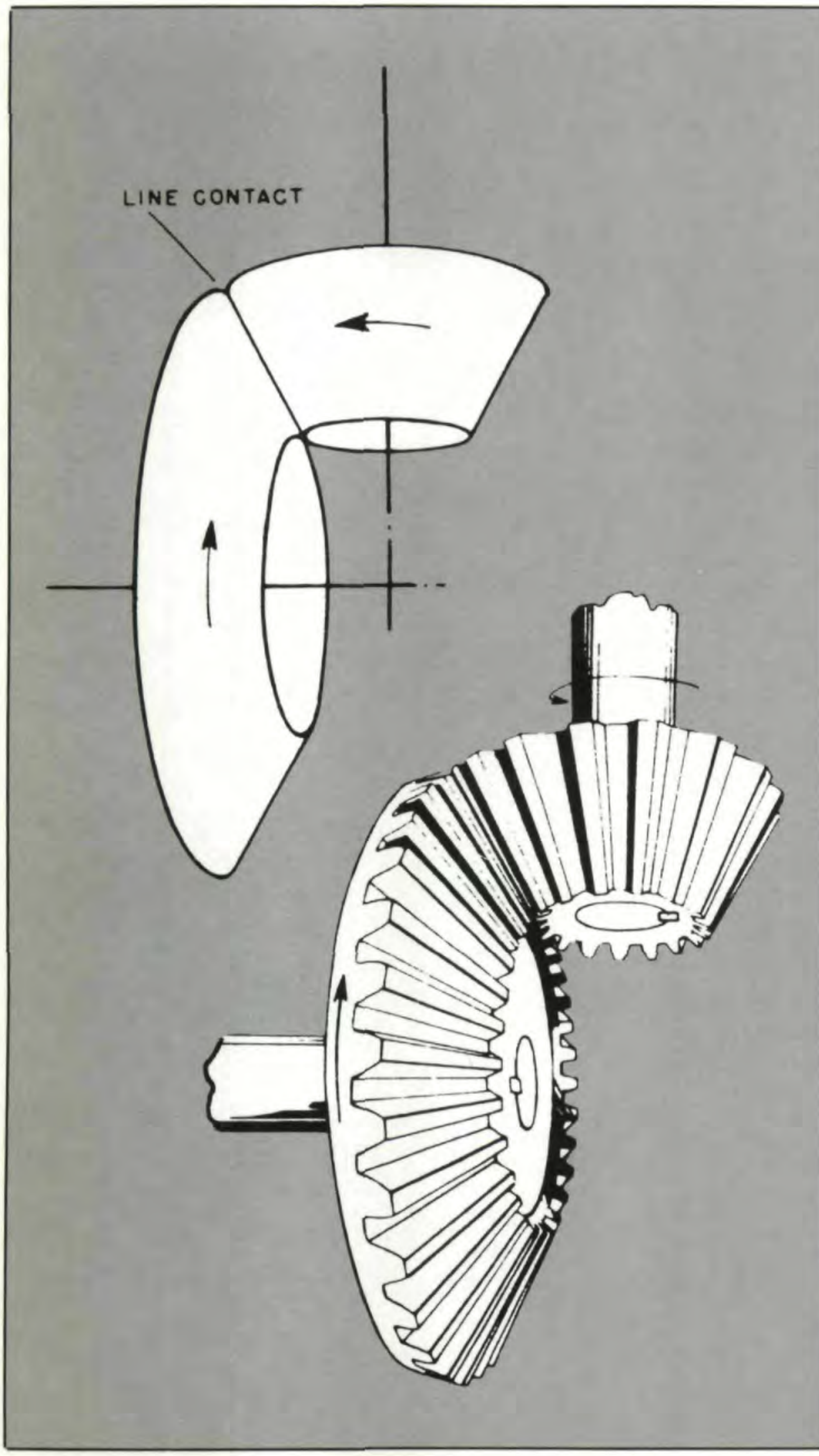

Fig. 1 (Left) – Bevel gears. These shafts intersect at a right angle, although bevel gears may also be used between shafts that intersect at larger or smaller angles. (Courtesy Mobil Oil Corporation.)

This article is an excerpt from Machine Design Fundamentals, John Wiley & Sons, Inc., Publisher.

Transmission of power between nonparallel shafts is inherently more difficult than transmission between parallel shafts, but is justified when it saves space and results in more compact, more balanced designs. Where *axial* space is limited compared to *radial* space, *angular* drives are preferred despite their higher initial cost. For this reason, angular gear motors and worm gear drives are used extensively in preference to parallel shaft drives, particularly where couplings, brakes, and adjustable mountings add to the axial space problem of parallel shaft speed reducers.

In angular drives, the gears not only rotate in different planes, but contact is frequently diagonal across the face of mating teeth (Fig. 1). Such gears are generally more difficult to design, manufacture, and install and thus cost more than equivalent spur and parallel-axis helical gears. They are also more sensitive to mounting and manufacturing errors. In addition, mounting on overhanging shafts makes some types sensitive to shaft deflections. As with spur and helical gearing, optimum design becomes a compromise. Two general classifications cover the right-angle gears: *coplanar* types, which have intersecting axes, and *offset* types, which have nonintersecting or skew axes (their axes do not lie in a common plane).

Bevel Gears

Bevel gears provide the most *efficient* means of transmitting power between intersecting shafts. The related friction wheels are frustrums of cones, and the

Gears For Nonparallel Shafts

by
Dr. Uffe Hindhede
Black Hawk College
Moline, IL

gears developed on these conical surfaces are called bevel gears. If teeth are cut straight across the faces of conical blanks, the gears are called *straight* bevel; when the teeth are twisted along a curved path, the gears are termed *spiral* bevel (Figs. 1 and 2.) The involute tooth form is used.

Customarily, tooth dimensions are determined in a transverse plane (perpendicular to the common element of the pitch cones) at the *large* end of the teeth (Fig. 3*a*). Intersection of tooth surfaces with this plane gives a tooth profile as shown in Fig. 3*b*. Fig. 3*a* also shows that the shaft angle equals the sum of the pitch angles. Thus

$$\sum = \Gamma_P + \Gamma_G \qquad (1)$$

where

Σ(sigma) = shaft angle; deg
Γ_P(gamma) = pitch angle of pinion; deg
Γ_G(gamma) = pitch angle of gear; deg

Fig. 3*c* indicates that the following relationship exists for $\Sigma = 90$ deg.

$$\tan \Gamma_P = \frac{d}{D} = \frac{N_P}{N_G} \qquad (2)$$

$$\tan \Gamma_G = \frac{D}{d} = \frac{N_G}{N_P} \qquad (3)$$

where

d = pitch diameter of pinion; mm, in.
D = pitch diameter of gear; mm, in.

N_p = number of teeth in pinion
N_G = number of teeth in gear

Nomenclature and symbols commonly used for straight bevel gears are shown in Fig. 4. The similarity to spur gearing should be noted. With few exceptions, the nomenclature also applies to spiral bevel gears.

Equivalent spur gears is a term commonly used in connection with bevel gears. Two bevel gears roll on each other in the same manner as a pair of spur gears with pitch diameters equal to those of the bevel gears. In Fig. 4 the equivalent spur gear would have a pitch diameter D_G.

AUTHOR:

DR. UFFE HINDHEDE *is an Associate Professor in the Engineering Related Technology Department at Black Hawk College, Moline, Illinois. He is a graduate of the Technical University of Denmark and the University of Illinois. Hindhede has authored several technical papers and articles. He is the principal author of* <u>Machine Design Fundamentals</u> *and sole writer of the chapter on Gears for Non-Parallel Shafts.*

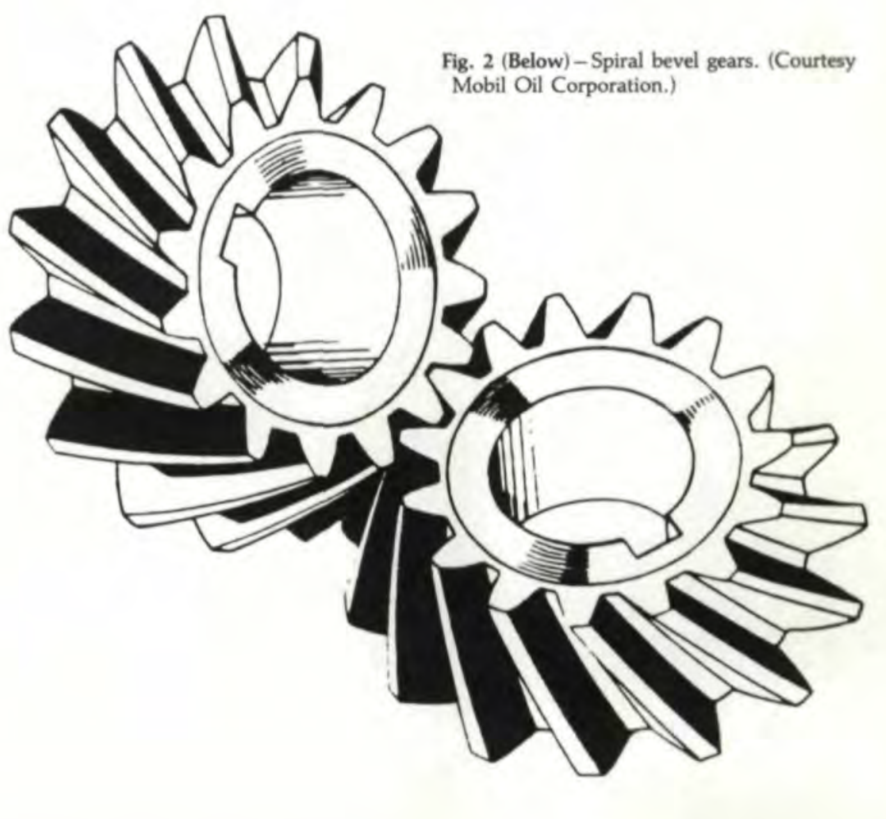

Fig. 2 (Below) – Spiral bevel gears. (Courtesy Mobil Oil Corporation.)

Nomenclature

C = center distance
d = pitch diameter of bevel pinion and worm
D = pitch diameter of bevel gear or worm gear
D_G = pitch diameter of worm gear
D_w = pitch diameter of worm
e = efficiency
L = lead of worm
m = module
m_G = speed ratio
n_G, n_w = speed of gear and worm, respectively
N_p = number of teeth in pinion
N_G = number of teeth in gear
N_w = number of teeth in worm
p_a = axial pitch
p_c = circular pitch
P_d = diametral pitch
TR = thermal rating
λ(lambda) = lead angle
Γ(gamma) = pitch angle
Σ(sigma) = shaft angle
ψ(psi) = helix angle
θ(theta) = friction angle

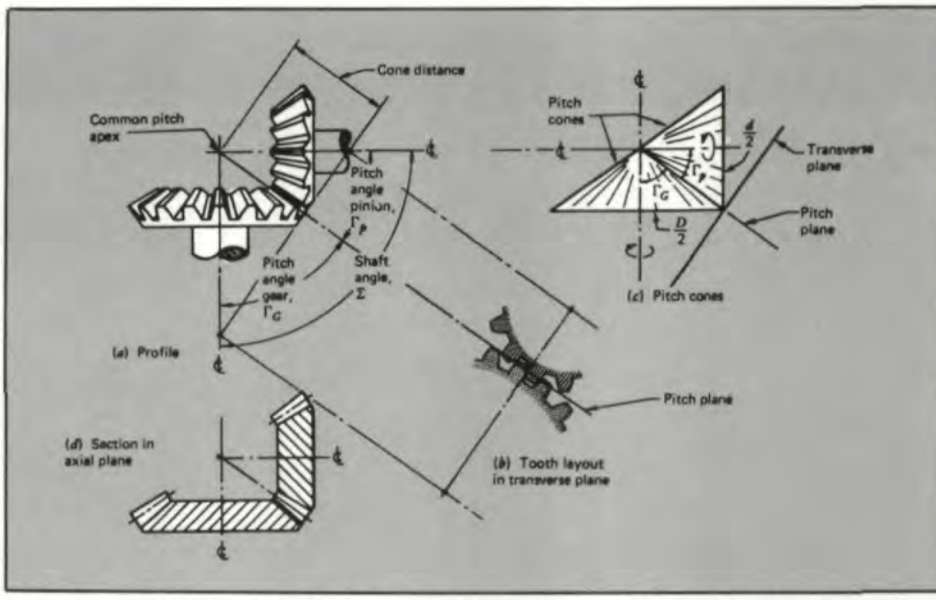

Fig. 3 – Basic bevel gear sections. (Courtesy General Motors Corporation.)

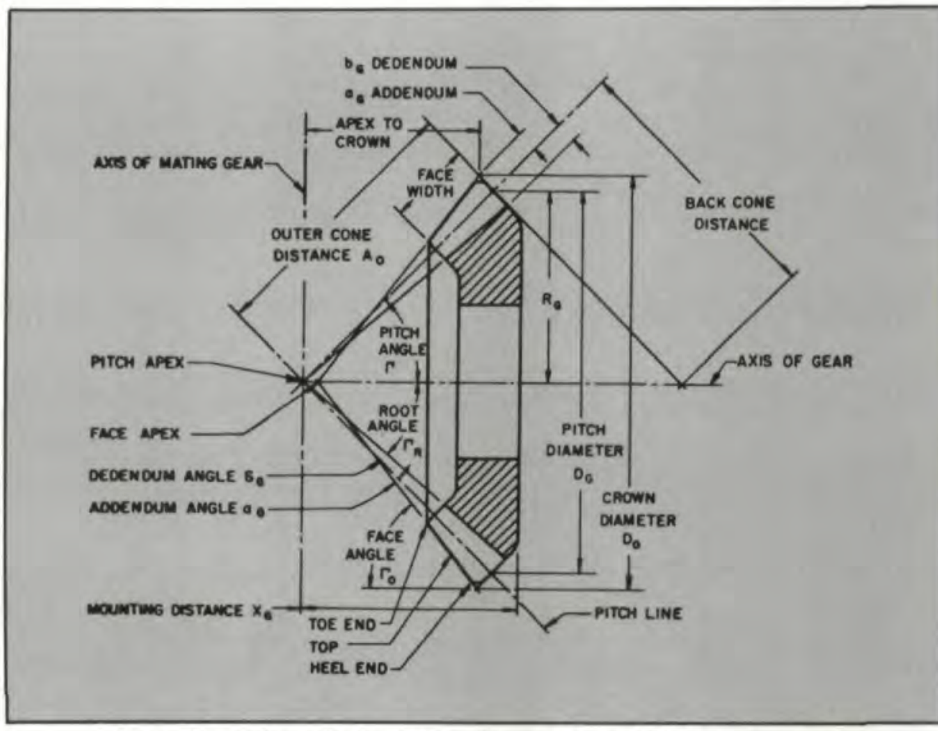

Fig. 4 – Nomenclature for bevel gears. (Courtesy General Motors Corporation.)

The difference between spiral and straight bevel gears is that spiral teeth have a *gradual* pitch line contact and a larger number of teeth in contact. Their teeth, instead of engaging in a full line contact at once, engage with one another gradually. This continuous contact makes it possible to obtain smoother action than is possible with straight bevels.

Arrangement

Bevel gears are widely used where a right-angle change in direction of shafting is required, although the shafts occasionally may intersect at acute or obtuse angles (Fig. 5). When of equal size and mounted on shafts at right angles, they are referred to as *miter* gears (Fig. 5*b*). A bevel gear with a right (90 deg) pitch angle is a *crown* gear (Fig. 5*e*). Internal bevel gearing, like internal spur or helical gearing, is sometimes used in planetary or internal gear arrangements (Fig. 5*f*).

Application

Straight bevel gears, like spur gears, are well suited for manual and low-speed operations, such as in small hoists, valves, gates, or doors. When greater speed and more power are required, spiral bevel gears are preferable.

Mounting

Bevel gears require larger shaft diameters and heavier bearings because they impose high reaction loads on bearings.

Speed Ratio

As in spur gears, the speed ratio is the ratio of tooth numbers. For bevel gears, it is also the ratio of corresponding pitch radii or diameters of the pitch cones (Fig. 4).

Design of Bevel Gears

Bevel gears are simple modifications of spur gears. Beam straight and surface durability determine size and surface hardness. The AGMA formulas used are therefore simple modifications of the formulas used for calculating spur gears.

Example 1

A pair of straight-toothed bevel gears

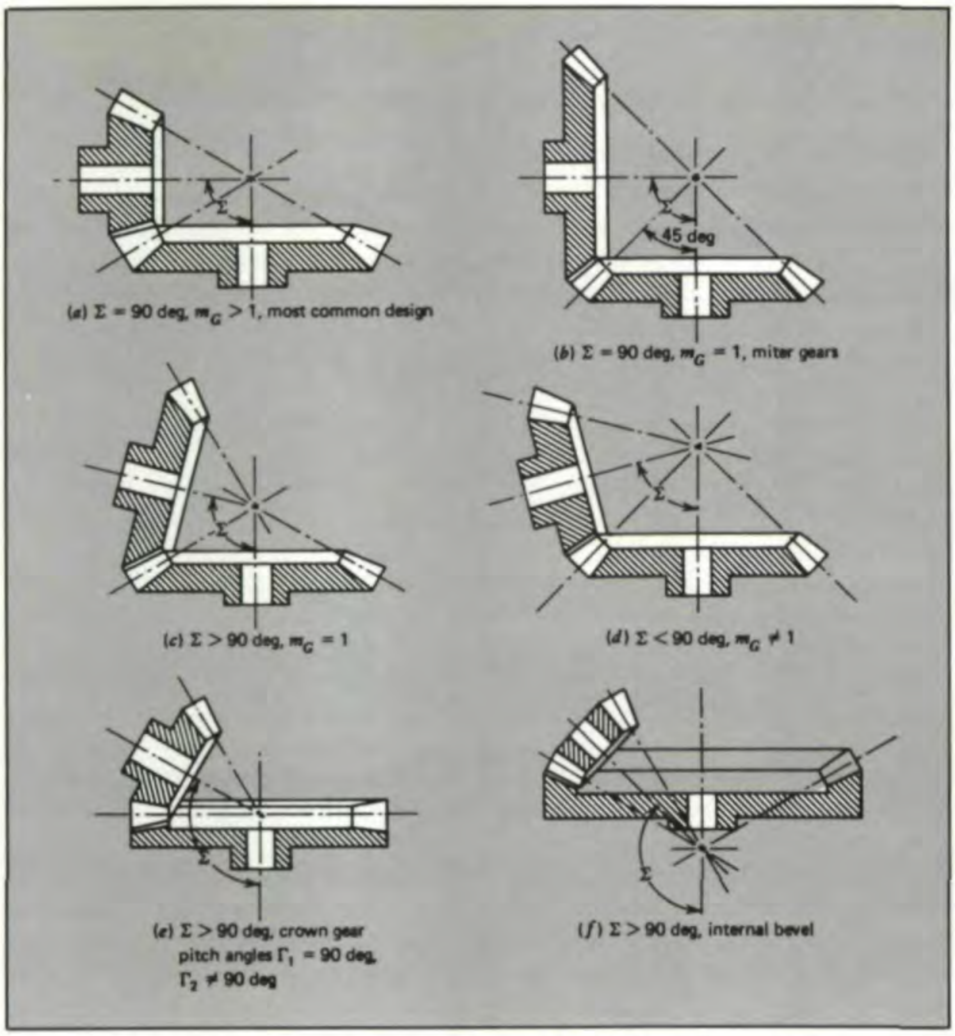

Fig. 5 – Bevel-gear arrangements. (Courtesy General Motors Corporation.)

are to be designed for a shaft angle of 90 deg and a reduction ratio of roughly 3:1. If the pinion is to have a minimum of 17 teeth, find pitch angles and the number of teeth in the gear.

Solution

$N = (3)(17) + 1 =$ **52** leads to a hunting ratio equal to 3.06:1. Assuming a module m, we obtain for the equivalent spur gears:

$$d = m\ (17\ \text{mm}) \qquad D = m\ (52\ \text{mm})$$

$$\tan \Gamma_p = \frac{N_p}{N_G} = \frac{17}{52} \longrightarrow \Gamma_p = \mathbf{18.1\ deg}$$

$$\tan \Gamma_G = \frac{N_G}{N_p} = \frac{52}{17} \longrightarrow \Gamma_G = \mathbf{71.9\ deg}$$

Check:

$$\sum = \Gamma_p + \Gamma_G = 18.1\ \text{deg} + 71.9\ \text{deg}$$
$$= 90\ \text{deg}$$

Hypoid Gears

Hypoid gears closely resemble spiral bevel gears except that the pinion does not meet the ring gear at its center. It meets it at a *lower* point (Fig. 6). The pitch surfaces are hyperboloids from which the term "hypoid" was derived. Curved teeth contribute to smooth, *noiseless* operation even at high speed.

Hypoid gears grew out of a need for *silent* automotive differentials that would also allow the drive shaft to be placed well below the centerline of the rear axle, thus contributing to a lower body design. Because the two shafts do not intersect, (1) two rear axles, instead of one, can be successively driven from the same transmission shaft, and (2) bearings can be mounted on both sides of the pinion. Although the altered tooth shape results in more sliding, lower efficiency, and the need for special lubricants, it provides a perfectly smooth drive and solves a major automotive problem – noise.

Helical Gearing

Helical gearing is a term applied to all types of gears whose teeth are of helical form. Helical gears work equally well to connect parallel shafts and nonparallel, nonintersecting shafts. In the latter case, however, a distinction must be made be-

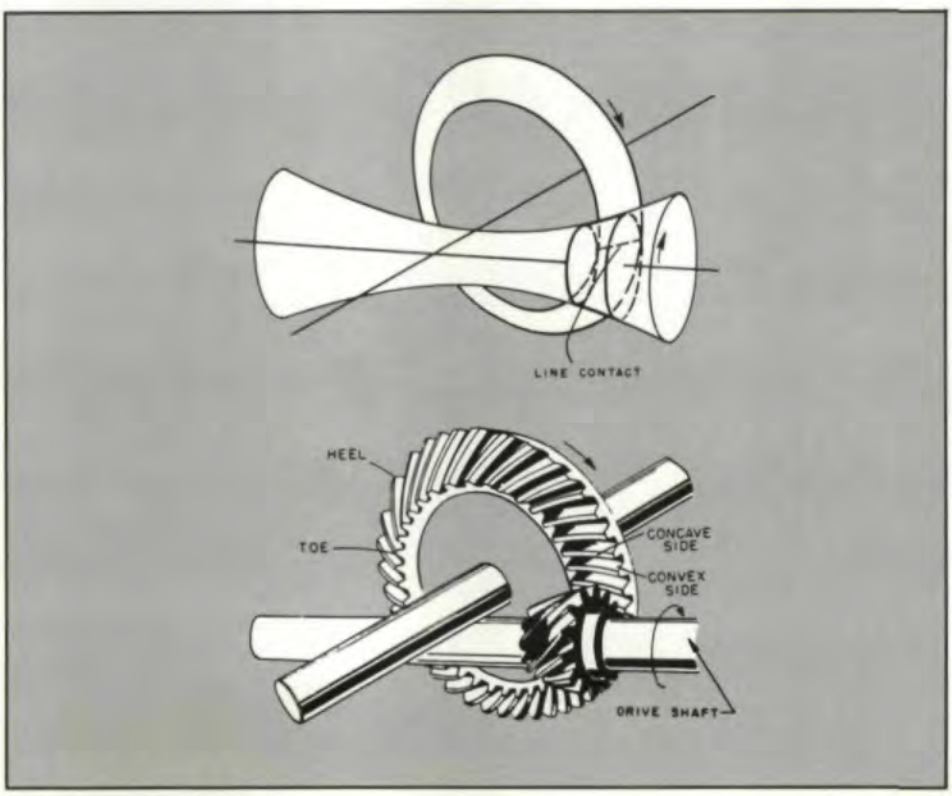

Fig. 6 (Bottom Left) – Hypoid gear and pinion. These gears transmit motion between nonintersecting shafts crossing at a right angle. The pitch surfaces are hyperbolic in form. (Courtesy Mobil Oil Corporation.)

Fig. 7—Crossed helical gears. These gears transmit motion between nonintersecting shafts crossing at an acute angle. The teeth are developed on cylindrical pitch surfaces. Since only point contact exists between the gears, this arrangement is rarely used to transmit loads of any magnitude. (Courtesy of Mobil Oil Corporation.)

tween a gear and a worm, even though both have helical teeth. As seen in Fig. 7, the teeth on this gear make only a *fraction* of a revolution on the base cylinder. That the tooth curvature is helical is not even obvious. What the teeth lack in length, however, they make up for in number, which always exceeds 10.

Crossed Helical Gearing

Fig. 7 shows this form of gearing. For what they can do kinematically, crossed helical gears are the acme of simplicity. Tooth contact, however, is only a point which greatly limits their power transmission capability.

Worm Gearing

Worm gear drives are used on right-angle applications with nonintersecting shafts. They provide smooth, quiet action and maximum reduction ratios for a given center distance. These favorable characteristics are obtained by using a worm gear combination. As seen in Fig. 8, the gear has teeth inclined at the same angle as the threads in the worm. For speed reduction or torque amplification, the worm is the driver.

In a *worm*, the number of teeth *rarely* exceeds 10 (one to four teeth is common, as shown in Figs. 8 and 9). Each tooth, however, makes at least one revolution on the base cylinder. If only one tooth is used, it winds around the base cylinder several times like a screw thread.

Worm gearing derives its characteristics from the two simple machines of which it is composed: the screw and the lever. From the screw it obtains a *large* mechanical advantage but a somewhat *lower* efficiency because of larger friction forces. The conjugate tooth action is identical to that of a large spur gear and rack (Fig. 8). As the worm revolves, the thread form advances along its axis and the worm gear rotates a corresponding amount. The presence of a screw instead of a rack ensures a vastly greater output torque on the gear shaft. The net effect is a torque converter of superior capacity but, because of inherent sliding action, one of reduced efficiency.

Worm gear terms are shown in Fig. 9. In this particular case the *lead*, the distance advanced during one revolution, is three times greater than the pitch. Triple-threaded worms are more efficient than single-threaded worms (due to less friction), but their reduction ratio is only one-third that of the single-threaded worm.

Fig. 10 shows the basic difference between single- and double-thread worms. The slope or helix angle of the double-thread worm is *twice* that of the single-thread worm, as is the lead. Thus, for one revolution the double-thread worm will advance or turn its mating gear an angle *twice* that of the single-thread worm.

Tooth breakage from bending action is not prevalent in worm gear sets. With relatively high sliding velocities, the design criteria are usually based on scoring and pitting. *Scoring* is wear resulting from failure of the lubricant film due to localized overheating of the mesh, per-

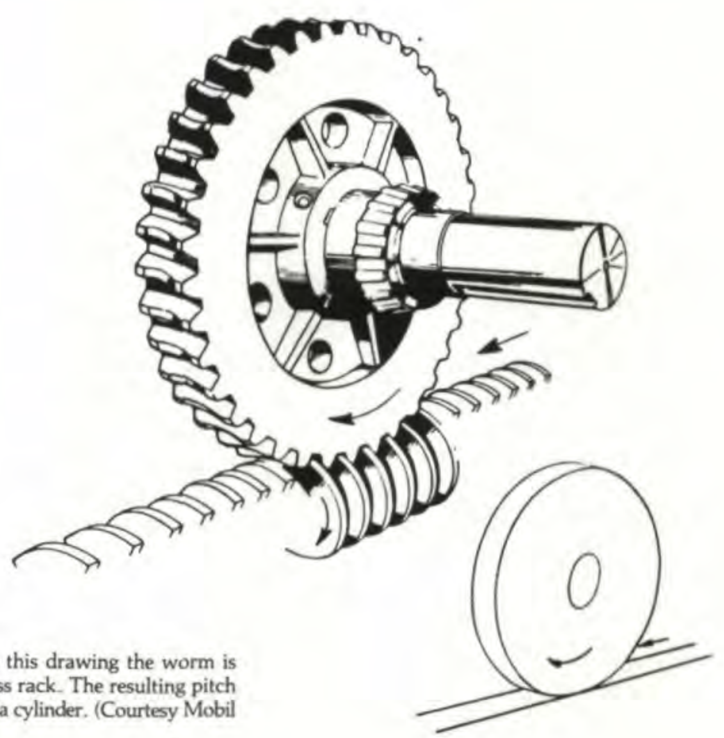

Fig. 8—Worm gear. In this drawing the worm is represented as an endless rack. The resulting pitch surfaces are a plane and a cylinder. (Courtesy Mobil Oil Corporation.)

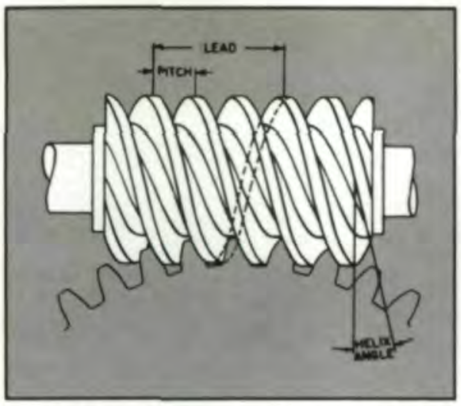

Fig. 9—Worm gear terms. (Courtesy Mobil Oil Corporation.)

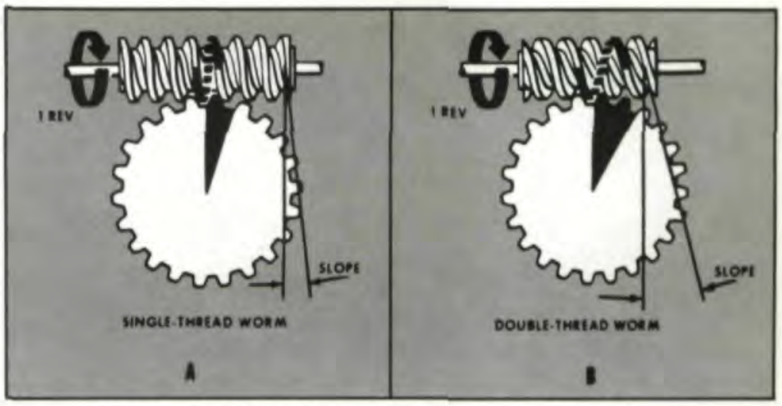

Fig. 10—The difference between a single- and a double-thread worm. (Courtesy Bureau of Naval Personnel.)

mitting metal-to-metal contact. Because more teeth are in contact simultaneously, worm gearing provides smoother operation than involute gearing. The contact area is also larger. Thus load capacity is high despite sliding action and line contact. Entering side wedges are produced on modern worm gears to generate a load-supporting oil film.

The advantages of worm gearing compared to spur and helical gearing are:

1. A more compact design for the same reduction ratio or power capacity.
2. Much greater speed reduction and torque amplification in a single step.
3. Smooth and silent operation that can withstand higher shock loads and higher momentary loads.

The disadvantages compared with ordinary gearing are:

1. Lower and varying efficiency.
2. Greater axial forces requiring costlier bearings.
3. Overheating that limits duration and capacity for power transmission.

Worm Gear Terminology and Kinematics

Fig. 11 shows worm gear terminology and development of a worm thread. For reasons of clarity, a triple-threaded worm was used. A worm can be single, double, triple, quadruple, or multithreaded, plus left or righthanded. Threads in excess of 10 are rarely advantageous.

Axial pitch (p_a) of a worm (Fig. 11) is *the distance measured axially from a* point on one thread to the corresponding

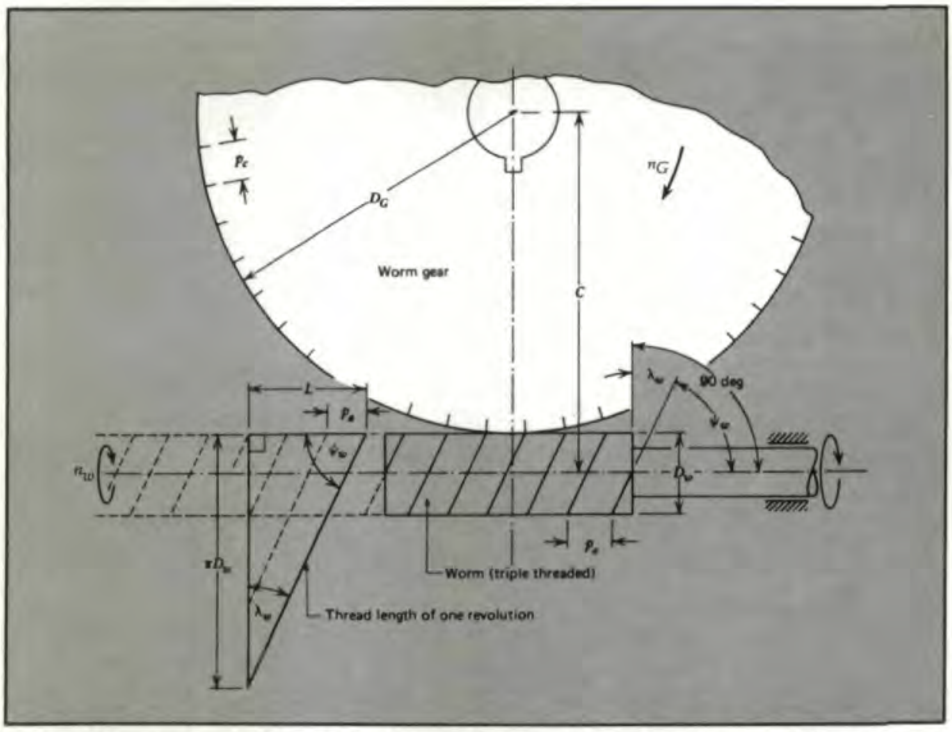

Fig. 11 – Worm gear terminology and development of a worm thread. (For clarity, a multithreaded worm was used.)

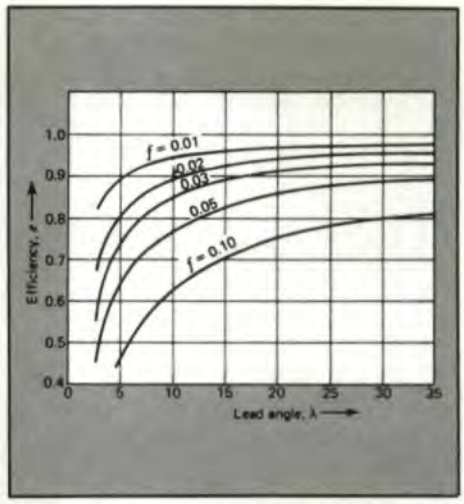

Fig. 12 – Efficiency as a function of lead angle and coefficient of friction.

point on the next thread. For proper mesh, p_a must equal the circular pitch p_c of the gear.

Lead (L) is the distance L that a thread advances in one turn of the worm. Thus

$$L = N_w p_a \tag{4}$$

where N is the number of threads on the worm; e.g., $N_w = 2$ for a double-threaded worm.

Lead angle (λ_w) is the angle between a tangent to the thread at the pitch diameter and a plane normal to the worm axis.

Velocity ratio (m_G) is the ratio of pitch circumference of gear to lead of worm, which equals tooth ratio. It is also the ratio of worm speed to gear speed. Thus

$$m_G = \frac{p_a N_G}{L} = \frac{N_G}{N_w} = \frac{n_w}{n_G} = \frac{D_G}{D_w \tan \lambda_w} \tag{5}$$

For worm and gear to mesh properly, the lead angle of the worm must equal the helix angle of the gear ($\lambda_w = \psi_G$), and axial pitch of the worm must equal circular pitch of the gear ($p_a = p_c$). Since the circumference of the pitch circle of the gear can be expressed as πD_G or $p_c N_G$, this leads to

$$p_c = \frac{\pi D_G}{N_G} = p_a \tag{6}$$

Substitution into Eq. 5 gives

$$n_G = \frac{L}{\pi D_G} n_w \text{ rpm} \tag{7}$$

as another expression of the speed relationship.

Development of one turn of the worm leads to a triangle, as shown in Fig. 11. This triangle shows that

$$\tan \lambda_w = \frac{L}{\pi D_w} \tag{8}$$

Center distance is 0.5 ($D_w + D_G$), which can also be expressed as

$$C = \frac{L}{2\pi} (m_G + \cot \lambda_w) \tag{9}$$

Thermal Ratings

When worm gear teeth slide across the surfaces of mating worm threads, far more heat is generated than when the same load is carried by any other type of gearing. These thermal conditions raise the operating temperature of the oil, thereby reducing its load-carrying capacity. To keep oil temperatures below critical levels, manufacturers publish thermal ratings for each unit that indicate the maximum power input that produces a safe rise in oil temperature. Because common gear lubricants deteriorate rapidly at temperatures above 90°C (195°F), operating levels are usually kept at or below 75°C (170°F). Clearly, design of worm gearing must include temperature effects, as well as strength and wear, as a limiting factor. Of the three, overheating is the controlling parameter. For example, a worm gear may have a thermal rating of 5 kW and a mechanical rating of 7 kW for the higher speed ranges. This means that the gearing is capable of transmitting more than 5 kW as far as strength and wear are concerned – but not without overheating. Recently, however, the use of computers has improved worm geometry, thereby narrowing the gap between thermal and mechanical capacity.

Efficiency of Worm Gearing

While spur and helical gearing exhibit very high and virtually constant efficiencies (0.98 to 0.99), those of worm gearing may range from a low of 0.50 to a high of around 0.98. Generally, efficiency varies inversely with speed ratio provided the coefficient of friction does not change. The various parameters determining efficiency do not have a linear relationship (Fig. 12). Instead, efficiency e increases with decreasing coefficients of friction. Efficiency is greatly influenced by the lead angle for small values, but less and less as λ increases. A maximum is reached for $\lambda = 45$ deg.

For a well-designed, well-lubricated unit, the following is a fair approxima-

Fig. 13 (Right) – Typical worm gear reduction unit. (Courtesy Bodine Electric Company.)

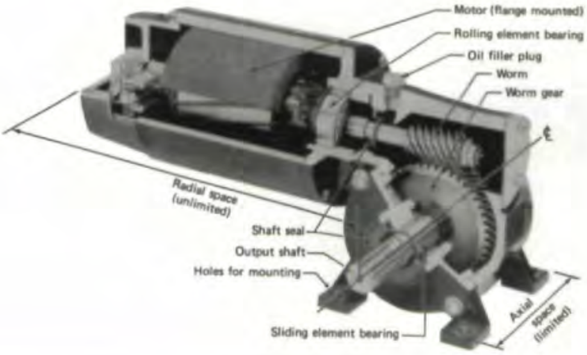

tion to efficiency.

$$e = \frac{\tan \lambda}{\tan(\lambda + \theta)} \tag{10}$$

where

$\theta = \arctan f =$ friction angle

Back-driving is the term used when the gear drives the worm. In this reverse action speed is increased at the expense of force. Back-driving can thus be used to advantage in speedup drives for centrifuges and turbochargers. The corresponding expression for efficiency is

$$e = \frac{\tan(\lambda - \theta)}{\tan \lambda} \tag{11}$$

Theoretically, back-driving is possible only for $\lambda > \theta$, that is, when the lead angle is greater than the friction angle. In reality, this reverse action occurs for higher values of θ. Vibration, present in most mechanical equipment, effectively lowers friction, thereby reducing "self-locking" to "a mechanical fringe benefit." Only a brake can effectively prevent back-driving.

Optimum Design

Even though worm gear drives are among the oldest mechanisms, they are one of the least understood. Because of their inherent complexities, precise analytical methods have not evolved, so design relies heavily on trial-and-error testing. Worm gears have, however, reached a high degree of perfection. Thus, by analyzing the expression for efficiency, we may single out major design parameters and compare them with the industrial end product.

Low coefficients of friction are obtained by (1) using dissimilar metals for worm and gear, (2) providing smooth tooth surfaces, and (3) ensuring adequate lubrication. For instance, hardened and ground steel worms are used with gears of phosphor bronze or cast iron. Special lubricants are available for worm gearing.

Large lead angles are also desirable, but are obtained at the expense of lower speed ratios. Consider the following equation.

$$\tan \lambda = \frac{L}{\pi D_w} = \frac{p_a N_w}{\pi D_w} \qquad (12)$$

A large efficiency requires a large lead; therefore the worm should be multithreaded. Consequently, when worm gearing is designed primarily for transmitting power, it should be multithreaded, as is common practice.

To obtain a given ratio, some number of worm wheel teeth divided by some number of worm threads must equal the ratio. Thus, if the ratio is 6:

$$m_G = \frac{6}{1} = \frac{12}{2} = \frac{18}{3} = \frac{24}{4} = \frac{30}{5} = \frac{36}{6} = \frac{42}{7}$$

Any of these combinations may be used. The numerators represent the number of worm wheel teeth, and the denominators are the number of worm threads. As the total number of teeth increases, so does efficiency, but only at higher initial cost.

The expression for λ also indicates that a small worm diameter D_w is most desirable because it lowers rubbing velocity. As can be seen in Fig. 13, the worm diameter is small relative to the thread height.

Example 2

A right-angle speed reducer has a triple-threaded worm and a 41-tooth gear. Find the speed ratio, lead, lead angle, helix angle, pitch diameter of gear, center distance, efficiency, power output, and transmitted force for the following data.

$p_c = 32$ mm $\qquad n = 900$ rpm

$D_w = 44$mm

$f = 0.05 \qquad P = 0.75$ kW (input)

Will the unit back-drive?

Solution

$$m_G = \frac{N_G}{N_p} = \frac{41}{3} = \mathbf{13.67}$$

From Eq. 4:

$$L = N_w p_a = 3(32 \text{ mm}) = \mathbf{96 \text{ mm}}$$

From Eq. 8:

$$\lambda_w = \arctan \frac{L}{\pi D_w}$$

$$= \arctan \frac{96 \text{ mm}}{\pi (44 \text{ mm})} = \mathbf{34.78 \text{ deg}}$$

For proper mesh, the lead angle of the worm must equal the helix angle of the gear. Thus $\psi_G = \lambda_w =$ **34.78 deg**

As can be seen in Fig. 12

$\psi_w = 90 \text{ deg} - \lambda_w =$ **55.22 deg**

From Eq. 6:

$$D_G = \frac{p_a N_G}{\pi}$$

$$= \frac{(32 \text{ mm})41}{\pi} = \mathbf{417.62 \text{ mm}}$$

From Eq. 9:

$$C = \frac{L}{2\pi}(m_G + \cot \lambda_w)$$

$$= \frac{96 \text{ mm}}{2\pi}(13.67 + \cot 34.78 \text{ deg})$$

$$= \mathbf{230.86 \text{ mm}}$$

From Eq. 10:

$$e = \frac{\tan \lambda_w}{\tan(\lambda_w + \theta)}$$

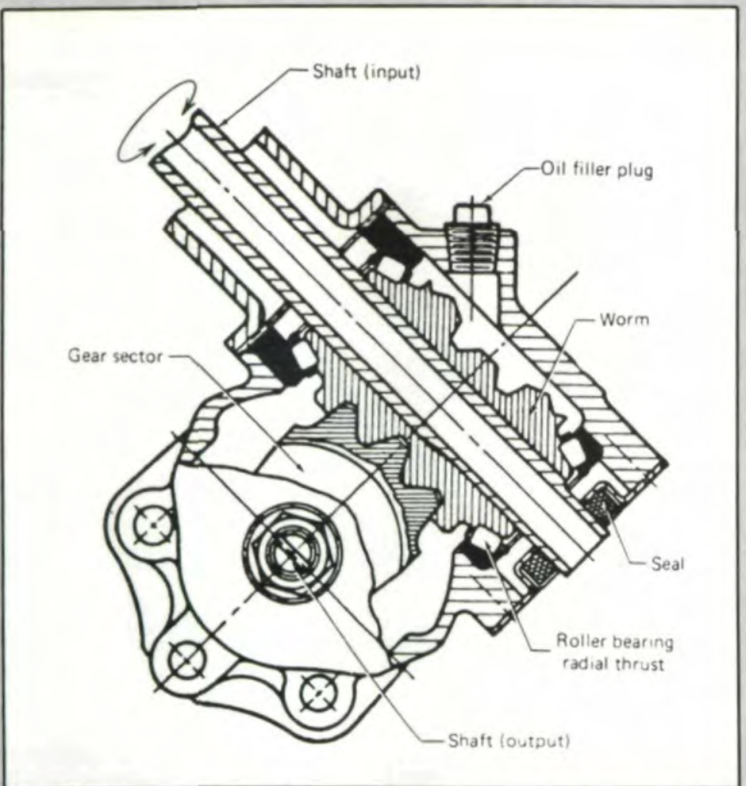

Fig. 14 – Steering mechanism. Note that only a gear sector is needed. (Courtesy The Timken Company.)

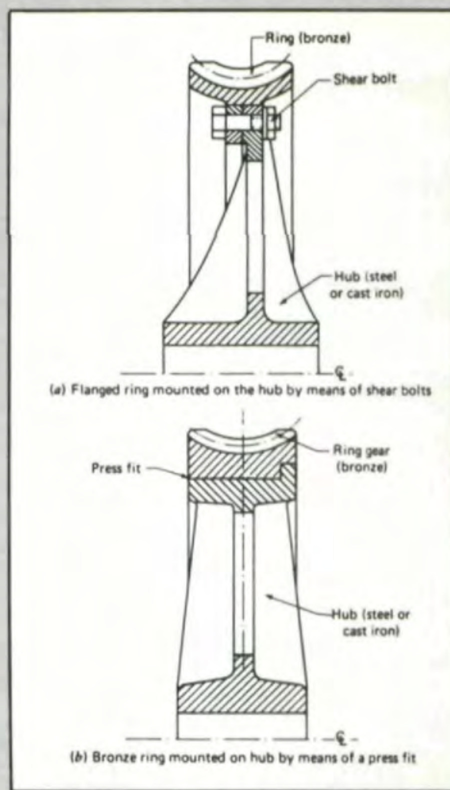

Fig. 16 – Design of a large worm gear.

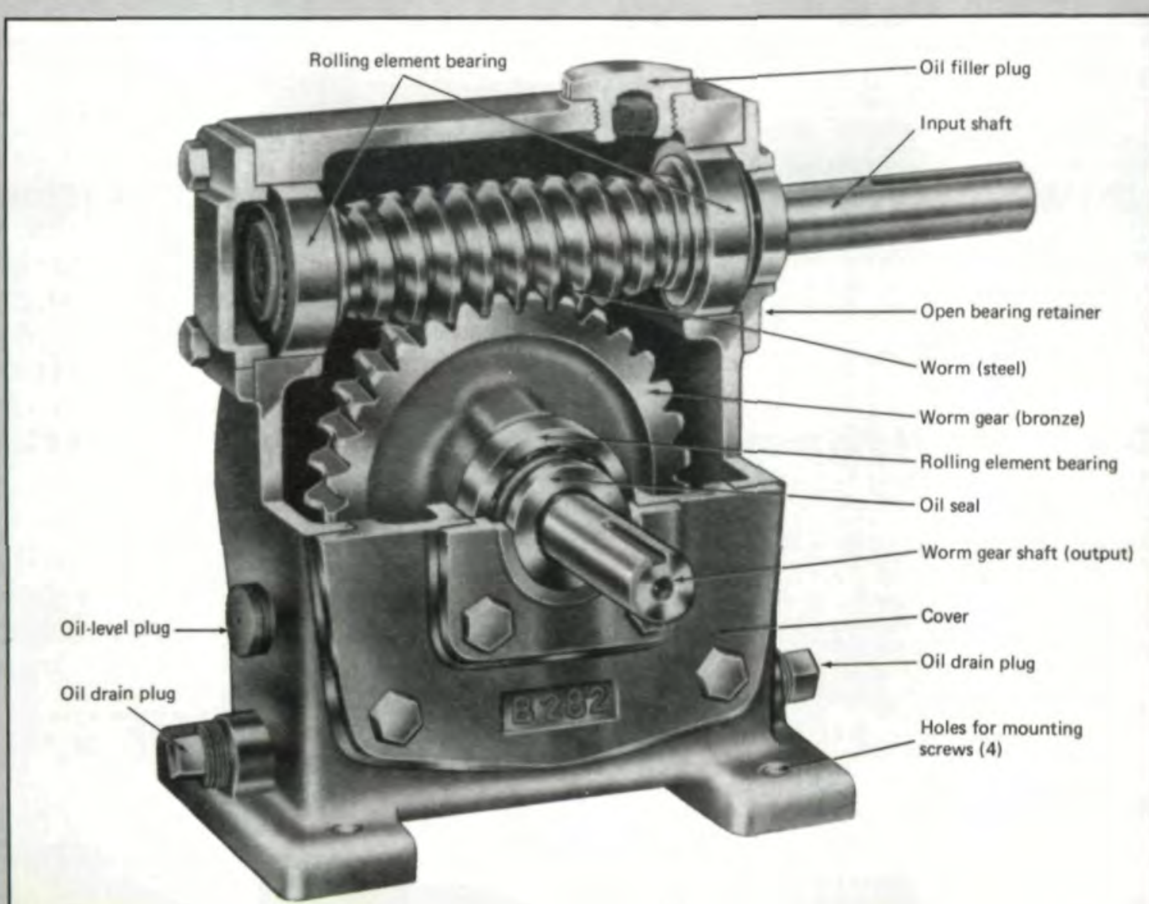

Fig. 15 – Typical medium-size worm gear speed reducer. (Courtesy of Morse Industrial Corp., subsidiary of Emerson Electric Co.)

(continued on page 63)

CLASSIFIED

Rates: Classified Display—$100 per inch (minimum 3") Type will be set to advertiser's layout or *Gear Technology* will set type at no extra charge. **Word Count:** 35 characters per line, 7 lines per inch.

Payment: Full payment must accompany classified ads. Mail copy to *Gear Technology*, P.O. Box 1426, Elk Grove Village, IL 60007. **Agency Commission:** No agency commission on classifieds.

Closing date: Ads must be received by the 25th of the month, two months prior to publication. **Acceptance:** Publisher reserves the right to accept or reject classified advertisements at his discretion.

HELP WANTED

GEAR ENGINEER

Spur and helical production gear manufacturing company has opening for engineer and manager of engineering.

Ideal candidate will have experience in manufacturing, project and process engineering, as well as automation and state-of-the-art technology.

These positions are being created by internal growth.

Reef Industries
50903 E. Russell
Schmidt Blvd.
Mt. Clemens, MI 48045

SUBCONTRACT WORK

SPRIAL BEVEL GEARS

Coniflex bevels to 34" diameter
Prototype or production up to 60" diameter
Breakdown work — fast turnaround
Complete machining, heat treat, lapping and testing
CALL US!

B&R MACHINING
PO Box 536
Sharon, TN 38255
1-800-238-0651

CIRCLE A-34 ON READER REPLY CARD

FOR SALE

AVAILABLE:

Rebuilt galvano meters for EPSCO, BRUSH and SANBORN tube type recorders.

PRECISE INSPECTION
27380 Gratiot Avenue
Roseville, Michigan 48066
313-445-6959

CIRCLE A-32 ON READER REPLY CARD

THE DRIVING FORCE

The drive to excel in technology is a prime motivator at **Rockwell International's Automotive Operations.** It's evident at our Troy Technical Center, the largest and most advanced of it's kind. Our technical professionals continually strive to perfect automotive components technology. This is proven by the number of our Engineers who have won Rockwell International's prestigious "Engineer of the Year" award. If you're driven to excel, consider our current opportunity.

GEAR DESIGN ENGINEER

The ideal candidate would possess a BSME with a minimum of 5 years hands-on gear design experience. Specific knowledge of Hypoid/Spiral Bevel gear design required, along with a working knowledge of gear manufacturing techniques. Familiarity with Spur and Helical gear design a plus.

Rockwell International offers an outstanding compensation and benefits package including relocation assistance. For further information, please send resume, including salary history, in confidence to: **Technical Services Personnel (GT9/10), Rockwell International, Automotive Operations, 2135 W. Maple Road, Troy, Michigan 48084.** Equal Opportunity Employer M/F.

Rockwell International

...where science gets down to business

GEAR MANUFACTURING ENGINEER

Cloyes Gear is a rapidly expanding manufacturer of automotive gears and sprockets. Our growth requires that we seek an engineer with knowledge in gear manufacturing processes to join the staff of our manufacturing plant in Arkansas. We are in need of an individual with a strong hobbing and shaving background willing to take a "hands on" attitude toward troubleshooting gear manufacturing processes.

For a chance to work with state of the art gear machinery including 6 axis CNC hobs and CNC gear inspection equipment, please submit your resume and salary history to:

CLOYES®

CLOYES GEAR & PRODUCTS, INC.
P.O. BOX 511
WILLOUGHBY, OHIO 44094

(continued from page 60)

$$= \frac{\tan 34.78 \text{ deg}}{\tan(34.78 \text{ deg} + 2.86 \text{ deg})} = \mathbf{0.90}$$

Output: $P = 0.90(0.75\text{ kW}) = \mathbf{0.675\text{ kW}}$

The unit will back-drive because the lead angle of the worm (λ_w = 34.78 deg.) is much greater than the friction angle Θ where

Θ = arctan f

= arctan 0.05 = 2.86 deg. $\ll$ 34.78 deg.

From the power equation:

$$W_t = \frac{9550\,P}{(0.5\,D_w)n}$$

$$= \frac{9550(0.675\text{ kW})}{0.5(0.044\text{m})(900\text{ rpm})} = \mathbf{326\text{ N}}$$

Applications

As indicated in Fig. 12, worm gear efficiency varies widely from 0.5 to 0.98. It also varies inversely with speed ratio or mechanical advantage. Thus, single-threaded worm gear drives yield large reduction ratios, but at the expense of efficiency. In contrast, a multithread speed reducer will have high efficiency, but a somewhat lower reduction ratio. This fact leads to three major areas of application for worm gearing.

1. *Intermittent, infrequent* operations where a small, low-cost motor moves a heavy load, as in small hoists. Efficiency, of minor importance, is thus

(continued on page 64)

IMPROVED GEAR LIFE . . .

(continued from page 18)

References

1. FUCHS, H., Shotpeening Effects and Specifications, ASTM Special Technical Publication No. 196-1962.
2. DALY, J., "Boosting Gear Life Through Shot Peening," *Machine Design*, May 12, 1977.
3. "Shot Peening of Metal Parts," MIL-S-13165B Amendment II, June 25, 1979.
4. *Shot Peening Applications*, Metal Improvement Company, Sixth Edition, 1980, Figs. 2, 6, 8 and 9.
5. McCORMACK, DOUG, "Shot Peen Gears for Longer Life," **Design Engineering**, July, 1981.
6. FUCHS, H.O., "The Effect of Self Stresses on High Cycle Fatigue," JTEVA Vol. 10, No. 4, July, 1982.
7. LAWERENZ, MARK, *Shot Peening and its Effect on Gearing*, SAE paper #841090.
8. SEABROOK, JOHN B. and DUDLEY, DARLE W., "Results of Fifteen Year Program of Flexural Fatigue Testing of Gear Teeth," 1963.
9. TOWNSEND, DENNIS P. and ZARETSKY, E.V., "Effect of Shot Peening on Surface Fatigue Life of Carburized and Hardened A151, 9310 Spur Gears," Lewis Research Center, Cleveland, Ohio, NASA 2047.
10. *Lloyd's Register of Shipping*, June 6, 1975, Letter.

Reprinted with permission of the American Gear Manufacturer's Association. First presented at AGMA's Fall Technical Meeting, October, 1985.

PRACTICAL ANALYSIS OF HIGHLY LOADED . . .

(continued from page 26)

Conclusion

Based on the DIN/ISO formulae for scoring capacity, a simplified method adopting a modified scoring index has been developed. As can be seen from typical applications, this method works with sufficient accuracy.

The calculation of scoring capacity will become more and more important in parallel with an increasing demand in transmitted power per gear volume. The practical experience with highly-loaded gears with regard to scoring will give more safety in the application of this calculation method and will possibly permit a reduction of the safety margins used today.

References

1. HIRT, M. "An Improved Method to Determine the Scoring Resistance of High Power High-Speed Gearing." Proc. of 1984 Turbomachinery Symposium. Texas A&M University, Houston
2. AGMA 217.0, "Gear Scoring Design Guide for Aerospace Spur and Helical Power Gears."
3. BLOK, H., "Theoretical Study of Temperature Rise at Surface of Actual Contact Under Oiliness," Lubricating Conditions. Proc. Gen. Disc. Lubric. IME London Bd 2(1937) Sh. 225.35.
4. DIN 3990, Part 4: "Basic Principles for the Calculation of Load Capacity of Spur and Helical Gears, Calculation of Scuffing Load Capacity," Draft (1980).
5. DUDLEY, D., Gear Handbook, McGraw Hill (1962).
6. HIRT, M., "Design and Calculation Methods for High Speed Gears of Advanced Technology", Proceedings of the Twelfth Turbomachinery Symposium, Texas A&M University, College Station, Texas (1983).
7. NIEMANN, G. and WINTER, H., Maschinenelemente Part II, Springer (1983).
8. WINTER, H. and MICHAELIS, K., "Scoring Load Capacity of Gears Lubricated with EP-Oils," AGMA Paper 219.17 (Fall, 1983).

GEARS FOR NONPARALLEL SHAFTS . . .

(continued from page 62)

sacrificed to obtain a large mechanical advantage. Typical applications are standby pumps, large valves, and gates.

2. *Intermittent, manual* operations requiring a *large mechanical advantage, such as in steering mechanisms and* opening and closing of valves and gates by means of handwheels (Fig. 14).
3. *Motorized, nearly continuous* operations where worm gearing competes with gear reduction units. When space is at a premium, as in machine tools, packaged, motor-driven worm reduction units are used in preference to gear reducers (Fig. 13). Depending on size and application, the unit may be self-contained or built integrally with an electric motor. Because of silent operation, such units are preferred in machine tools and also in elevators. These units all require multithreaded worms and ratios not exceeding 1:18. Larger ratios are achieved by connecting two units in series.

Design Detail of Worm Gearing

The unit shown in Fig. 15 is a typical, medium-size worm gear speed reducer. Smaller units of this type usually have housings of cast aluminum alloys for maximum thermal rating. For larger units the preferred material is cast iron. The worm is case-hardened and ground alloy steel of integral shaft design. The gear is cast bronze with generated teeth and keyed to the output shaft. Larger worm gears are often composed of a ring of bronze mounted on a center or hub of less expensive material. A common design utilizes a flanged rim mounted on the hub by means of shear bolts (Fig. 16*a*). Equally common is mounting by means of a press fit (Fig. 16*b*) assisted by a pin connection. The output shaft is high-quality, medium-carbon steel, ground to close tolerances. The worms and output shafts are frequently mounted on roller bearings. All shaft extensions are equipped with lip style, synthetic oil seals.

Lubrication

Generally, oil is contained within the housing and directed by splash to the bearings and to the zone of tooth and thread contact. Natural splash may be augmented by flingers, scrapers, and cups attached to the gear. Channels or ribs may be furnished inside the housing to help direct oil to the bearings.

Summary

Despite higher initial cost, gears for nonparallel shafts are justified because they often save space and lead to a better design. Kinematically, these gears all perform the very difficult task of changing the plane of rotation. With the exception of crossed helical gears, all have reached a high degree of perfection and a long, useful life of transmitting power. Hypoid gears for automotive differentials, for instance, rarely fail during the life of a car. The versatility of worm gearing is due to the inverse relationship of efficiency to torque and reduction ratio. Table 1 summarizes comparative characteristics of speed reducer gear families.

References

1. BUCKINGHAM, E. K. "Taking Guesswork Out of Worm-Gear Design." Machine Design, March 20, 1975.
2. MacFARLAND, W. C. "Straight Talk About Speed Reducers." Machine Design, September 18, 1975-October 2, 1975.
3. *WILL, R. J. "Selecting Speed Reducers."* Machine Design, September 8, 1977.